NOVEL METHODS TO REDUCE SHUNT CATHETER OBSTRUCTION IN THE TREATMENT OF HYDROCEPHALUS

by

Carolyn Anne Harris

A dissertation submitted to the faculty of
The University of Utah
in partial fulfillment of the requirements for the degree of

Doctor of Philosophy

Department of Bioengineering

University of Utah

May 2011

The University of Utah Graduate School

STATEMENT OF DISSERTATION APPROVAL

The dissertation of **Carolyn Anne Harris**

has been approved by the following supervisory committee members:

James P. McAllister, II	, Chair	**3/3/11** Date Approved
Robert W. Hitchcock	, Member	**3/3/11** Date Approved
Vladimir Hlady	, Member	**3/3/11** Date Approved
John R.W. Kestle	, Member	**3/3/11** Date Approved
Patrick A. Tresco	, Member	**3/3/11** Date Approved
Marion L. Walker	, Member	**3/3/11** Date Approved

and by **Patrick A. Tresco**, Chair of the Department of **Bioengineering**

and by Charles A. Wight, Dean of The Graduate School.

ABSTRACT

Shunt catheter obstruction due to the foreign body host response is a serious problem in the treatment of hydrocephalus. Our goal was to reduce inflammatory cell adhesion on silicone catheters in an effort to limit shunt obstruction. We investigated chemical and mechanical cues that may influence macrophage and astrocyte adhesion, and using this knowledge, examined pertinent catheter modifications. A novel *in vitro* bioreactor, capable of measuring dependencies between macrophage and astrocyte adhesion, intracranial flow rate, pressure, pulsation frequency, and protein concentration, was developed and tested. Results demonstrated that a combination of chemical cues (particularly surface chemistry) and mechanical cues (particularly shear stress) influenced macrophage and astrocyte attachment to shunt catheters. The surface chemistry of the catheter was modified using long term coatings with anti-inflammatory capabilities including poly(ethylene) glycol and N-acetyl-L-cysteine, both of which significantly inhibited macrophage and astrocyte adhesion when tested in the bioreactor. Additionally, the shear stress through ventricular catheter drainage holes was manipulated by changing the diameter of these openings. Data generally suggested that macrophage and astrocyte adhesion decreases with increasing hole size. Two barriers were overcome in this research: (1) the development of an *in vitro* system capable of testing catheter constructs in a method superior to standard static *in vitro* culturing; (2) significant surface and architecture modifications that inhibit inflammatory cell adhesion

which could be used in future studies to inhibit inflammatory-derived obstruction. Together, the implementation of this system and the modifications to current catheter design will help answer questions of how and why catheters fail.

To my husband, Dan.

“The treatment of hydrocephalus in infancy remains one of the most unsatisfactory and discouraging problems the neurological surgeon is called upon to treat. Penfield’s statement made in 1935 that ‘all surgeons who continue to face the hydrocephalus problem require the support of fortified optimism’, is just as pertinent today.”

- Ingraham

TABLE OF CONTENTS

LIST OF TABLES

LIST OF ABBREVIATIONS

Abbreviation	Defining Term
13F	Tridecafluoro-1,1,2,2,-tetrahydrooctyl1-1-trichlrosilane
ABC	Avidin-biotin complex
Alb	Albumin
ANOVA	Analysis of Variance
ASD	Anti-siphon Device
ATCC	American Type Culture Collection
BBB	Blood-brain barrier
CNS	Central Nervous System
CSF	Cerebrospinal Fluid
Da	Dalton
DAPI	4', 6-diamidino-2-phenylindole dihydrochloride
DI	Deionized
DNase	Deoxyribonuclease
DPBS	Dulbecco's Phosphate Buffered Saline
dRGB	Digital Red-Green-Blue
DRIE	Deep Reactive Ion Etching
EDC	1-ethyl-3-(3-dimethylaminopropyl) carbodiimide
e-PTFE	Expanded Polytetrafluoroethylene

ETV ..... Endoscopic Third Ventriculostomy

EVD ..... External Ventricular Drain

FAS ..... Fluoroalkylsilane

FBR ..... Foreign Body Response

FITC ..... Fluorescein isothiocyanate

Fn ..... Fibronectin

g ..... Gravity

GFAP ..... Glial Fibrillary Acidic Protein

H + L ..... Heavy and Light

HBSS ..... Hank's Balanced Salt Solution

Hep ..... Heparin

HEPES ..... 4-(2-hydroxyethyl)-1-piperazineethanesulfonic acid

HSCB ..... Hydrocephalus Shunt Catheter Bioreactor

Hyaluronan ..... Hya

IACUC ..... Institutional Animal Care and Use Committee

Iba-1 ..... Ionized calcium binding adapter molecule 1

ICAM-1 ..... Inter-Cellular Adhesion Molecule 1

ICP ..... Intracranial Pressure

IFNγ ..... Interferon-gamma

IgA ..... Immunoglobulin A

IgG ..... Immunoglobulin G

IL-1 ..... Interleukin-1

IL-1β ..... Interleukin-1 Beta

IL-6 ..... Interleukin-6

iNOS ..... Inducible Nitric Oxide Synthase

MCP-1 ..... Monocyte Chemotactic Protein-1

NAC ..... N-Acetyl-L-cysteine

NFκB ..... Nuclear Factor Kappa-Light-Chain-Enhancer of Activated B Cells

NHS ..... N-Hydroxysuccinimide

OH ..... Hydroxylated

OTS ..... Octadecyltrichlorosilane

PBS ..... Phosphate Buffered Saline

PDMS ..... Polydimethylsiloxane

PEG ..... Polyethylene glycol

PEG5K ..... Polyethylene glycol with Molecular Weight 5000 Da

PEG604 ..... Polyethylene glycol with Molecular Weight 604 Da

pHEMA ..... Poly-2-hydroxyethyl methacrylate

PS ..... Polystyrene

PTFE ..... Polytetrafluoroethylene

PVP ..... Polyvinyl Pyrrolidone

RGB ..... Red-Green-Blue

RMS ..... Root Mean Square

SAS ..... Subarachnoid Space

SEM ..... Scanning Electron Microscopy

TEM ..... Transmission Electron Microscopy

TNF-α..... Tumor Necrosis Factor Alpha

XPS ..... X-ray Photoelectron Spectroscopy

ACKNOWLEDGEMENTS

Without the support of my colleagues, friends, and family, completion of this dissertation would have been impossible. I would like to thank my advisor and role model, Dr. Pat McAllister, for his mentorship, encouragement, guidance, and friendship. Pat opened his lab to me, and for that I am grateful. His daily scientific input helped me understand the kind of scientist I aspire to become. Thank you to Dr. Walker and Dr. Kestle for pushing me to do the most clinically relevant work and for being such good friends along the way. I know I will always have a Utah family. I would like to thank my PhD Advisory Committee, Drs. McAllister, Tresco, Hlady, Hitchcock, Walker, and Kestle for their inspiration and for continually urging me to go beyond my preconceived limitations. Additionally, I would like to thank our collaborators who have been phenomenal supporters, including Dr. Del Bigio, Dr. Fults, Dr. Resau, Eric Hudson, and Rich West. I am most appreciative of the technical aid provided by William Grever, Lyn Pedone, and Brian Baker as well as the editorial assistance by Kristin Kraus. I would also like to thank my co-workers Kelley Deren, Candice Moon, Missy Packer, Ramin Eskandari, Jenn Forsyth, and Phillip Smith for their constant support. I think we figured out how to have fun and be productive at the same time. Thank you to my friends in the Midwest, especially Michelle and Jess, for reminding me that not even a thousand miles or crazy work schedules can keep us from staying close. A huge thank you goes to my family. Mom, Dad, Philip, and Andrew - you're the greatest! I couldn't have done any of this without you guys. Last but not least, I'd like to thank my husband and love of my life, Dan. Thank you for being my rock, for believing in me, and for constantly inspiring me.

CHAPTER 1

INTRODUCTION

1.1 Hydrocephalus

1.1.1 Clinical aspects

Hydrocephalus, an imbalance between cerebrospinal fluid (CSF) production and absorption, is a chronic disorder caused by impairment to the normal fluid pathway in the cranial cavity and spine. Genetic malformations, meningitis, subarachnoid hemorrhage, stroke, trauma, tumors, or unknown reasons can restrict or completely block CSF outflow within the ventricles (obstructive or intraventricular hydrocephalus) or the subarachnoid space (SAS, communicating or extraventricular hydrocephalus). This impairment in CSF outflow often causes elevated intracranial pressure (ICP) because the CSF production rate exceeds the volume of the ventricles and subarachnoid space by 2-3 times in a normal state [1]. The brain responds to ventriculomegaly with compensatory reactions such as partial CSF absorption into interstitial spaces to create edematous tissue and/or by decreasing the rate of CSF production, but in many cases these mechanisms are not capable of controlling ICP, and thus periventricular regions of the brain (especially the cerebral cortex) become compressed and distorted, and a multitude of secondary injury mechanisms are initiated [2]. If untreated, hydrocephalus usually causes serious neurological deficits such as learning disabilities, mental retardation, epilepsy and

spasticity, visual system impairments, reproductive dysfunction, and often death [3]. The incidence of hydrocephalus is about 1 in 500 people, but the prevalence of hydrocephalus is constantly increasing. In Sweden, Fernell and colleagues have shown that these increases in prevalence have caused the percentage of patients with neurological deficits to rise as much as 78% [4].

1.1.2 Anatomy most pertinent to hydrocephalus

The cerebral ventricular system consists of the lateral, third, and fourth ventricles with a total volume of approximately 22.4 mL in adult humans [5]. The lateral ventricles are the largest compartments of the ventricular system. They form two C-shaped arcs, are lateral to the midline, and are each composed of an anterior frontal horn, an intermediate body, a posterior occipital horn, and an inferior temporal horn. The midline third ventricle separates the two thalami. The fourth ventricle narrows to the obex where communication to the cisterna magna and the spinal cord occurs. The lateral ventricles and the third ventricle communicate through two foramina of Monro, the third and the fourth through the cerebral aqueduct (also known as the aqueduct of Sylvius), and the fourth and cisterna magna through the paired foramina of Luschka and the midline foramen of Magendie. Of all the communication pathways, the cerebral aqueduct has the smallest diameter with a cross section measuring 0.1 to 1.0 mm^2 at its most restrictive point [6]. Because of the small width of the cerebral aqueduct, pathologically it is a common site for resistance to CSF outflow (termed aqueductal stenosis).

The choroid plexus is a tissue consisting of choroidal epithelium, blood vessels, and interstitial connective tissue found on the floor of the lateral and fourth ventricles and on the roof of the third ventricle [5]. CSF is produced by the parenchyma (30%) along perivascular spaces and axon tracts [7] and by the choroid plexus (70%) by actively and passively transporting filtrate of arterial blood from the anterior and posterior choroidal arteries [8]. Following production, CSF flows slowly through the ventricular system, exits the fourth ventricle to gain access to the subarachnoid space, and finally is absorbed by the vascular system through the cranial dural venous sinuses, the veins adjacent to the spinal nerves, and the lymphatics surrounding some cranial nerves [9-10] (Figure 1). Although there is no direct way to measure CSF production rate, it can be interpreted through MRI studies or through ventricular tapping. As calculated using MRI, the average normal CSF production rate is expected to be about 0.3-0.36 mL/min [11]. At this rate, the volume of CSF exceeds the volume of the ventricular system in about 1.25 hours.

CSF serves as a protective cushion around the brain, nourishes the brain with glucose, essential amino acids, essential proteins, and vitamins, may serve as a pathway for diffusible neuromodulators and trophic substances, and provides a conduit in which waste can be excreted [12-14]. Depending on the integrity of the blood-brain barrier (BBB) and the pathological state, the total CSF protein concentration is approximately 20-40 mg/dl and from highest to lowest concentration (mg/dl) include albumin (11.5-19.5), immunoglobulin G (IgG, 0.7-2.0), transferrin (0.3-1.2), α_1-antitrypsin (0.4-1.0), α_2-macroglobulin (0.3-0.65), fibronectin (0.1-0.3), immunoglobulin A (IgA, 0.1-0.3), α_1-

acid glycoprotein (0.1-0.25), haptoglobin (0.075-0.4), ceruloplasmin (0.07-1.0), and fibrinogen (0.065). The relatively low concentration of protein in CSF compared to blood is due to macromolecular filtration of the blood by the choroid plexus and the blood-brain barrier.

1.1.3 Dynamics of hydrocephalus

CSF dynamics are influenced by CSF production, circulation, and drainage. The production rate of CSF under normal conditions is constant but the average patient with chronic hydrocephalus has a decreased production rate of 0.25 ml/min [15-16]. Normally, CSF circulates throughout the ventricular system, through the foramen of Magendie and the foramina of Luschka, into the SAS. Circulation is essential for nutrient exchange and protection of the structures of the CNS. If drainage is inhibited or CSF cannot be absorbed, brain homeostasis is disturbed. Compensatory mechanisms such as intraparenchymal fluid absorption can cause cellular damage and a cortical inflammatory response which are common pathophysiologies of hydrocephalus [2, 17-18].

1.1.4 Known pathophysiology of hydrocephalus

While the pathophysiology of hydrocephalus is multifactorial and involves a wide variety of brain injury mechanisms [2, 17, 19-20], neuroinflammation plays a major role and results in the activation of inflammatory cells throughout the cerebrum. Dilation of the ventricles (ventriculomegaly) from an impediment to CSF flow causes the brain to

become compressed and distorted. This process undoubtedly creates primary injury resulting in secondary pathophysiologic mechanisms such as inflammation. Stretch, BBB breakdown, cerebral ischemia, and edema lead to hypertrophy and proliferation of microglia and astrocytes within hours of initial insult [2], which accelerates pro-inflammatory cytokine responses and releases neurotoxic mediators [21]. Microglia migrate to sites of brain lesions and sites of physiological stress, but also target astrocytes by producing biochemical mediators/cytokines, such as tumor necrosis factor alpha (TNF-α), interleukin-1(IL-1), and interleukin-6 (IL-6) [22], and secrete other pro-inflammatory cytokines (e.g., monocyte chemotactic protein-1 (MCP-1) and interleukin-1 beta (IL-1β) [23]). Generally, inflammatory reactions occur in the periventricular white matter (especially in the white matter adjacent to the dorsolateral angle of the frontal horns), in subcortical structures and throughout the cortical mantle [2, 17, 24]. That is, hydrocephalus generates activated inflammatory cells. These reactions are prominent in the hydrocephalic brain.

1.2 Hydrocephalus Treatment

In the United States, two of the most common methods to treat hydrocephalus are surgical management by endoscopic third ventriculostomy (ETV), and shunting [25]. An endoscopic third ventriculostomy is a surgical procedure done to create an alternative pathway for CSF outflow from the third ventricle to the SAS. ETVs are successful mainly in treating obstructive hydrocephalus [26] and are usually only appropriate for patients with aqueductal stenosis. This procedure is not recommended for premature

infants or early neonates because these patients usually have an underdeveloped SAS. Following surgery, gliotic scarring of this artificial channel can block flow. It is estimated that up to 75% of ETVs fail within six months of surgery [27]. ETV failure is higher in children less than six months of age than in older patients [28] and is especially common in patients in their first two to four months of life [29]. Unfortunately, these factors cause a high percentage of patients to seek treatment through shunting.

Shunting is the most common treatment for hydrocephalus and can include the implantation of an externalized drain (external ventricular drain), an internalized drain, or insertion of a ventricular catheter and closed shunt reservoir (often termed Ommaya Reservoir). An external ventricular drain (EVD) is placed to temporarily relieve high intracranial pressure. This is an in-patient procedure that is often done in the case that infected or blood saturated CSF must be diverted before a permanent internalized shunt system can be inserted or in the case where high ICP can be alleviated in a short time. An Ommaya Reservoir is inserted in premature infants or infants less than 2000 grams who tend to have an underdeveloped immune system that may not tolerate insertion of an internalized shunt system. It consists of a ventricular catheter and a closed bulbous reservoir that allows the neurosurgeon access to the ventricular space. In order to remove any accumulating CSF from the ventricular system, the Ommaya Reservoir must be intermittently tapped. In most cases of hydrocephalus, however, a patient becomes dependent on a permanent internalized drain (herein referred to as a shunt system) comprised of a proximal and distal polydimethylsiloxane (PDMS, silicone) catheter joined in series by a pressure valve to chronically drain excess CSF out of the ventricles.

Proximal catheters are placed in the ventricular or lumbar system where the distal catheter is inserted into a drainage site (usually the abdominal peritoneum, cardiac atrium, or subcutaneous/subgaleal space as noted in Figure 2). Shunt systems are the primary treatment for hydrocephalus, but residual deficits (listed above) occur often in up to 78% of patients [4]. Most importantly, the failure rate for shunts is one of the highest of all neurosurgical procedures equating to a disproportionately high revision to total cost ratio [30-32]. Shunt revisions due to shunt failure account for 70% of hydrocephalus-related surgeries [33]. The costs to our society can be measured by lives lost following shunt failure, morbidity, lower quality of life for patients and their families, and the annual $1.4-2 billion direct cost of hospital care for pediatric hydrocephalus alone [33-34].

1.3 Current Technologies and Their Limitations

Why do these shunt systems fail? (1) *The complex and variable etiologies of the disorder*: The pathology of hydrocephalus is multifactorial and includes primary (ischemia/hypoxia, compression, BBB breakdown) and secondary (gliosis, cell death, and CSF stagnancy) injury mechanisms that can contribute to shunt failure in a patient-dependent manner. Other patient-dependent variables such as rate of cortical re-expansion can shift catheter orientation and cause obstruction. We are only beginning to understand these complex relationships by studying the pathophysiology of hydrocephalus. (2) *Shunt infection:* After initial shunt placement, CSF infection rates are approximately 11.7% per patient and 7.2% per procedure [35]. The chance of

infection is related to patient health and immune response, surgical technique and site preparation (operating room and patient), and long term care. Latent infections can occur and are treated by shunt externalization, shunt removal/external drainage insertion, and antibiotic treatment [36]. In the United States, infection rates are on the decline but they are still unacceptably high. Clinical trials using antibiotic loaded catheters (Bactiseal®) may or may not advance this field [37-38]. (3) *Shunt design:* The modern shunt catheter is made from silicone, a hydrophobic elastomer. At the ventricular end, the catheter walls have access holes for CSF outflow from the ventricular space into the catheter. Downstream, a pressure valve regulates flow but flow parameters through the shunt system can also change as a result of patient positioning and can result in flow stagnancy for as long as 10 min (Joseph Madsen, personal communication). From the valve to the absorption site, a distal catheter transfers CSF. Because of the synthetic nature of the silicone polymer and the overall design of the system, shunts malfunction. The shunt system was designed in 1955 [39]. Since then, the valve characteristics have been manipulated (including the addition of differential pressure valves, programmable valves, valves that protect against siphoning, and valves that regulate outflow based on CSF production), but adaptations to the catheter's overall design or material properties have been limited [40]. But, shunts still fail, primarily because the focus has not been on preventing the most common type of shunt malfunction directly.

The most common type of shunt malfunction is tissue obstruction [41-43]. In the United States, complications due to tissue obstruction occur in up to 61% of patients [44]; 40% of shunt systems become obstructed after two years and 85% are obstructed

after ten years [45-46]. Obstruction is the major cause of shunt complications in under developed areas as well. In sub-Saharan Africa, 54% of shunts are removed because of obstruction [47]. Obstruction of catheters is multifaceted [42] and can include obstruction via whole tissue choroid plexus, inflammatory cells, connective tissue, red blood cells, platelets, and cell debris.

A tabulated outline of significant findings from studies of malfunctioned shunts (Table 1) exposes profound evidence of inflammatory reactions in or around many obstructed shunt systems. A thorough study on the histopathology of tissue obstructing catheters revealed that 14% of catheter obstructions included acute inflammatory cells, 49% possessed chronic inflammatory cells, 40% contained glial tissue, and 48% having granulomatous cells [48-49]. A study by Gower and his colleagues suggested that the development of CSF eosinophilia (enhancement of the concentration of white blood cells) was correlated to shunt failure [50]. This response is persistent until host cells completely encapsulate the shunt system and is indicative of a foreign body response (FBR) initiated by inflammatory cell adhesion (see section 1.4). The significance of this problem increases because patients with multiple revisions appear to have a greater chance of developing an immune reaction to the shunt system [51]. Since most patients with hydrocephalus receive a shunt, and because most shunts fail repetitively, we would expect the number of patients with an inflammatory derived occlusion to dramatically increase over time.

Although analysis of explanted shunts has revealed the types of cells bound to the catheter, the mechanisms by which cell obstruction occurs is still somewhat speculative.

Cells from CSF, from the parenchyma, and from the blood can infiltrate the local space around the catheter and adhere to and encapsulate the catheter, infiltrate the holes, or infiltrate the holes and occlude the catheter lumen. The CSF of a hydrocephalic patient can be filled with multinucleated cells of the monocyte/macrophage family, glia, ependymal cells, and lymphocytes [52-53]. Because the catheter is bathed in CSF, these cells can bind to the catheter through individual cell-catheter contact. These cells may have a parenchymal or blood-borne origin. Neoplastic cells from the parenchyma may migrate to the CSF to contact the shunt system purposefully (via an inflammatory response to the catheter) or accidentally (through shedding of the ependymal cell lining or periventricular white matter as an effect of high ICP). Blood-borne cells may cross the blood brain barrier (BBB) due to BBB breakdown. As a result of these mechanisms, cells are found scaling the wall of the catheter, attached and activated, invaginating catheter drain holes, and encapsulating the catheter in its entirety.

1.4 The Foreign Body Response to Central Nervous System Implants

1.4.1 Initiation of the foreign body response: exudate/tissue

The foreign body response (FBR) is a series of events that produce a local inflammatory and wound healing response around an implanted medical device, prosthesis, or biomaterial. This reaction sequence can occur in tandem to activation of inflammatory cells by hydrocephalus. The FBR to a shunt system is similar to the FBR seen around most other medical devices [54], but it differs compared to non-CNS implants by cell type (although some cells cross the BBB) and because of the protection

mechanisms of the BBB (despite some BBB malfunctioning through implant insertion [55] and hydrocephalic insult [56]). Currently, it is assumed that the FBR to the shunt system is identical to other CNS implants and is described in this background as such, but direct exposure of the ventricular catheter to high pressure and pulsatile CSF flow rather than direct brain tissue contact may drastically alter the reaction/rate of reaction.

Initiation of the FBR occurs during surgery. Despite attempts to minimize invasive procedures, most surgeries cause injury and trauma at the surgery site. Trauma due to shunt insertion causes infiltration of blood into extracellular space, damage to extracellular matrix components, and an influx of chemokines and phagocytes. These reactions can accelerate blood brain barrier dysfunction around the catheter [57], effectively increasing CSF protein concentration. Following this, a localized nonspecific acute response develops where inflammatory products from the parenchyma infiltrate the CSF [58]. To accelerate the inflammatory response, circulatory proteins like complement proteins promote mast cell degradation to increase vascular permeability and increase local chemotactic substances. The activation of T-lymphocytes from outside the leaky BBB occurs through dendritic cells in the choroid plexus and meninges. Active T-lymphocytes then cross the BBB in order to recognize antibody-antigen complexes as nonself. Phagocytes such as microglia, supraependymal macrophages, astrocytes, and blood-derived neutrophils and monocytes (later activated macrophages) increase proinflammatory cytokines and release reactive oxygen free radicals among others in a cyclic process which continues into a chronic inflammatory response [59]. This persistent response is commonly found surrounding CNS implants [60] and can lead

to the formation of an astrocytic capsule around the implant like those found surrounding the ventricular shunt catheter. Chronic contact with the meninges may further accelerate this inflammatory response [55].

In the treatment of hydrocephalus, the initiation of the FBR causes trauma to cortical tissue and to vasculature already impaired with the neuroinflammatory responses of the hydrocephalic brain. Thus, both the insertion of the ventricular catheter and the secondary responses to hydrocephalus produce cells that are known to obstruct catheters. Combined with concurrent inflammatory signals that are part of the injury mechanisms associated with hydrocephalus, the FBR induces a chronic inflammatory response.

1.4.2 Initiation of the foreign body response: biomaterial

Simultaneous to inflammatory reactions occurring in tissues and in the CSF surrounding the catheter is the reaction that occurs directly at the CSF-shunt catheter interface. Here, opsonization occurs, the process by which the material is covered by any available molecule that might enhance phagocytosis. Opsonins like CSF and tissue fluid proteins, complement, and antigens adsorb to the catheter within seconds of implantation in response to the nature of the surface, specifically via electrostatic interactions, hydrogen bonding, dispersive forces, and the hydrophobic effect. Opsoninization results in surface bound ligands that can provide sites for specific inflammatory cell and antibody attachment in order to initiate the innate and adaptive immune response [61]. Monocytes, microglia, and macrophages bind to the surface in an effort to phagocytose the catheter and by this reaction alone, genes encoding

inflammatory mediators are enhanced [62]. Through alternative activation involving the surrounding active T lymphocytes and macrophage mannose receptor upregulation, macrophages and microglia fuse to become foreign body giant cells. This process lasts the duration of the implant, and in the last stages of implant efficacy, astrocytic end feet and collagen form a sheath around the catheter [54]. The end-stage encapsulation of the shunt system is a reaction similar to the fibrotic scarring around any other medical device [63-65] but varies in rate of action because of the location of the implant. Specific surface modifications have been employed to inhibit the initiation of the foreign body response, as discussed in more detail below.

1.5 What Is the Best Model for Inflammatory Cell Adhesion on Shunts?

Modeling the inflammatory response to shunting without using the human body is quite a challenge. There are several excellent *in vivo* congenital and experimental models of hydrocephalus that can be shunted with down-sized or clinical hardware. Rats can be shunted with down-sized hardware; clinical hardware cannot be used because of size constraints of the rat skull. However, alteration to the dimensions of the hardware can alter binding mechanics as is evident with failure of down scaled vascular grafts [66]. The skull size of felines permits the insertion of clinical hardware and is an excellent *in vivo* model of hydrocephalus [67] but the cost of these large animals restricts their use. Collectively, *in vivo* models have demonstrated that cell death, reactive astrocytosis and microgliosis, errors in neuronal connectivity and transmission, and neurotoxicity via BBB breakdown all occur as part of the multifactorial pathophysiology of hydrocephalus [2,

18, 68]. Because obstruction of the shunt system is a multimodal problem, it is difficult to test problems univariably in any *in vivo* model. *In vitro* modeling is quite controllable in this way. Because the design of this work is driven by specific mechanistic hypotheses, an *in vitro* model was chosen. *In vitro* modeling is capable of narrowing our search parameters for an ideal modification to the shunt device in an inexpensive manner.

There is a need for an *in vitro* system that could measure adhesion of cells on catheter tubing material in a physiological environment because shunt failure is undoubtedly an effect of poor understanding of shunt failure mechanisms. There is a rich literature base on *in vitro* models designed specifically to mimic particular *in vivo* conditions. The most applicable current model is the parallel-plate flow chamber aimed to simulate *in vivo* shear stress effects on bound cells including endothelial and bone. Previous work done with this model has demonstrated that mechanical stresses influence the orientation of bound cells [69]. The parallel-plate flow chamber could be used to measure cell spreading under fluidic conditions seen in hydrocephalus and could be adapted to measure initial cell adhesion by propelling cells through the system as has previously been done with platelets [70]. However, the rectangular dimensions of the flow chamber do not mimic the boundary conditions of a catheter used to treat hydrocephalus which may change flow vector fields [71]. The focus of Chapter 2 is to adapt the parallel-plate flow model to measure initial macrophage and astrocyte adhesion on catheter material while mimicking intra-ventricular conditions and maintaining similar luminal geometry of the catheter tube. Once developed and tested, this model will help

us gain an understanding of how the catheter environment influences adhesion (Chapter 3).

1.6 Modifications to Reduce Inflammatory Cell Binding

When designing a device, an engineer must consider the desired life and location of the implant, processing restrictions, and the implant composition (mechanical properties, bulk chemistry, molecular weight, morphology, geometry, and surface properties such as surface functional groups, charge, roughness, and energy). To design a shunt system used in the treatment of hydrocephalus, these design factors must be considered, but there is little historical evidence to suggest that all of these parameters were explored when the shunt system was first designed. As a consequence, the shunt system has undergone adaptations.

Since the invention of the shunt system, there have been many adaptations to the shunt valve (not discussed), but there have been only a few attempts to combat rates of obstruction; these include removal of the obstruction during surgery (Table 2) and modifying the catheter material or architecture in the laboratory (Table 3). Unfortunately, most of these strategies have failed due to inconsistencies in the technique, injury to the surrounding tissues, or insufficient data collection. For instance, use of electrocautery to clear a catheter that afterward remains implanted is not standard practice because of the potential risk for thermal injury [72]. Here, essential modifications to the catheter material and design are discussed.

1.6.1 Modifications to surface properties to reduce inflammatory cell binding

In 1955, silicone was chosen as the primary shunt material since it is unusually stable at extreme temperatures [39, 73]. In elastomer form, silicone is 95% cross-linked and has a high tensile strength, and high resistance to tear and fatigue flexing. These mechanical properties are optimal for chronic implantation of shunt systems because of the material's allowance to contort its shape depending on the state of the ventricular space without causing additional harm to the fragile nature of the ventricular lining. Silicone is manufactured by condensation copolymerization of dimethyldichlorosilane with water [73] which can permit further polymerization with additives that can enhance radiopacity like barium sulfate [74]. The geometry of present day catheters is created using a cast molding process where tubes are formed with a closed ventricular tip. Holes are subsequently made in the catheter wall using a mechanical punch. Silicone can be sterilized by ethylene oxide, dry heat, or irradiation, has an indefinite shelf life at ambient temperature, and after its initial use in 1955 was considered generally inert, non-degradable, and biocompatible [75-76].

Because silicone fit so many design requirements, it is easy to understand why silicone was first used and why it is still used. Today, silicone polymers have a wide range of applicability including implants made for ophthalmology, plastic/reconstructive surgery, orthopedic surgery, cardiology (blood-contact), and microfluidic devices [77]. However, there is a high demand to tailor the surface chemistry of silicone. Silicone, a hydrophobic polymer (detailed below), can elicit an inappropriate response at some implantation sites because of undesired protein adsorption and cell adhesion [77-79].

Chapters 4 and 5 will focus on the modification of the surface wettability and surface available functional groups of silicone using the developed and tested *in vitro* model of Chapters 2 and 3.

The term surface wettability describes the phenomenon where water is attracted to certain surfaces but is repelled by others. This is likely due to a balance between surface adhesive and cohesive forces. Hydrophobic surfaces can be described as those with less Lewis acid or base functional groups that can interact with water, so they are non-wettable and water fearing. Hydrophilic surfaces, or more wettable and water loving surfaces, can interact with water through water-water hydrogen bonding driven by surface energy. These interactions, in combination with other inter- and intramolecular forces, drive protein adsorption [80-82]. On a hydrophobic surface like silicone, a biological response can be initiated through an entropic drive for the hydrophobic moieties of proteins in solution to bind onto the implant. In most conditions, this response will be stronger on hydrophobic materials inducing more cellular activation and spreading than on hydrophilic materials [83]. For instance, hydrophobic polytetrafluoroethylene used in blood-contact devices has been shown to activate monocytes [84]. However, there is certainly a broad range of literature suggesting that cell attachment is minimal at both hydrophobic and hydrophilic extremes [85]. For example, tissue culture polystyrene, with a more hydrophilic surface composition than nonmodified polystyrene, is well known to support adhesion more than its nonmodified counterpart [86]. Modifying the degree of wetting (wettability) is an extremely useful parameter in guiding biological interaction [87]. Others have suggested that the

relationship between surface wettability and adhesion is dictated not only by alterations in surface properties but also by environmental conditions, charge [58, 88], and roughness [89] in which the material is surrounded [79, 90].

In 1991, a new ventriculo-subdural shunt system was used in a small clinical trial made entirely of poly-2-hydroxyethyl methacrylate (pHEMA), a hydrophilic polymer that often has a gel-like consistency in water [91]. Out of the eight patients who had the new catheter inserted, three patients' intracranial pressure returned to normal without a change in ventricular size and four patients improved but still had signs of progressive hydrocephalus. This study focused on the revival of the abandoned ventriculo-subdural shunt approach and the use of pHEMA was only briefly discussed. In one case, the material caused only a mild tissue reaction and was patent upon removal seven months after insertion. However, histological analysis of the other six removed catheters suggested that a fibrous membrane originating in the subdural space spread and encapsulated the entire device. The reason for this encapsulation was not speculated upon but could be due to either the material (pHEMA) or the atypical use of a ventriculo-subdural shunt. The use of pHEMA and the ongoing success of some hydrogels in inhibiting protein deposition on contact lenses and other materials [92-93] might suggest that pHEMA may have reduced or delayed scarring compared to controls, but we cannot come to this same conclusion here because of the multiple variables in the study. Since cells often bind more efficiently to hydrophobic surfaces [85] and less effectively to soft modulus materials like hydrogels [94-95], pHEMA (with its hydrophilic and gel-like quality) seems to be an excellent candidate material that should be pursued as

modification to current catheter design in future studies. This study underscores the necessity to study how alterations in the material or surface type impact device encapsulation independently.

Another modification to the silicone shunt system was the coating of polyvinyl pyrrolidone (PVP) onto the surface of silicone. PVP is a hydrophilic water-soluble polymer. Applied onto a shunt catheter, PVP was marketed as Bioglide® by Medtronic® and sold as a catheter that would increase lubricity in order to ease insertion [96]. Bioglide was used by many neurosurgeons until it was taken off the market in 2010 because the catheter was so lubricious that it failed to stay attached to the polymeric joints linking the ventricular catheter to the valve. Although Bioglide® is now viewed by many as a failed modification, there is no study to date that describes the longevity of these coatings grafted onto silicone and there is no correlation between the coatings and inflammatory cell adhesion.

Although this study will not compare proposed surface coatings to Bioglide catheters, the scientific rationale behind their ability to reduce macrophage or astrocyte attachment (i.e., hydrophilic surface modification) is similar. Protein adsorption and cell adhesion on photochemically immobilized PVP and polyethylene glycol (PEG) on silicone have been compared in other work which suggested that the PEG surfaces elicit very low pro-inflammatory cytokine secretions from monocytes; the degree of monocyte adhesion between PVP and PEG on silicone was not significantly different [97]. We have chosen two coating types (discussed below, including PEG) that may begin to help us understand the mechanisms behind adhesion under fluidic conditions. Future work

will expand on this need and will explore other material types like Bioglide® that can be correlated to shunt failure rate.

1.6.2 Modifications to drainage architecture to reduce inflammatory cell binding

One of the primary failure sites of current shunt devices is in and surrounding the holes of the ventricular catheter. The ventricular end of the shunt system typically includes 32 500 μm diameter holes oriented in four rows that permit CSF outflow from the ventricular space. Perhaps manipulation of the catheter design can inhibit obstruction. Like surface properties, there is knowledge to be gained from the literature on other medical devices such as studies on porous materials, flow, and shear.

Porous materials, with holes of varying morphology, are commonly found in dialysis equipment, hernia repair, and tissue engineering applications. A comparison of adhesion and infiltration on and through porous materials and ventricular catheters is limited, primarily because of their dissimilar implant environment and the estimated 100 fold difference in hole size. However, we may be able to gain inspiration from previous work on porous materials and apply this knowledge to the architecture of the ventricular catheter. For instance, studies that suggest that the biological response to porous materials is greater when the morphology of the pores is mesh-like compared to when it is composed of cylindrical holes [98-99]. Conceivably a similar correlation should be studied by examining differences between cylindrical holes and mesh-like drainage systems. Other inspired correlations may follow.

Perhaps the degree of inflammatory-derived obstruction is dependent on another component to shunt design: the configuration of the drainage holes. In the porous membrane literature, components of the foreign body reaction are dictated by the pore(hole) size of porous materials [100-101]. On devices under flow, the literature implies that adhesion is dependent on shear stress [102-103]. Shear stress through the holes of ventricular catheters can be manipulated through alterations to the flow impedance through each hole. This can occur by adapting bulk flow (pharmacologically or through manipulation of the diameter of the catheter), by altering the number of drainage holes, or by altering the diameter of the holes. There are no publicly available records indicating why the number of holes, the size of each hole and the distance between holes was chosen when shunts were originally designed. The focus of Chapter 6 is to determine if inflammatory cell adhesion is dependent on the diameter of ventricular catheter drainage holes.

There is clearly an urgent need to inhibit occlusion of catheters used in hydrocephalus. Data suggesting that a high percentage of obstructive lesions contain inflammatory cells together with evidence suggesting that this foreign body response is one of the major contributors to shunt failure inspire us to study these interactions. Currently we do not understand how macrophage and astrocyte binding is impacted by physiological parameters such as flow, pressure, or pulsation frequency, nor do we know how adhesion changes under these conditions as a function of surface chemistry or shear stress. In an effort to understand cell-contact induced obstruction and to find ways in which mediators of occlusion can be inhibited, we develop and test a model that

measures inflammatory cell adhesion under fluidic conditions seen in hydrocephalus. With a team of highly skilled and motivated neurosurgeons, physiologists, and engineers, we can begin to fill these gaps in our knowledge and design a catheter that inhibits inflammatory cell adhesion from occluding catheters.

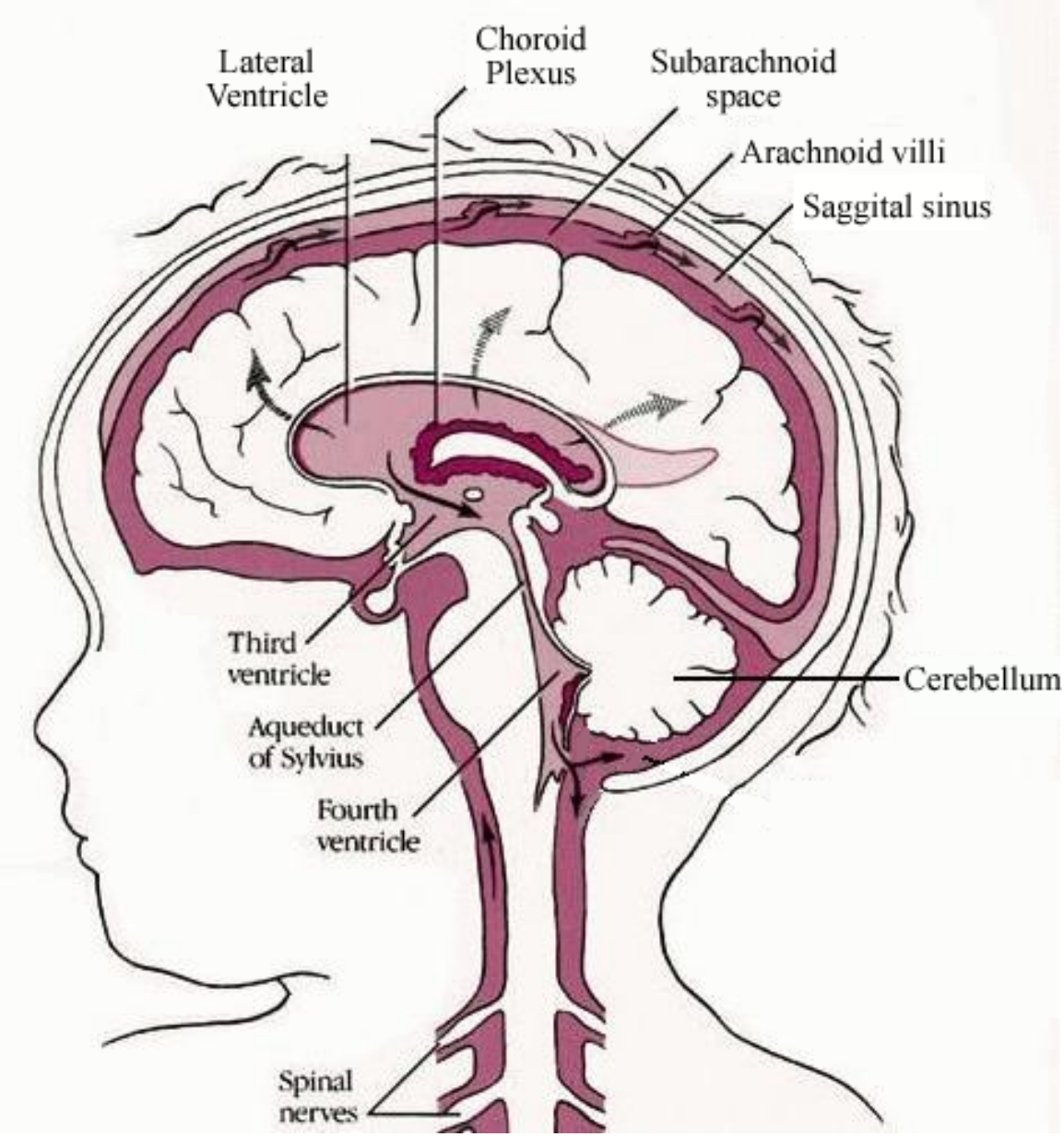

Figure 1 Schematic of CSF flow. Through communication of the lateral, third, and fourth ventricles, cerebrospinal fluid can escape to the subarachnoid space where it can be absorbed through the arachnoid granulations or out to lymphatic sites. Image adapted from the World Chiari Malformation Association [104].

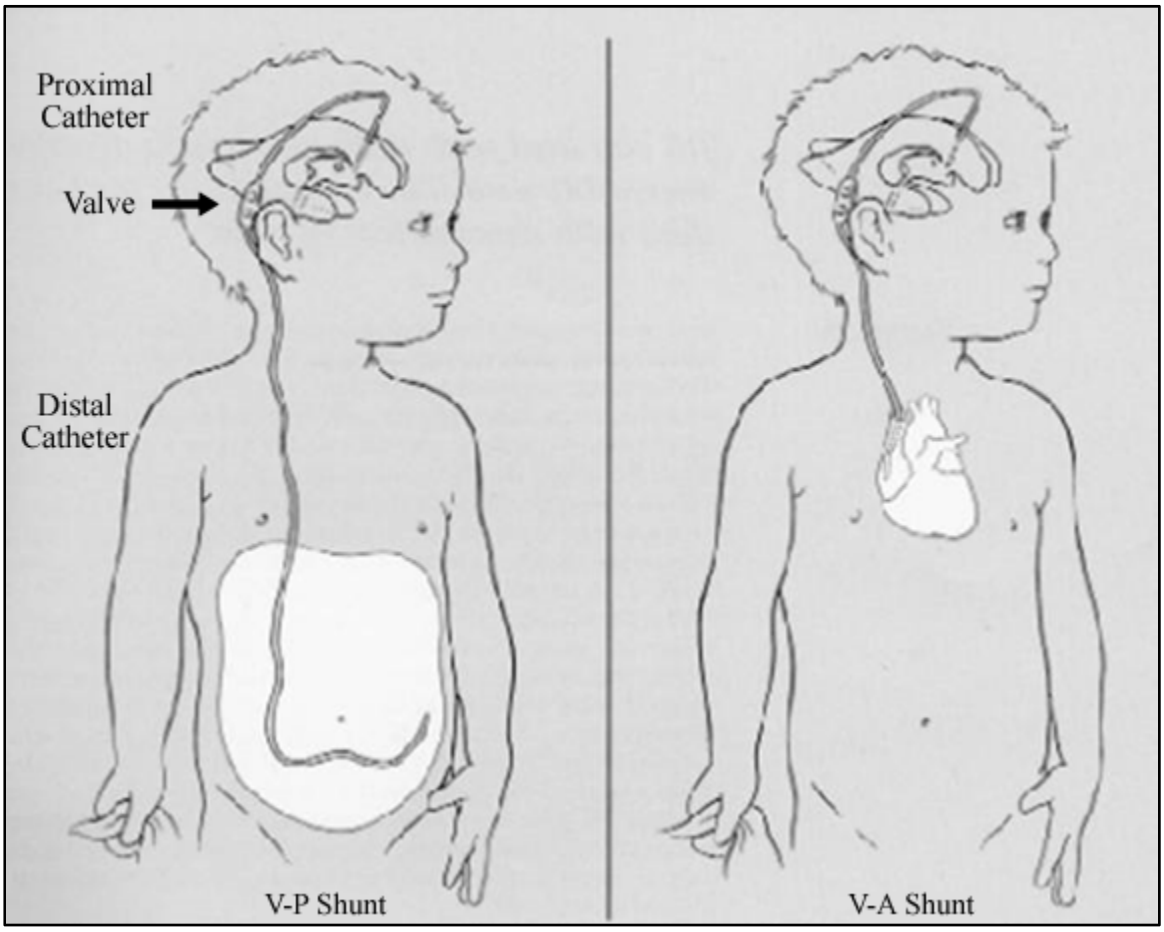

Figure 2 Common types of shunt systems are described as ventriculo-peritoneal (V-P) or ventriculo-atrial since they divert cerebrospinal fluid from the ventricles to either the peritoneal cavity or the cardiac atrium where fluid can be absorbed. Image adapted from the Hydrocephalus Association [105].

Table 1 Significant findings from catheter explants

Year	Author [ref]	Implant Type	Methodology	Scientific Contribution
1981	Go [106]	Malfunctioning ventricular shunts	Histological	Dead cell debris-related obstruction month one; Choroid plexus related obstruction 3-6 months following insertion
1982	Sekhar [49]	Malfunctioning ventricular shunts	Histological	Top five tissue types found: connective, chronic inflammatory, granulomatous, glia, choroid plexus
1984	Gower [107]	Malfunctioning and non-malfunctioning (elective removal) distal shunts	SEM	Malfunctioning and non-malfunctioning both had bound protein layer; Non-malfunctioning: single cells and rare clusters; Malfunctioning: more cells, cell clumps, reactive with foot processes
1985	Bigner [53]	Malfunctioning ventricular shunts	Cytological	Histiocytic giant cells and ependymal cells in cerebrospinal fluid; Choroid plexus in ascitic fluid benign
1986	Del Bigio [108]	Silicone tubing	Histological, TEM, SEM	Silicone chemical factors and mechanical factors (pressure, stretch) may correlate to periventricular reaction and reaction at silicone-tissue interface
1989	Kossovsky [109]	Malfunctioning shunts (patients with repeat failures)	Pathological	Obstructions associated with repeat failures Abundance of eosinophils and evidence of active inflammatory processes
1989	Snow [51]	Malfunctioning shunts (ventricular, valve, abdominal)	Pathological	Patients with three or more revisions (48% of study population): eosinophils and giant cells in tissue enveloping shunt
1991	Schoener [44]	Shunts	Histological, SEM	Foreign body tissue reaction on all explants; Defects caused luminal tissue migration or adherence Migration of choroid plexus or glial cells to 14% inner lumen

Table 1 continued

Year	Author [ref]	Implant Type	Methodology	Scientific Contribution
1991	Tung [52]	Malfunctioning shunts	SEM	CSF eosinophilia is correlated to shunt failure
1992	Koga [110]	Malfunctioning shunts	Histological, SEM	Inner lumen filled with granulomatous connective tissue, reactive glial tissue, and giant cells; reaction may correlate to aged silicone (material breakdown)
1998	Del Bigio [48]	Literature Review	N/A	Mechanically obstructed by mostly vascularized glial tissue and/or choroid plexus; inflammatory cells on over half of samples
2004	Cinalli [111], Clyde [112]	Malfunctioning distal shunts	N/A	Cracks in silicone caused by barium sulfate impregnation (for radiopacity) instigate an inflammatory response
2004	VandeVord [113]	Malfunctioning distal shunts	Molecular Techniques	Enhanced protein deposition resulting in increased immunologic response
2008	Ellis [114]	Malfunctioning shunts	CSF analysis	Unpolymerized silicone may increase failure via persistent eosinophilia and hypersensitivity
2009	Czernicki [115]	Shunts (ventricular, lumbar, peritoneal)	Histological	Focally attached cells (RBC, WBC, platelets, lymphocytes, macrophages, mast cells); cells in fibrin networks (RBC, WBC, mast cells); destroyed cells (RBC)
2010	Thomale [116]	Malfunctioning Shunts	Histological	Obstructive tissue involves glia, connective, and inflammatory cells

Table 2 Surgical device modifications to remove or avoid shunt obstruction

Year	Author [ref]	Model	Method	Time	Significant Findings
1976	Ono [117]	Human	Combined aspiration and modified spinal needle	Postocclusion	80% of patients' catheters patent post procedure that were otherwise occluded
1994	Ventureyra [118]	N/A	Electrocautery within the Catheter Lumen powered by Radiofrequency Current	Postocclusion	Concept proposal only; comments suggest that technical problems may be difficult to overcome
2003	Kehler [26]	Human	Peel away ventricular sheath	Preocclusion	Within one year, 13% less shunts required revision presumably due to less parenchymal intrusion during insertion (insignificant sample size)
1999	Pattisapu [119]	Human	Electrocautery of Catheter Lumen	Postocclusion	85% success rate
2006	Ginsberg [120]	*In vitro* Sheep Choroid Plexus, Human	Ultrasonic Cavitation	Postocclusion	Low frequency ultrasound removed at least 90% of the occluded holes
2010	Camlar [121]	Cadaver	Peel away ventricular sheath	Preocclusion	Significantly less plugged holes following insertion with the peel away covering

Table 3 Modifications to catheter material or design to prevent obstruction

Year	Author [ref]	Species	Implant Type	Target to Inhibit or Regulate	Scientific Contribution
1967	Ames [122]	Human	Polyethylene Shunts	Inflammatory and Whole Tissue	Obstruction occurred within days to weeks
1974, 1976, 2006	Zumstein [123], Haase [124] and Browd [42]	Human	Flanges (Portnoy Catheter)	Choroid Plexus/Whole Tissue	Added flanges to prevent tissue infiltration, Zumstein suggests little success, Haase suggested inhibits choroid plexus obstructions; Browd suggested no decrease in obstruction rate
1982	Nakamura [125]	Human	Floating catheter	Inflammatory and Choroid Plexus/Whole Tissue	Air cell to inhibit obstruction by maintaining a distance between tissue and the catheter tip; functioned well over first 19 months but further analysis suggested the device was unsuccessful
1991	Wong [91]	Canine	Ventriculosubdural pHEMA catheters	Inflammatory and Whole Tissue	38% functioned but subdural design prevented pHEMA specific conclusions
1992	Gower [50]	Rat, Human	Expanded polytetrafluoroethylene (e-PTFE)	Bacteria	Did not prevent bacterial adhesion; e-PTFE occluded rapidly with tissue
2001	Watson [126]	N/A	Polyether sulfone or other porous fiber membrane	Whole Tissue	Patent suggests small holes of porous materials may prevent whole tissue ingrowth but analysis not conducted
2001, 2008	Medtronic® Product, Ellis [114] Report	Human	Extracted silicone (removal of unpolymerized oligomers)	Inflammatory	May work well for patients with immune hypersensitivity to silicone but no formal report to date

Table 3 continued

Year	Author [ref]	Species	Implant Type	Target to Inhibit or Regulate	Scientific Contribution
2004	Medtronic® Product, Cagavi [127], Boelens [128] Report	*In vitro* culture	BioGlide® (polyvinylpyrrolidone grafted)	Bacteria (not marketed as such but tested)	Decreases initial bacterial colonization; May induce abscess formation
1981	Codman® Product, Bayston [37, 129]	*In vitro* culture	Bactiseal®	Bacteria	Effectiveness was dependent on impregnation method, inhibition sufficient for continued work
2003	Medtronic® Product, Lin [130-131]	Benchtop	Rivulet™ (graduated inlet hole diameter, compressed inlet placement)	Flow	Flow through each hole is equalized (standard catheters have minimal flow at tip), effects on obstruction unknown
2005	Medow [132]	Benchtop	Cellulose Acetate Ventricular Catheter	Choroid Plexus	Sufficient flow can be produced from porous materials, may inhibit whole tissue infiltration
2006	Patel [133]	*In vitro* rat culture	Silicone sheets modified with silanes, Heparin, and Hyaluronan	Inflammatory and Whole Tissue	Heparin and Hyaluronan increased astrocyte and choroid plexus cell growth compared to PDMS; silanes reduced astrocyte but not choroid plexus cell growth compared to PDMS
2006	Liang [134]	*In vitro* culture	Cast molded Rifampicin/Silicone	Bacteria	Cast molding decreases burst effect; rifampicin decreases initial bacterial colonization

Table 3 continued

Year	Author [ref]	Species	Implant Type	Target to Inhibit or Regulate	Scientific Contribution
2006, 2008	Lee [135-136]	*In vitro* murine culture	Magnetic microactuators	Inflammatory and Whole Tissue	Microactuators removed an average of 37% adherent cells; cell clearing capability increased dependent on actuation duration and angle of deflection.
2009	Izci [137]	Human	Silver-impregnated polyurethane tubing	Bacteria	CSF cultures were negative after use when initially positive however no conclusions about bacterial adhesion were made
2010	Thomale [116]	Human	Decreased number of drainage holes	Parenchyma	Without decreasing total flow velocity, fewer holes may decrease the risk of tissue infiltration but further study required

CHAPTER 2

DEVELOPMENT AND TESTING OF A NOVEL *IN VITRO* MODEL TO SIMULATE MACROPHAGE AND ASTROCYTE ADHESION ONTO SILICONE CATHETERS USED IN HYDROCEPHALUS

2.1 Introduction

One of the main impediments facing hydrocephalus treatment is the high rate of shunt failure, which is commonly caused by shunt obstruction [42, 44, 138-139]. Cytological analysis of ventricular catheter explants has revealed a definite inflammatory response manifested as layers of microglia/macrophages and astrocytes surrounding catheters, infiltrating the flow input holes, and clogging the lumen [48].

A major obstacle to reducing inflammatory-based shunt obstruction is that current *in vitro* systems, which hold great potential for univariable and hypothesis-driven modeling of cell and tissue adhesion, do not incorporate pertinent physiological parameters. Instead, most models used to test inflammatory cell–derived shunt obstruction consist of static environments that lack the dynamics of CSF flow, pressure, and pulsatility [133]. *In vitro* models that do incorporate flow, like the parallel plate flow model [71], do not mimic the appropriate flow vector fields seen within a catheter under intracranial conditions. These technical barriers impede our understanding of why inflammatory cells block catheters in the cerebral ventricles and slow development of

new strategies to inhibit obstruction. This needs-based study begins to close these technical barriers through the development and testing of an *in vitro* flow system tailored to study shunt obstruction [140] through incorporation of flow, pressure, pulsatility, and protein concentration that mimic intracranial conditions.

2.2 Materials and Methods

2.2.1 Development of the hydrocephalus shunt catheter bioreactor

The Hydrocephalus Shunt Catheter Bioreactor (HSCB) was developed to improve analysis of the interactions between the polydimethylsiloxane (PDMS, silicone) shunt catheter and inflammatory cells *in vitro*. The traditional waterfall model for sequential progress [141], where design, implementation, and verification are based on defining user needs and system requirements, was generally followed. The user needs of this system include the capability to (1) suspend viable adherent cells in a fluid cell carrier; (2) adjust flow rate; (3) adjust pressure; (4) adjust fluid pulsation rate; (5) adjust fluid protein and cell concentration; and (6) remove and analyze a sample region for cell attachment. The system requirements include (1) output of flow, pressure, pulsation rate, and protein concentration in a physiological range (0.25–0.30 mL/min, 70–200 pulses/min, ≤ 25 mmHg, and 20–40 mg/dL total protein, respectively), and (2) minimal loss in cell viability.

Adjustable flow and pulsation rates were achieved using a three-channel peristaltic pump (Watson-Marlow® 401U/DM3, Cornwall, England), Marprene Tubing (thermoplastic polymer with inner diameter 0.2–0.5 mm, 64 Shore, Watson-Marlow), in-

line transport tubing (PDMS with inner diameter 1.5 mm), a removable PDMS sample region (inner diameter 1.5 mm), and low total protein albumin-rich medium (0.5% fetal bovine serum (FBS) with an albumin additive). A schematic is shown in Figure 3. Shear stress, flow rate, and pulsation frequency were calculated using this proposed design (Table 4). After initial development and confirmation that set parameters fell within given deviations, the cell type and cell concentration were chosen, the cell viability on the catheter and in solution (with respect to each system component and with respect to time) were analyzed, the most appropriate technique to measure cell attachment was determined, and the sample type (catheter lumen, catheter holes) was decided.

2.2.2 Measurement of deviances from set parameters

To assure that flow rate, pulse rate, and pressure readings were consistent with the values in which they were set, tolerated deviations were defined such that the system's parameters fell within a particular range: ± 0.05 mL/min (flow), ± 1 pulses/min (pulsatility), and ± 0.5 mmHg (average pressure). Bulk total flow of the fluid cell suspension was measured over time by measuring the total fluid output (mL) after 10 min. Pump manufacturer pulsation rate specifications were confirmed by manually counting the number of times tubing was compressed over 1 min. Pressure was measured using a calibrated digital manometer zeroed at atmospheric pressure. Readings were then confirmed manually using a water column. A sample size of three was used in each verification test.

2.2.3 Choice of cell type: macrophage

Mus musculus IC-21 macrophages derived from SV-40 transformed peritoneal macrophages with phagocytic properties were used primarily because of their mature phenotype [142] and characteristic similarity to supraependymal macrophages found bound to central nervous system (CNS) implants [23, 143-144]. Because macrophages are involved in acute and chronic inflammation (see Introduction: Chapter 1.1.4 and 1.4) it was determined that observing adhesion would aid us in the understanding the inflammatory response to the shunt catheter.

Mus musculus IC-21 macrophages taken from a C57BL/6 mouse were obtained from ATCC (ATCC product number TIB-186). Macrophages were maintained in RPMI-1640 medium with 25 mM 4-(2-hydroxyethyl)-1-piperazineethanesulfonic acid (HEPES), 1% penicillin-streptomycin (Sigma, St. Louis, MO), 1% GlutaMAX (Sigma, St. Louis, MO), 1% sodium pyruvate (Invitrogen, Carlsbad, CA), and 10% fetal bovine serum (FBS, Sigma, St. Louis, MO). Cultures were split at 80% confluence.

Twenty-four hours before cell detachment for experimental analysis, cells were soaked in a low concentration of albumin-rich medium (0.5% FBS with 7.5 mg/mL Bovine Serum Albumin, SeraCare Life Sciences, Milford, MA). After several washing steps with noncationic Dulbecco's Phosphate-Buffered Saline (DPBS, Invitrogen), cultures were exposed to 1X TrypLE Express (Invitrogen) to initiate resuspension. After a 5-min incubation period, cells were removed. To facilitate macrophage removal, flasks were knocked sharply to mechanically dissociate cells from flasks. Subsequently, cells

were added to medium that was centrifuged at 275 x *g* for 10 min before cells were suspended in fresh medium.

2.2.4 Choice of cell type: astrocyte

Adhesion and eventual encapsulation of the catheter is highly dependent on the inflammatory astrocytic reaction (see Introduction: Chapter 1.1.4 and 1.4). Histological evidence suggests that an astrocytic response is prominently found surrounding many chronic implants of the CNS, is known to accompany hydrocephalus [2, 17], and is a major mediator of inflammatory-derived device failure [54, 145-148]. Testing astrocyte adhesion to catheters is imperative as these cells are a main component of encapsulation tissue. A primary cortical astrocyte cell line from *Rattus norvegicus* (Sprague Dawley strain) extracted at embryonic day 20 was chosen for this study because of its cell uniformity.

Astrocytes were separated from other cell types within cortical tissue using a shake-off procedure [149]. Immediately after the dam had been euthanized with carbon dioxide, rat fetuses were extracted for astrocyte cultures at day 20 of gestation. These procedures were approved by the Institutional Animal Care and Use Committee (IACUC) of the University of Utah in accordance with the National Institutes of Health Guide for Care and Use of Laboratory Animals. The meninges of the embryos were removed, and brain tissue was minced and suspended in PBS containing 1 mg/mL DNase with manganese and 1X Trypsin. After a 10-min centrifugation at 275 × *g*, the sample was resuspended, sieved through an 80-μm nylon mesh, and washed with Hank's Balanced

Salt Solution (HBSS). The suspension was seeded and allowed to reach confluency. A shake-off procedure separated adherent astrocytes from other cell types; flow cytometry confirmed the presence of high glial fibrillary acidic protein (GFAP) in the dissociated cells. Rat astrocytes were cultured in RPMI-1640 with 25 mM HEPES, 1% penicillin-streptomycin, 1% GlutaMAX, and 10% FBS. Cultures were split at 80% confluence. Similarly to macrophage detachment, astrocytes used for experimental analysis were removed from culture flasks after a 24-hour exposure to the low protein medium using 1X TrypLE Express.

2.2.5 Confirmation of cell type

To confirm that our cultures of IC-21 mouse macrophages and primary rat astrocytes expressed antigens specific to their respective cell types, cells in culture plates were immunohistochemically stained with 1:500 polyclonal rabbit anti-ionized calcium binding adapter molecule 1 (Iba-1,Wako) and 1:500 polyclonal rabbit anti-GFAP (Dako Cytomation, Glostrup, Denmark), respectively. Cells were treated with secondary goat anti-rabbit IgG biotinylated antibody (1:200, Vector Laboratories, Burlingame, California) for 45 min at room temperature. Avidin-biotin complex (ABC kit, Vector Laboratories) was added to the culture dishes for protein detection for 30 min and washed with 0.1 M PBS before samples were developed with diaminobenzidine (DAB Kit, Vector Laboratories). Astrocytes were also stained with Toluidine blue to stain the cell nuclei. Both cultures were analyzed using an inverted microscope (Carl Zeiss, Germany).

2.2.6 Choice of cell concentration

A concentration of approximately 3.00 $\times 10^6$/65 mL astrocytes or macrophages (46,000 cells/mL) was chosen for these experiments for two reasons: (1) astrocyte adhesion assays on silicone have used this cell concentration with conclusive results [133]; (2) preliminary data from animals with hydrocephalus show nuclear positive cells (some with macrophage and astrocyte positive staining) in the CSF averaging approximately 41,000 cells/mL. This estimate was used to support the cell concentration from the previously noted study [133].

2.2.7 Cell viability with respect to system components

After one cycle (time for all cells to be exposed to the components once) and again three days after exposure (to determine longer-term effects on viability), the total cell count and viability with respect to each system component were analyzed using the Trypan blue exclusion assay. Each group had a minimum sample size of three.

The effect on cell viability attributable to the compressive forces of the pump was tested using two groups: (1) flow facilitated by positive air pressure in a closed system with no pump contact, and (2) flow enabled by positive air pressure and exposure to the pump. The former group compressed tubing that did not contain the cell solution whereas the latter compressed tubing that housed the cell solution.

The effect on cell viability attributable to protein concentration was tested by comparing viability after exposure to cell culture medium with 10% FBS, medium with

0.5% FBS and an albumin additive, and human CSF (a collection of CSF from 18 patients, approved IRB protocol number 00036772 at the University of Utah).

The effect on cell viability attributable to the suspension flask was tested by comparing viability with and without exposure.

The effect on viability due to a decrease in tubing diameter (used to gate flow) was tested using either PDMS or Marprene tubing at the pump site. A known caveat of this approach is that, although the flow rates (and therefore shear) were fixed and equal using both tubing types, the pulsation rate varied from 7 to 100 pulses/min.

The effect on cell viability attributable to the type of transport tubing was tested by comparing viability after exposure to PDMS, PDMS tubing with the addition of surface hydroxyl groups (OH-PDMS), and polystyrene-coated PDMS tubing (PS-OH-PDMS). OH-PDMS was obtained by placing tubing into an oxygen plasma chamber under a pressure of 200 mTorr and a power of 50 W for 2 min. The polystyrene (STYRON® 666D) modification was performed on a subset of OH-PDMS samples by injecting 15% (w/v) polystyrene in toluene into the tubing lumen, distributing the solution using compressed air, and drying the samples overnight at 70ºC to remove residual solvent.

2.2.8 Cell viability and adhesion with respect to time

To determine the effects of reusing the flow system on cell viability (since reincubating the system with cells could potentially enhance the longevity of each experiment), eight 15-µL aliquots of the cell suspension were analyzed at incremental

time periods using the Trypan blue exclusion assay after initial exposure. Following the time period in which the total cell count was exhausted from the fluid suspension (see Results, approximately 20 hours), the system was resupplied with a second identical concentration. Finally, the system was resupplied 24 hours later for a total three-day incubation period. Cell viability data were graphed as the number of viable and dead cells over time and analyzed by integrating the area below the line of best fit for each curve. The number of cells at the beginning and end of each exposure period was also analyzed for significance using statistical methods outlined below.

To determine whether and to what degree cell adhesion had changed because of the additional incubation periods, samples were removed at the end of the three incubations and fixed with 4% (w/v) paraformaldehyde. Samples were cut longitudinally and fluorescently stained for analysis.

2.2.9 Cell viability of cells bound to sample material

Catheter tubing was inserted at the sample site and exposed to either the macrophage or astrocyte solution. Samples were removed from the system, cut longitudinally to expose the tubing lumen, and washed with 1X binding buffer. Samples and any adherent cells were then fluorescently stained with 1:20 FITC-Annexin V in buffer containing 0.1% bovine serum albumin and 0.1% NaN_3, 1:20 0.8 μM/μL ethidium homodimer III in PBS, and 1:20 500 μg/ml Hoechst 33342 in PBS to stain for apoptotic, necrotic, and healthy cells, respectively, as detailed in the PromoKine Apoptotic/Necrotic/Healthy Cell Detection Kit (PromoKine, Heidelberg, Germany).

After a 15-min incubation period at room temperature in the dark, samples were analyzed using an inverted fluorescent microscope (Carl Zeiss, Germany).

2.2.10 Confirmation of cell binding analysis technique

To find an appropriate technique to measure macrophage and astrocyte attachment after exposure to the flow system, fluorescent staining was attempted on longitudinally cut PDMS sample tubing after fixation with 4% (w/v) paraformaldehyde using actin, vinculin, and 4',6-diamidino-2-phenylindole (DAPI) to stain macrophages and GFAP and DAPI to stain astrocytes. A double staining technique of actin and vinculin was chosen to identify macrophage cytoskeletal structure and focal contacts on the catheter surface to obtain a detailed perspective of macrophage morphology and attachment. Samples were exposed to a 1:300 concentration of polyclonal sheep anti-actin (Chemicon, Temecular, CA) in 0.1 M PBS followed by a 1:100 concentration of polyclonal donkey anti-sheep IgG with a cyanine 3 (Cy3) conjugate in 0.1 M PBS labeled actin filaments. A mouse monoclonal anti-vinculin primary antibody (Chemicon) was then used at a 1:300 concentration identified with a 1:100 concentration of fluorescein isothiocyanate **(**FITC)-labeled polyclonal goat anti-mouse immunoglobulin G (IgG) with heavy and light (H+L) chains (Chemicon). GFAP was chosen to label astrocytes because of its repetitive appearance in astrocyte literature and its ability to portray astrocyte morphology (GFAP has been shown to partially control the shape and movement of the astrocyte [150]). A 1:300 concentration of monoclonal mouse anti-GFAP (Chemicon) in 0.1 M PBS was labeled using a 1:100 polyclonal goat anti-mouse

IgG - FITC conjugated secondary antibody (Chemicon). Unless otherwise stated, all samples were incubated for 1 hour in the respective antibodies at 37ºC. All samples were counterstained to identify the cell nuclei using DAPI diluted from 1 mg/mL stock to 1:1000 in 0.1 M PBS for 12 min at room temperature. Confocal imaging was performed using a Zeiss 510 microscope, and spectral epifluorescent images were obtained using a Nikon fluorescent CRI Nuance microscope system. Images were observed using the Zeiss LSM image browser.

Three methods to analyze samples were attempted. First, images were analyzed for the total DAPI surface area with respect to the total sample surface area. This was done by hand-selecting the areas with software aid (Stereo Investigator, MicroBrightField, Williston, VT). A second method involved analysis of the average percentage of blue in digital Red-Green-Blue (dRGB) space using the DAPI intensity of the images. Lastly, adhesion was analyzed by removing cells, cellular debris, and extracellular matrix (ECM) from the PDMS sample tubing and concentrating the cell mixture on a microscope slide using a Shandon Cytospin 3 Cytocentrifuge (Fisher Scientific, Hampton, NH). The quantity of cellular particulate on the slide was then quantified using pixel luminance photometry (Neurolucida, Microbrightfield). A sample size of 12 was used for each analysis technique.

2.2.11 Applicability of model to adhesion on ventricular catheters and through drainage holes

To determine the relevance of our model (testing luminal adhesion) to models where adhesion is measured on commercially available ventricular catheters, we

measured macrophage and astrocyte adhesion on: (1) the lumen of PDMS tubing with a 1.5-mm inner diameter and 3.0-mm outer diameter (inner and outer diameters which fall in the range of many clinical shunt catheter dimensions); (2) on the interior surface (the lumen) of commercially available ventricular catheters; (3) on the exterior surface of commercially available ventricular catheters. Adhesion on the lumen of PDMS tubing (with inner diameter 1.5 mm) was also compared to adhesion on the lumen of PDMS with an inner diameter of 500 μm (the approximate diameter of the holes in clinical catheters). While the latter comparison maintained laminar flow through the tubing lumen, the dramatic variation in luminal diameter permitted a comparison of calculated shear stress.

2.2.12 Statistical analysis

The Anderson-Darling normality test was used if groups were normally distributed and the Bartlett's test was used to examine the degree of homoscedasticity across data sets. Parametric data were compared using either a two-tailed Student's t-test or a one-way analysis of variance (ANOVA). Nonparametric results were compared using the Mann-Whitney U Test and the Kruskal-Wallis H Test with a confidence interval of 0.95 ($\alpha = 0.05$). If the null hypothesis was rejected using a Kruskal-Wallis H Test, an unplanned comparison of mean ranks test was applied using least significance in difference rank.

2.3 Results

2.3.1 Measurement of deviances from set parameters

Verification measurements were performed to confirm that flow rate, pulsation rate, and intraluminal pressure fell within tolerated deviances. The data revealed that flow (± 0.018 mL/min), pulsation rate (± 1 compression/min), and intraluminal pressure (± 0.24 mmHg) all fell within the tolerated deviances of ± 0.05 mL/min, ± 1 pulses/min, and ± 0.5 mmHg, respectively.

2.3.2 Confirmation of cell type

Macrophages were stained positively with Iba-1 and astrocytes were stained positively with GFAP (Figure 4). Adherent to the culture flask and without exposure to flow, both cell types exhibit extended processes.

2.3.3 Cell viability with respect to system components

The compressive forces of the pump did not cause a significant decline in cell viability, although macrophage and astrocyte viability decreased significantly immediately after exposure ($P < 0.01$) and 3 days after exposure ($P < 0.01$) to either system setup.

Protein concentration did not cause a significant decay in macrophage or astrocyte viability except when CSF was used rather than medium (Figure 6, $P < 0.01$ when comparing pre and post conditions). When comparing cell viability before, immediately after, and 3 days after incubation across groups, there was a significant difference in the

number of living macrophages caused by the addition of the suspension flask ($P < 0.01$) but by changes in the protein content ($P = 0.18$). When astrocyte viability was examined, exposure to CSF under flow conditions caused a significant decrease in cell viability compared with static cultures using 10% ($P < 0.05$) and 0.5% ($P < 0.05$) serum, but there was no significant difference in viability when comparing 0.5% serum with the albumin additive and CSF when cells were held in suspension with the suspension flask ($P = 0.95$).

Figure 7 illustrates that contact with the suspension flask caused a significant decline in the number of viable macrophages but not viable astrocytes. PDMS tubing and Marprene tubing (in combination with flow) both caused the number of viable macrophages and astrocytes to decrease significantly ($P < 0.05$), but the difference in viability between these two tubing types was not significant.

Compared with cell viability before contact, contact with PDMS and oxidized PDMS (OH-PDMS) each caused a significant decrease in viable macrophages ($P < 0.01$); PDMS ($P < 0.05$), OH-PDMS ($P < 0.01$), and polystyrene-coated PDMS (PS-OH-PDMS, $P < 0.01$) each caused a significant decrease in viable astrocytes (Figure 8). The difference in macrophage viability after exposure to PDMS, OH-PDMS, or PS-OH-PDMS was insignificant. Astrocyte viability was significantly greater when in contact with OH-PDMS than with PS-OH-PDMS ($P < 0.05$). Three days after exposure to PDMS, the number of viable cells was greater than after exposure to OH-PDMS ($P < 0.01$) or PS-OH-PDMS ($P < 0.01$).

2.3.4 Cell viability with respect to time

Based on the number of living cells in suspension, nearly 100% of 3.00×10^6 macrophages and astrocytes either bound to catheter tubing or were converted into cellular debris after approximately 20 hours of exposure to the HSCB (Figure 3). However, while the number of living macrophages and astrocytes in suspension decreased over time during the first 20 hours, the number of dead cells in suspension before exposure to the system (1411.25 macrophages/mL ± 219.63; 3148.90 ± 867.03 astrocytes/mL) was not statistically different from the number of dead cells after the 20-hour exposure (6788.46 ± 1630.95 macrophages/mL, $P = 0.06$; 3910.26 ± 1488.25 astrocytes/mL, $P = 0.77$).

The number of living macrophages and astrocytes in suspension decreased over time (Figure 9, Table 5); this phenomenon occurred at a quicker rate with each subsequent incubation such that the area under the curve for the first incubation was significantly greater ($P < 0.05$) than for the second and third incubations. The number of dead macrophages in suspension increased significantly in the second ($P < 0.05$) and third ($P < 0.01$) macrophage incubation compared with the first incubation. The number of dead astrocytes in suspension was not significantly different throughout each incubation, although qualitative analysis suggested that the number of dead astrocytes in suspension in the second and third incubations appeared to increase over the first few hours and then gradually decrease.

After analysis of viability of cells in solution, the degree of cell attachment was analyzed (Figure 10). At the end of the three consecutive incubations, there was no

significant difference in macrophage ($P = 0.17$) or astrocyte ($P = 0.26$) attachment compared with the degree of adhesion present after one incubation period.

2.3.5 Cell viability of cells bound to sample material

As seen in Figure 11, there is little to no evidence of apoptotic cells. A majority of the cells appear to be necrotic with a presence of some healthy cells.

2.3.6 Confirmation of cell binding analysis technique

Fluorescent staining and subsequent confocal imaging and cell removal were performed to determine an appropriate analysis technique. Each of the three techniques was completed and data were attained successfully (Table 6).

2.3.7 Applicability of model to adhesion on ventricular catheters and through drainage holes

There was no statistically significant difference in macrophage adhesion on the wall of the tubing lumen, on the wall of tubing lumen with a diameter equal to the diameter of the holes, or around the holes of the clinical catheter analyzed from the perspective of the lumen or the catheter exterior (Figure 12). Astrocyte adhesion results followed the same pattern: There were no statistically significant differences in groups except for a difference between adhesion on PDMS with the large (1.5-mm) and small (500-μm) inner diameters ($P < 0.05$). Qualitative image analysis of the clinical catheters suggested that macrophages and astrocytes accumulated around the drainage holes but not on the hole walls.

2.4 Discussion

2.4.1 Development of the hydrocephalus shunt catheter bioreactor

In this work, our *in vitro* flow system, the Hydrocephalus Shunt Catheter Bioreactor (HSCB), was developed and tested. The model was designed to expand current *in vitro* models to improve our understanding of macrophage and astrocyte adhesion on catheters by mimicking intracranial flow, pressure, and pulsation rate. After initial development, the cell type and cell concentration were chosen, cell viability was analyzed, the most appropriate technique to measure cell attachment was determined, and the sample configuration (catheter lumen, catheter holes) was decided.

2.4.2 System components

To model CSF flow without force from the vascular system at a physiologic rate, a pump must be used. A direct lift, displacement, velocity, buoyancy, or gravity pump could be used to attain such flow, but a peristaltic pump was chosen in order to simultaneously attain pulsation. A peristaltic pump mimics the fluid displacement demonstrated by many biological systems, such as the gastrointestinal tract, by displacing fluid using a rotor with attached rollers. A tube surrounding these rollers becomes compressed between the rollers and a stationary exterior surface to push the fluid forward. Data suggest that the use of a peristaltic pump that induces compressive forces does not (by itself) decrease cell viability. We can speculate that the decrease in viable cells (Figure 7) is due to interactions with tubing and high intraluminal pressure.

In the proposed model, we use a low-serum medium (0.5% serum plus an albumin additive) to mimic the total protein and albumin concentration of CSF. Low-serum medium did not cause a significant difference in the number of viable cells compared with CSF or high-serum (10%) medium. Speculatively, since a significant decrease in living macrophages and astrocytes was seen after exposure to CSF but not after exposure to the media solutions, a reduction in viability could have been due to factors other than protein concentration, including variations in amino acid concentration, glucose concentration, or added HEPES in the medium. Together, this information leads to the conclusion that medium with 0.5% serum plus the albumin additive may be used in subsequent experiments.

To keep cells in suspension, a standard 250-mL suspension flask (Kontes Cytostir, Kimble Chase, Vineland, NJ) was used. The suspension flask is made of borosilicate glass and is designed with a curved bottom to minimize cell adherence. Use of the suspension flask caused a significant decline in the number of viable macrophages but not in the number of astrocytes. A second suspension flask with a slightly different design (Wheaton Celstir, Braintree, MA) was used in a subset of experiments (data not shown), but results were similar, suggesting that the type of suspension flask does not alter viability. The use of a falcon tube was also attempted, but cells did not remain in suspension. Therefore, it was concluded that a standard suspension flask was required and that the decrease of the total number of viable cells should be noted but is unavoidable.

As was discussed, small-diameter tubing (0.2–0.5 mm) at the site of the pump was required to achieve simultaneous flow and pulsation rates in a physiological range. Marprene tubing was chosen because of its high durometer and known resistance to repetitive compressions [151]. The addition of Marprene tubing into the system did not significantly alter the number of viable macrophages and astrocytes compared with when PDMS tubing was used at the site of the pump. To maintain a similar bulk flow rate in both conditions, the pulsation rate varied from 100 pulses per min with Marprene tubing to 7 pulses per min without the tubing. Changes in viability could have been a result of this varying pulsation rate or could have occurred because of a difference in surface chemistry. Variability in shear could have caused a change in the number of viable cells in suspension. However, none of these factors resulted in a significant difference in macrophage or astrocyte viability in the proposed model. Importantly, the diameter of the Marprene tubing is similar to the diameter of the cerebral aqueduct in children [6]. Therefore, any cellular response attributable to the decreased diameter may be physiological when comparing the system with shunt systems implanted in the fourth ventricle. Together, this information leads to the conclusion that Marprene tubing may be used in subsequent experiments.

PDMS tubing was the originally proposed transport tubing, but to understand how the viability and total cell count change depending on surface composition, two modifications replaced PDMS in a subset of experiments: (1) an anti-adhesive PDMS surface modification (the addition of surface hydroxyl groups) to inhibit cell attachment; and (2) polystyrene (PS)-coated PDMS to enhance adhesion (previous work has shown

that the quantity of bound cells on PS is greater than that on PDMS [133]). A limitation to this study is that more surfaces were not tested. Results indicated that there was no significant difference in cell viability after exposure to PDMS, OH-PDMS, or PS-OH-PDMS, but 3 days after exposure to OH-PDMS macrophage viability was near zero and astrocyte viability after exposure to OH-PDMS or PS-OH-PDMS was near zero. Consequently, there is no clear advantage to using OH-PDMS or PS-OH-PDMS, but there are disadvantages, including potential protein activation by OH-PDMS surfaces [85] and changes in proinflammatory cytokine release on polystyrene surfaces [23, 65, 142]. PDMS transport tubing may still elicit a response, but may be preferred over OH- or PS-modified PDMS to minimize undesired changes in cellular response that do not occur *in vivo*.

2.4.3 Exposure period

We can predict that the loss of viable macrophages and astrocytes over time was due to adhesion to the tubing walls, flow-induced shear stress, and the potential for phagocytosis to mediate the conversion of living cells to cellular debris that is not counted as dead cells. To start with the chosen concentration of 46,000 cells/mL, an approximate 20-hour exposure period should be used for future studies using this model.

Analysis of adhesion after one incubation (20 hours) and after three consecutive incubations (20 hours + 24 hours + 24 hours) indicated there was no significant increase in adhesion with increased time or cell count. This may suggest that the maximum degree of adhesion was reached within the first 20 hours when surfaces were not

saturated with cells. These data are similar to data from other reports that suggest that cell adhesion onto polymers occurs over a short time when the materials are not yet cell saturated [90, 152-153]. This suggests that a 20-hour exposure period is most likely adequate. *In vivo*, however, PDMS catheters are introduced to multiple cell types at different time-points throughout the life of the implant, indicating that a 20-hour period *in vivo* might not necessarily be adequate. Future work should investigate these relationships.

2.4.4 Viability of bound cells

After a 20-hour exposure period, a majority of bound cells were necrotic, a minority of cells were healthy, and none of the cells were apoptotic. If we assume that the presence of the necrotic cells is not an artifact of the methodology, we question how the cells became necrotic. From data collected in this study we know that the number of dead cells in solution did not significantly increase over the first 20-hour incubation period. This would imply that the cell necrosis observed on the sample was likely not a result of cells in solution binding after death. Perhaps these cells became necrotic after they had bound to the PDMS sample. Although PDMS is not cytotoxic in the presence of protein and does not leach toxins [154], the low protein concentrations or the flow conditions at the fluid–material interface may not be conducive to viability binding. Clinically, the presence of necrotic debris in tissue occluding catheters is not uncommon [48-49, 107, 115].

2.4.5 Measuring intensity for analysis

Three data acquisition and analysis methods were compared. Determining the quantity of attached cells by measurement of DAPI intensity surpasses manually counting cell nuclei because of the potential for merged or overlapping cells, its wide acceptance in academic research [144, 155-156], and its capability to reduce human error and potential bias of manual counting despite double blinding. Using threshold values to count the nuclei area is a potential analysis method was but not tested here. Analysis by removing cells, cellular debris, and ECM from the PDMS sample tubing and concentrating the cell particulate on a slide for photometric analysis is sound in theory but could introduce error if all the cells are not completely removed from the sample. Photometric analysis is not very sensitive but can provide additional information on the cell debris and matrix that cannot be visualized with fluorescent staining. As seen in Table 6 the three methods were all successful. Because of these factors, measurement of adherent macrophages and astrocytes using DAPI intensity serves as the primary method of analysis.

2.4.6 Applicability of model to adhesion on ventricular catheters and through drainage holes

An insignificant difference in adhesion on the lumen of PDMS tubing (presumably where flow is laminar) and adhesion on commercially available ventricular catheters (where flow eddies could occur because of the catheter geometry) suggests that flow turbulence may not be a noteworthy factor in adhesion under in this system. The significant difference between adhesion through tubing with a small (with 0.2409 N/m^2

shear stress) and large (with 0.0089 N/m^2 shear stress) diameter suggests that perhaps adhesion is dependent more on changes in shear stress than possible flow turbulence around the catheter. This information leads to the conclusion that PDMS tubing with a diameter similar to that of clinical catheters can be used in this system to mimic adhesion on the inner surface of commercially available catheters but should not be interpreted as occlusion through the holes of the clinical catheters because of a potential dependence on shear stress. One aspect of Chapter 3 will focus on the effects of shear stress by modifying flow rate. Additionally, the flow system will be expanded in Chapter 6 to include analysis on commercially available hardware to determine how changes in the diameter of the holes (and presumably shear stress through the holes) impacts adhesion.

2.5 Conclusions

To minimize changes in macrophage and astrocyte viability, components of the flow system for future experiments may include a suspension flask, a low protein medium solution, a peristaltic pump, PDMS transport tubing, Marprene tubing at the site of the pump, a sample site, and macrophages/ astrocytes. Running the system for more than 20 hours appeared to have no significant impact on the degree of macrophage or astrocyte attachment. Adherent cells are primarily necrotic when bound to PDMS samples but we can speculate that this was caused after initial attachment and was not caused by inappropriate modeling. There was no statistically significant difference in macrophage adhesion on the wall of the tubing lumen, on the wall of tubing lumen with a diameter equal to the diameter of the holes, or around the holes of the clinical catheter.

Although the system is not without limitations, the Hydrocephalus Shunt Catheter Bioreactor can be used to begin to understand inflammatory cell adhesion on catheter material used to treat hydrocephalus. The field is long overdue for an incremental advancement that permits continued progress that may improve our knowledge of shunt obstruction. A provisional patent was recently filed [157].

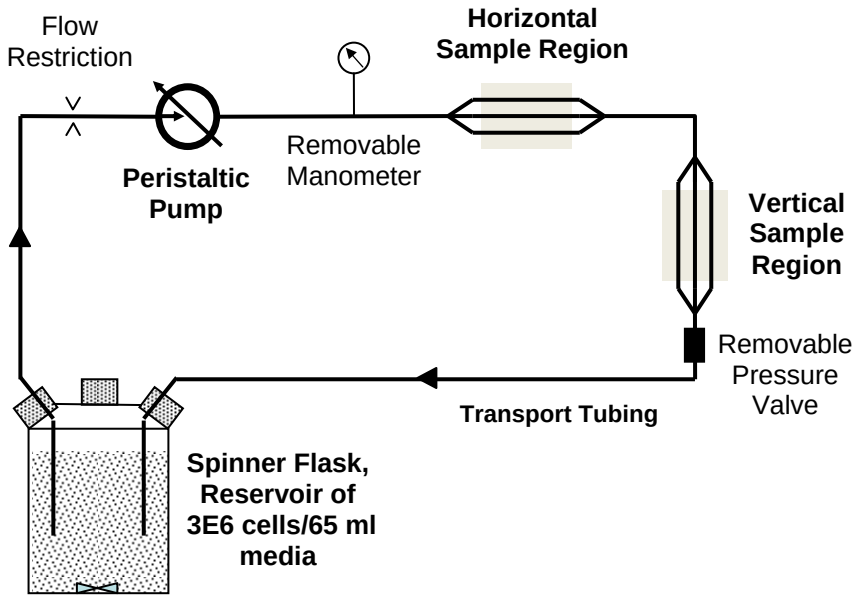

Figure 3 Diagram of the novel Hydrocephalus Shunt Catheter Bioreactor (HSCB). A peristaltic pump was used to propel a cellular suspension from the reservoir (denoted "Spinner Flask") through PDMS transport tubing (solid black line), through the point of flow restriction (referring to the variable diameter of Marprene tubing used to alter flow and pulsation rate), through PDMS samples (either horizontally or vertically placed), and back to the cellular solution reservoir. In this way, samples were exposed to pulsatile flow. Three parallel channels were used to decrease experimental error.

Table 4 Tubing dimensions and calculated shear stress

Marprene Inner Diameter (mm)	Marprene Shear Stress (N/m^2)	PDMS Inner Diameter (mm)	PDMS Shear Stress (N/m^2)	Outputted Bulk Volumetric Flow Rate (mL/min)	Outputted Pulsation Frequency (pulses/min)
0.5	0.0301	1.5	0.0011	0.25	70
0.38	0.0686	1.5	0.0011	0.25	100
0.25	0.2409	1.5	0.0011	0.25	200
0.38	0.0823	1.5	0.0013	0.3	120
0.25	0.2891	1.5	0.0013	0.3	280

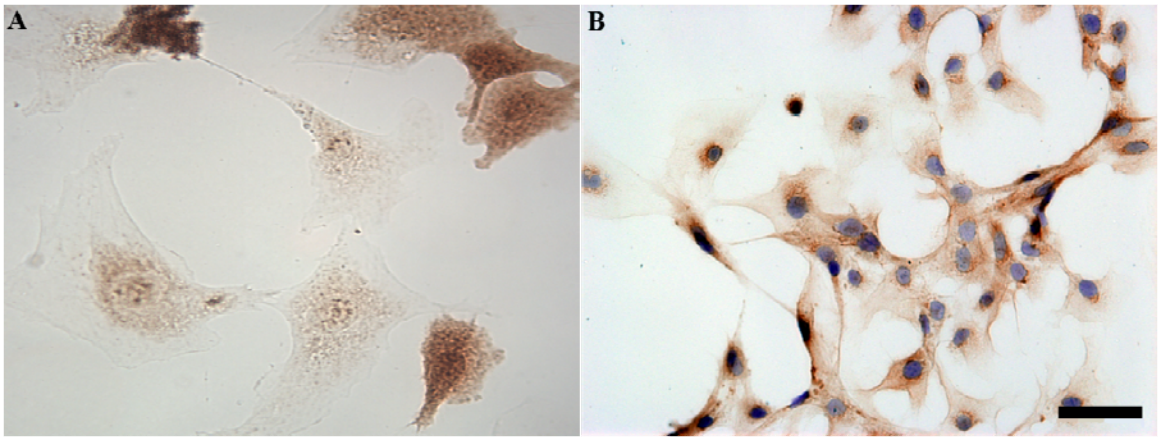

Figure 4 Representative illustrations of adherent living macrophages stained with Iba-1 (A), and astrocytes stained positively with GFAP and Toluidine blue (B) to confirm cell type. Adherent to the culture flask and without exposure to flow, both cell types exhibit extended processes. Scale bar denotes 20 μm.

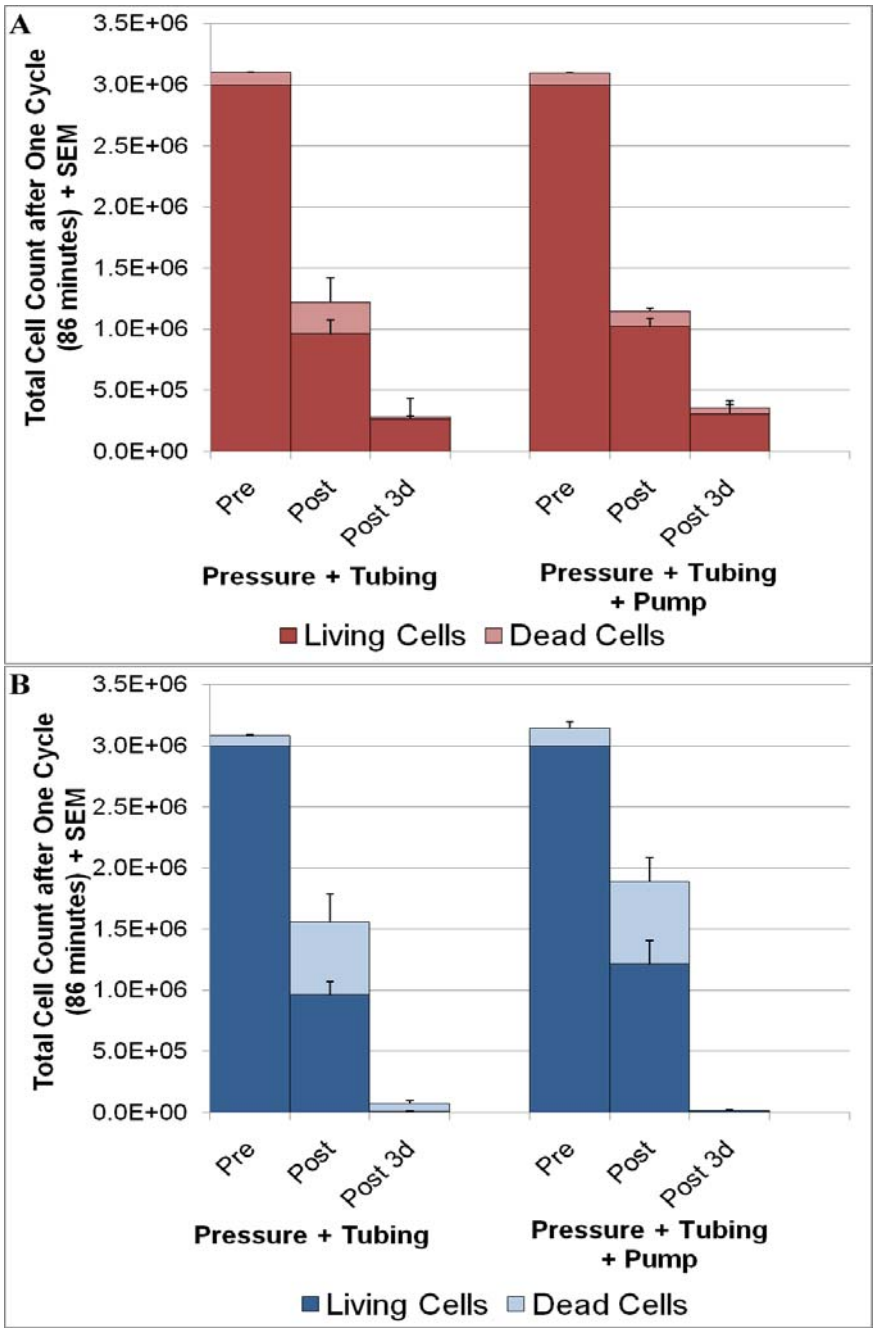

Figure 5 Macrophage (A) and astrocyte (B) count in suspension after exposure to flow conditions with and without the use of the peristaltic pump. The compressive forces of the pump did not cause a significant decline in cell viability. All statistically significant differences were determined using a one-way ANOVA as outlined in the text.

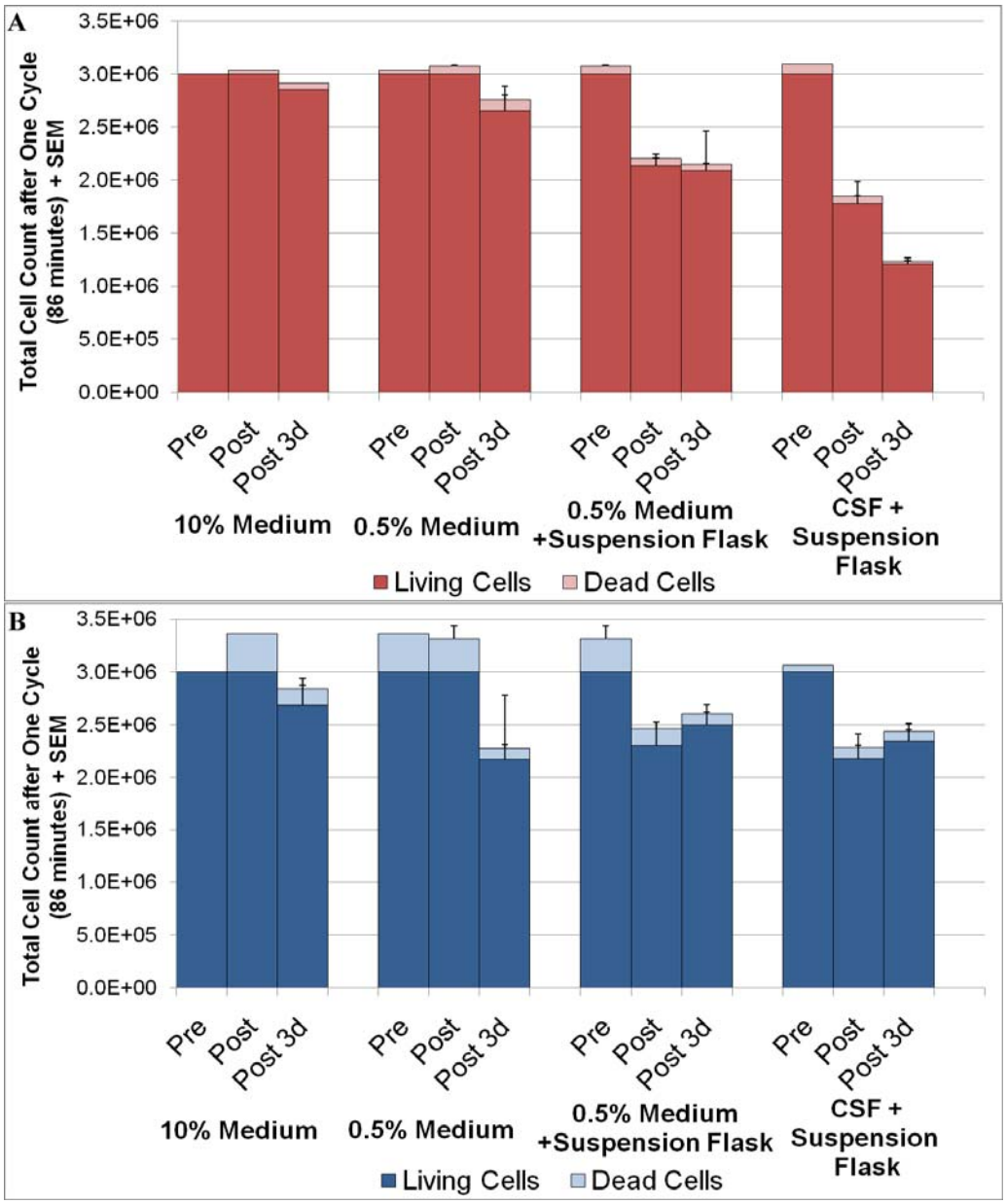

Figure 6 Macrophage (A) and astrocyte (B) count in suspension after exposure to varying protein concentrations. Of particular interest among the results shown is the insignificant difference between 10% medium and 0.5% medium or between 0.5% medium and CSF while using the suspension flask. All statistically significant differences were determined using a one-way ANOVA as outlined in the text.

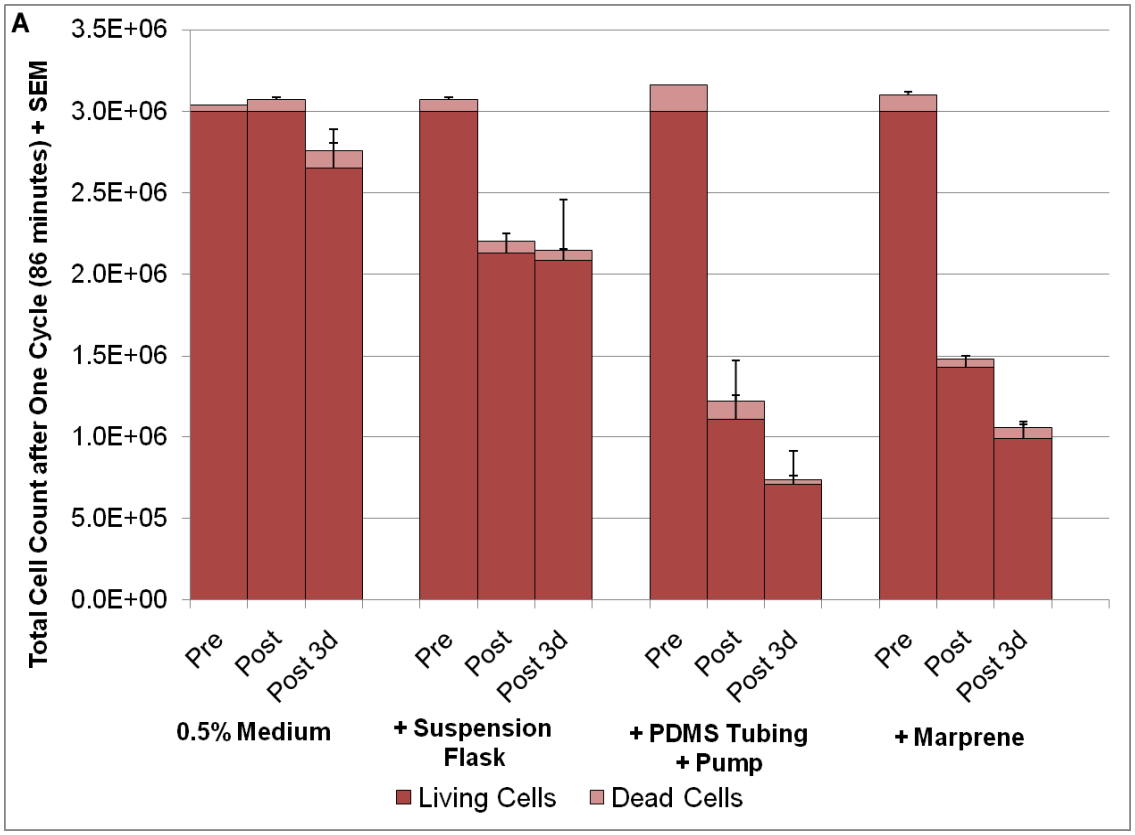

Figure 7 The effect of flow system components on macrophage (A) and astrocyte (B) count in suspension. Here, "+" denotes that a component has been added to the preceding condition. Contact with the suspension flask caused a significant decline in viable macrophages but not viable astrocytes. PDMS tubing and Marprene tubing (in combination with flow) both caused the number of viable macrophages and astrocytes to decrease significantly, but the difference in viability between these two tubing types was not significant. All statistically significant differences were determined using a one-way ANOVA as outlined in the text. Figure continued on the next page.

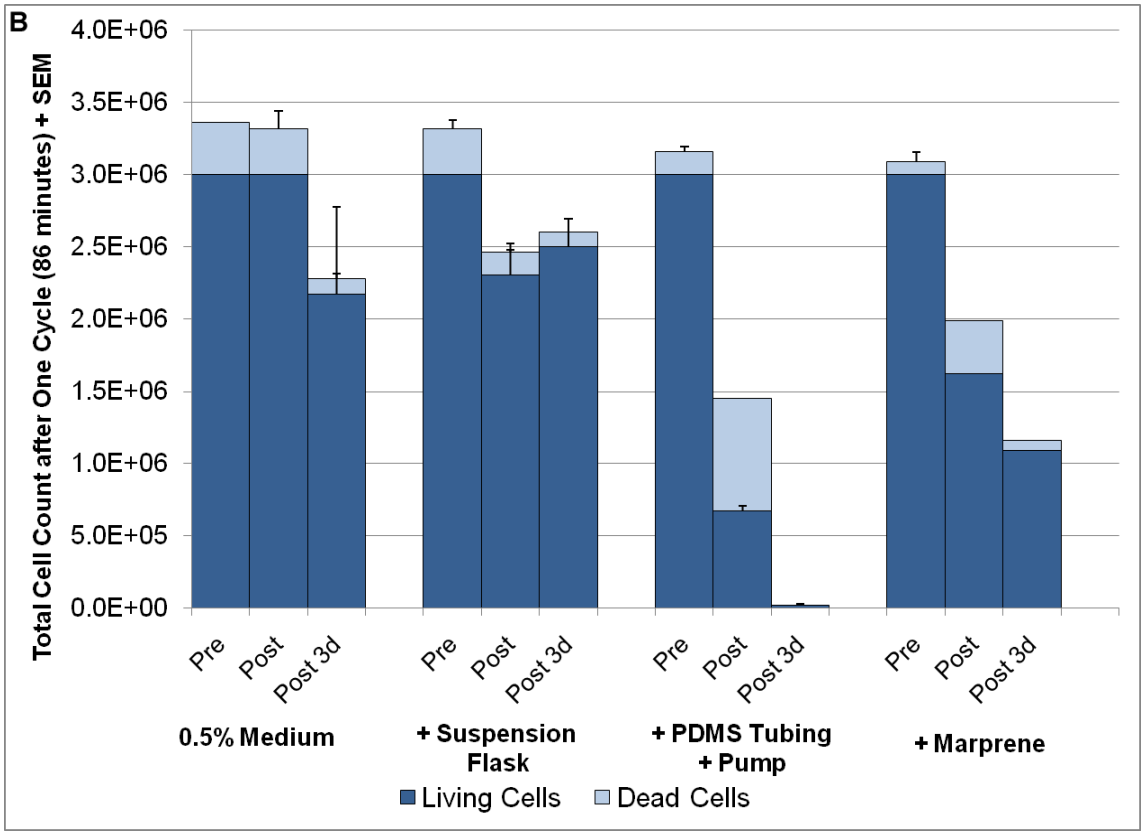

Figure 7 continued

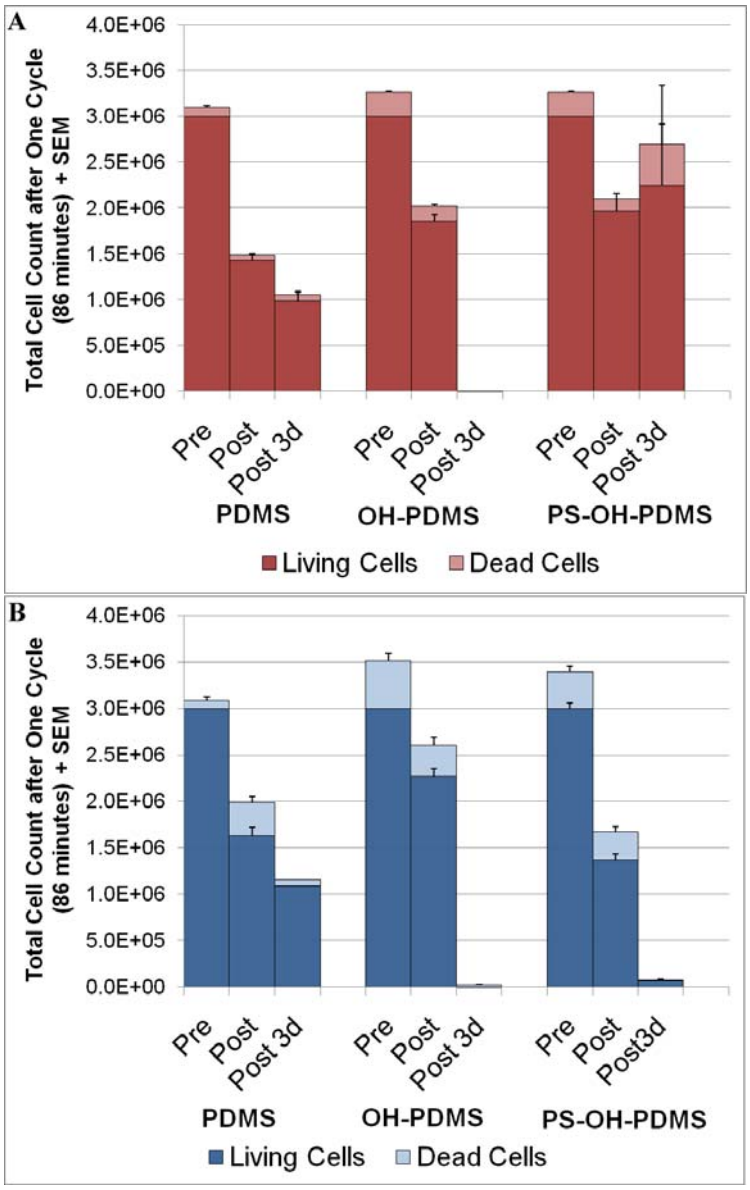

Figure 8 Macrophage (A) and astrocyte (B) count in suspension after exposure to varying surface chemistries of transport tubing. The data suggest that there is no significant difference in cell count with the use of PDMS, OH-PDMS, or PS-OH-PDMS transport tubing immediately after exposure. All statistically significant differences were determined using a one-way ANOVA as outlined in the text.

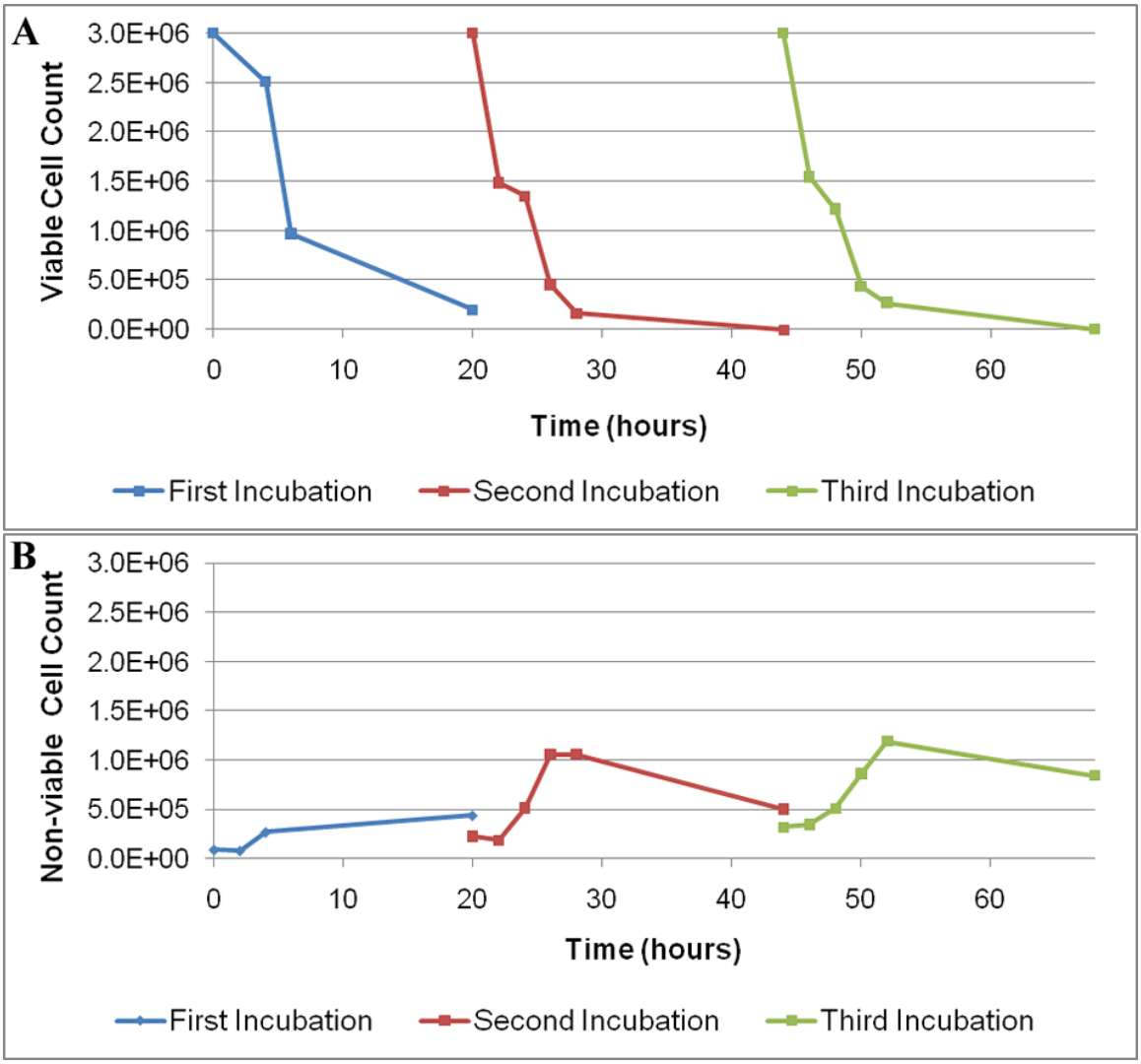

Figure 9 Living (A) and dead (B) macrophage and living (C) and dead (D) astrocyte concentration over time. Generally, the number of living cells in solution decreased over time, but the number of dead cells did not proportionally increase over time. All statistically significant differences were determined using a one-way ANOVA as outlined in the text. Figure continued on the next page.

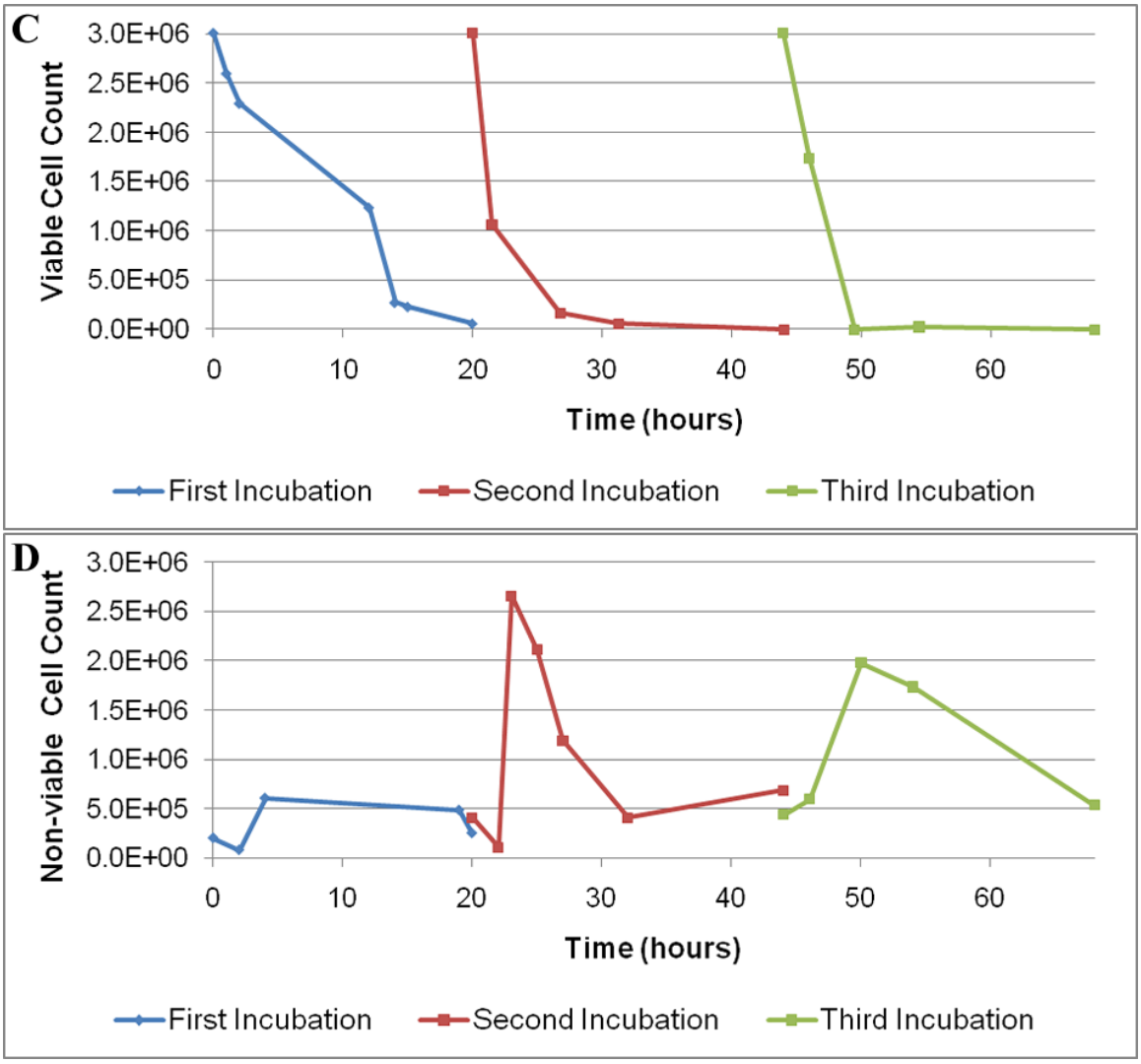

Figure 9 continued

Table 5 Average living cell count in solution with respect to time (± SEM)

	First Incubation (0-20 hours)	**Second Incubation (20-44 hours)**	**Third Incubation (44-68 hours)**
Astrocyte	20,368,180 ± 6,985,370	5,763,396 ± 937,508	7,588,020 ± 1,059,452
Macrophage	20,074,310 ± 3,848,177	10,790,979 ±1,029,678	12,106,250 ±880,545

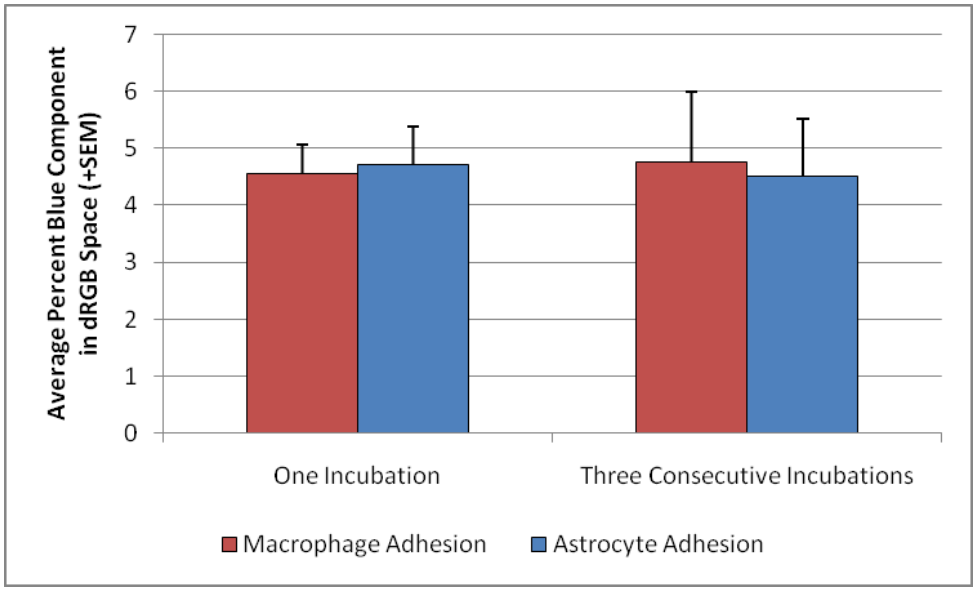

Figure 10 The degree of macrophage and astrocyte adhesion was analyzed after one or three consecutive incubations, and no significant difference was found between groups using a Kruskal Wallis H Test.

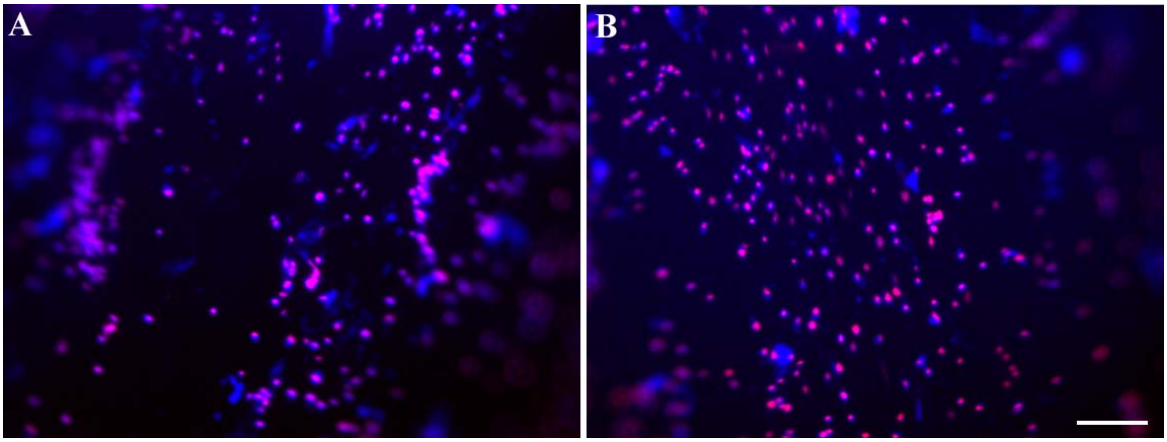

Figure 11 Bound macrophages (A) and astrocytes (B) on PDMS samples stained for apoptotic cells (green co-localized with blue), necrotic cells (red co-localized with blue), and healthy cells (blue alone) using the PromoKine Apoptotic/Necrotic/Healthy Cell Detection Kit. While a majority of cells appear to be necrotic, there are some healthy cells and no apoptotic cells. Images acquired using a 10X objective. The scale bar denotes 100 μm.

Table 6 Quantitative values for each analysis technique

	DAPI Area (Average Percent Area Occupied) ± SEM	**DAPI Intensity (Average Percent Blue Component in dRGB Space) ± SEM**	**Luminance of Concentrated Debris (Pixel Luminance) ± SEM**
Macrophage	1.31 ± 0.33	4.55 ± 0.54	171.70 ± 0.36
Astrocyte	1.86 ± 0.26	4.71 ± 0.69	173.50 ± 2.61

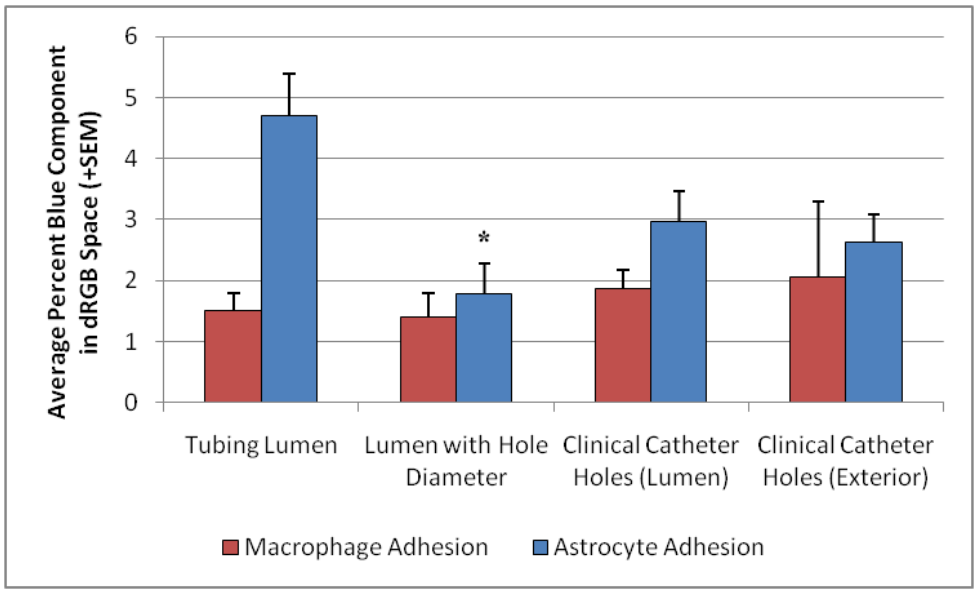

Figure 12 Degree of macrophage and astrocyte adhesion as determined by the average percent blue component in dRGB space (fluorescently stained nuclei). While there is no significant difference in macrophage adhesion across groups, there is a significant difference in astrocyte adhesion when comparing adhesion on the tubing lumen (larger inner diameter, approximately 1.5 mm) and adhesion on the tubing with inner diameter equal to the diameter of a clinical catheter hole (500 μm); significance denoted with an asterisk (*) and determined using a Kruskal-Wallis H Test.

CHAPTER 3

MECHANICAL CONTRIBUTIONS TO MACROPHAGE AND ASTROCYTE ADHESION USING A NOVEL *IN VITRO* MODEL OF CATHETER OBSTRUCTION[1]

3.1 Introduction

Hydrocephalus is a neurological disorder that results from an imbalance between formation and absorption of cerebrospinal fluid (CSF). It is often associated with increased and pathological intracranial pressure (ICP), which usually causes expansion of the cerebral ventricles. Treatment for this chronic disorder must be individualized because variations exist in CSF flow rate, pulsation frequencies, and ICP. However, over the last 50 years there has been little modification of the standard treatment, which involves implanting a silicone catheter into the lateral ventricle to drain CSF [158]. Although this type of treatment is usually effective in draining (shunting) excess CSF temporarily, surgical revisions are often necessary. The results of one retrospective study indicated that 85% of shunts malfunction within 10 years of implantation [45]. Another study reported that the incidence of shunt failure was about 40% after one year and 50%

---

[1] Reprinted from Experimental Neurology with minor additions and revisions, 222(2), Harris, CA; Resau, JH; Hudson, EA; West, RA; Moon, C; McAllister JP "Mechanical contributions to astrocyte adhesion using a novel *in vitro* model of catheter obstruction," 204-10, Copyright (2010), with permission from Elsevier.

by the second year after insertion [42]. Indeed, tissue obstruction of the ventricular catheter is one of the most common causes of shunt failure [41-43, 49].
The most abundant cell types and tissues found attached to shunt catheters are choroid plexus, ependyma, and glial cells [49], which likely bind in part due to the chronic/foreign body inflammatory response [50, 107, 159].

While the cell types found to obstruct catheters are known, the causes for adhesion and eventual obstruction are still somewhat speculative and are probably at least partially dependent on changes to intraventricular conditions such as changes in flow rate, pressure, and pulsation frequency. Normal CSF flow is approximately 0.3 mL/min [11] but decreases as a compensatory reaction to hydrocephalus to approximately 0.25 mL/min [15]. Previous studies have suggested that changing the overall flow rate can change cellular function [160] and cell tethering rate [102], so we hypothesized that a change in flow rate would change the quantity of bound cells. The pressure within the ventricles and the pressure within the catheter change frequently and in most patients as a consequence of the disorder, but studies have indicated that pressure may alter the expression of specific integrins that impact receptor-ligand cell adhesion [161]. We hypothesized that an increase in pressure would decrease adhesion. Finally, the average frequency of pulsations within the ventricles ranges between 70-200 pulses/min dependent on the age and activity of the patient. Pulsatile flow as compared to static culture alters focal adhesion sites [162], and compared to oscillatory flow impacts cytoskeletal reorganization of cells and decreases nuclear factor kappa-light-chain-enhancer of activated B cells (NFκB, involved in inflammation) [163]. We hypothesized

that an increase in pulsation rate would decrease adhesion. By altering parameters of pressure, pulsation rate, and flow rate in an *in vitro* bioreactor univariabily, we can determine if each factor has an impact on the degree of macrophage and astrocyte adhesion as part of the initial inflammatory response.

3.2 Materials and Methods

3.2.1 Astrocyte extraction, isolation, and maintenance

Procedures were approved by the Institutional Animal Care and Use Committee of the University of Utah in accordance with the National Institutes of Health Guide for Care and Use of Laboratory Animals. Primary rat astrocyte cultures were attained from rat astrocytes collected on day 20 of gestation. Immediately after the dam had been euthanized, rat fetuses were extracted, the meninges of the embryos were removed, and brain tissue was separated. Tissue was minced and suspended in phosphate buffer solution containing 1mg/mL DNase with manganese and 1X Trypsin. The cellular solution was centrifuged for 10 min at 275 × g. Following resuspension, the tissue particulate was sieved through an 80-μm nylon mesh and washed before it was seeded and allowed to reach confluency. A shake-off procedure separated adherent astrocytes from other cell types. Cells were analyzed using flow cytometry to confirm the presence of high GFAP in the dissociated cells. Astrocytes were cultured in RPMI-1640 with 25 mM HEPES, 1% penicillin-streptomycin, 1% GlutaMAX, and 10% FBS. Cultures were split at 80% confluence.

3.2.2 Acquisition and maintenance of macrophages

Mouse peritoneal IC-21 macrophages were attained from ATCC. Cells were quickly thawed and washed with cold DPBS before being cultured in RPMI-1640 with 25 mM HEPES, 1% penicillin-streptomycin, 1% GlutaMAX, 1% sodium pyruvate, and 10% FBS. Similarly to the astrocyte cultures, macrophage cultures were split at 80% confluence.

3.2.3 Macrophage and astrocyte detachment for passaging and experimental analysis

Twenty-four hours before cell detachment for experimental analysis, cells were soaked in a low concentration of albumin-rich medium (0.5% FBS with an albumin additive). Both cell types were washed separately with DPBS and were subsequently incubated in 1X TrypLE Express at 37° C to initiate resuspension. After a 5-min incubation period for astrocytes and a 10-min incubation for macrophages, cells were removed and added to medium, centrifuged, and resuspended in fresh medium. The Trypan blue exclusion assay, viable cells were counted. Viable cells were seeded and suspended at a density of 180.175 cells/mm^2 in either the static culture or the bioreactor.

3.2.4 Design of static culture systems

Silicone surfaces were prepared in 6-well culture plates to represent a static *in vitro* culturing environment in which cells were seeded onto silicone rather than the culture dish base polymer polystyrene. Silicone was prepared using the Sylgard 184 Silicone Elastomer Curing Agent and Base (Dow Corning, Midland, MI) at a ratio of

10:1. Approximately 1 mL of the combined solution was injected into each well and allowed to cure at a temperature of 60°C for 4 hours before seeding with astrocytes.

3.2.5 Cell attachment and viability in static culture systems

Using methods similar to those in a direct contact cytotoxicity assay [164], samples were analyzed for acute cell maturation and growth. Macrophages and astrocytes (0.098×10^6 cells) were seeded onto a silicone surface to yield a density of 180.175 cells/mm^2. Cells were incubated for 20 hours at 37°C.

3.2.6 Design of the hydrocephalus shunt catheter bioreactor

In methods analogous to those used in static culture, macrophages and astrocytes were suspended on a silicone surface at 180.175 cells/mm^2 equating to a final cell suspension of 4.615×10^4 cells/mL (3×10^6 cells total) in the HSCB. Cells were propelled through the bioreactor at 37°C. The cells were distributed using an autoclaved 250-mL spinner flask (Cytostir). A three-channel peristaltic pump (Watson-Marlow 401U/DM3, Cornwall, England) initiated flow propagation through a series of tubing including Marprene double manifold tubing (Watson-Marlow), barium-impregnated regions of silicone catheters, and barium-free silastic tubing (Silastic Rx Medical Grade Tubing, Dow Corning, Midland, Michigan). The rate of flow was set to mimic conditions within the ventricular cavity such that variations in pressure, flow rate, and pulsatility were independent parameters (pump settings were chosen based on Watson-Marlow pump and tubing specifications). Conditions of high pressure (16.43 ± 0.24

mmHg) were induced using in-line high-pressure valves (Baxter Heyer-Schulte Mini-LPV High Pressure Valves, Deerfield, IL), whereas low-pressure conditions (-1.66 ± 0.02 mmHg) resulted from inherent pressure within the system with no valve used. Flow rate and pulsation rate were manipulated in combination by varying the diameter of the Marprene tubing: 0.25 mL/min and 100 pulses/min was simulated using 0.38-mm inner diameter tubing; 0.3 mL/min and 120 pulses/min also using 0.38-mm inner diameter tubing; 0.25 mL/min and 70 pulses/min using 0.50-mm inner diameter tubing, and 0.25 mL/min and 200 pulses/min using 0.25-mm inner diameter tubing. When measuring adhesion under varying conditions of flow, no pressure valve was used and pulsation rate was set to 100 pulses/min; when measuring adhesion under varying conditions of pressure, 0.25 mL/min flow rate and 100 pulses/min were used; when measuring adhesion under varying conditions of pulsatility, no pressure valve was used and flow rate was set to 0.25 mL/min. A removable in-line manometer was used to record mean pressure within the catheter. Sample regions of medical-grade silicone shunt tubing impregnated with barium were fixed in horizontal and vertical positions to mimic prolonged supine and up-right orientation, respectively. Sample tubing was obtained from the Neurosurgery Division of Medtronic (Goleta, CA).

3.2.7 Pressure measurements

An Extech HD700 Handheld Digital Manometer was used to measure pressure within the flow system. The total pressure in all components of the flow system was obtained when the manometer was set to zero at atmospheric pressure. The pressure of

fluid flow was determined when the manometer was zeroed in line with the system turned off. Pressure values were confirmed manually using a water column.

3.2.8 Staining procedure for static cultures and the bioreactor

Following cell exposure to silicone, macrophages and astrocytes bound to each substrate were fixed in 4% (w/v) paraformaldehyde in PBS for two hours at ambient temperature. All samples were removed from solution, immediately rinsed, stored in 0.1 M PBS overnight at 4°C, and then longitudinally cut to prepare for staining. Samples inoculated with macrophages were batch stained using a double staining technique to label actin and vinculin. Samples were subsequently incubated in 1:300 polyclonal sheep anti-actin (Chemicon, Temecular, CA) in 0.1 M PBS followed, 1:100 polyclonal cyanine 3 (Cy3)-conjugated secondary antibody in 0.1 M PBS, 1:300 monoclonal mouse anti-vinculin (Chemicon), and 1:100 polyclonal FITC-labeled goat anti-mouse IgG H+L (Chemicon). Samples inoculated with astrocytes were batch stained with a 1:300 concentration of monoclonal mouse anti-GFAP (Chemicon, Temecula, CA) in 0.1 M PBS to label astrocytes. A 1:100 polyclonal goat anti-mouse IgG (H+L) fluorescein conjugated secondary antibody (Chemicon, Temecula, CA) was applied for one hour at 37°C to localize the GFAP primary antibody. Both macrophage- and astrocyte-inoculated PDMS samples were counterstained with a 1:1000 concentration of 1 mg/mL stock using established methods.

3.2.9 Imaging and quantification for static cultures and the bioreactor

Confocal images were taken using a Zeiss 510 microscope, and spectral epifluorescent images were obtained using a Nikon fluorescent CRI Nuance microscope system. The confocal images were observed using the Zeiss LSM image browser. For semiquantitative image analysis, 2 random spots on each tube half and on each static culture sample were investigated using DAPI-positive nuclei tracing (n = 12, where each sample included both portions of the catheter tubing for HSCB analysis). Data were analyzed and represented as the percent of total blue component in dRGB space (analyzed using software to analyze fluorescent intensity). Data for each condition were pooled and represented as the percent change from 255, with 255 representing complete light emission at each measured pixel.

3.2.10 Statistical analyses

After analysis of data normalcy using the Anderson-Darling normality test, results were compared using either a one-way ANOVA or the Kruskal-Wallis H Test with a confidence interval of 0.95 ($\alpha = 0.05$). In cases in which two dependent hypotheses were tested simultaneously, the Bonferroni correction set significance at 0.025. In instances where the null hypothesis was rejected, suggesting that the groups did not come from the same distribution, either a post-hoc Scheffe test or an unplanned comparison of mean ranks test was implemented using least significance in difference rank. Power analysis was used to determine the beta error level and statistical power between group comparisons.

3.3 Results

3.3.1 Flow-dependent adhesion

Calibration using 0.1 M PBS at corresponding pump settings and Marprene tubing diameters confirmed flow rates of 0 mL/min (static culture), 0.25 mL/min, and 0.30 mL/min. As seen in Figure 13, Figure 14, and Figure 15, fluid flux altered the quantity of binding macrophages and astrocytes within a 20-hour time period. Separate one-way ANOVA tests for each cell type followed by a post-hoc Scheffe test indicated that there was a significant difference in astrocyte adhesion when exposed to static or fluidic cultures ($P < 0.05$). There was no statistically significant difference in macrophage adhesion although a trend suggested that adhesion increased with flow. Therefore, our hypothesis that adhesion would be altered by flow is correct in the case of astrocyte adhesion, but not for macrophage adhesion.

3.3.2 Pressure-dependent adhesion

Using the digital manometer, total mean recorded intraluminal pressure was confirmed to be -1.66 ± 0.02 and 16.43 ± 0.24 mmHg with and without in-line high-pressure valves, respectively. Confocal images in Figure 16 and Figure 17 show no obvious variation between adhesion under conditions of low or high pressure. There was no significant difference between groups. Therefore, our hypothesis that adhesion would increase dependent on an increase in pressure was not correct. As is apparent in the graphical representation of the data in Figure 18), an increase in pressure did not significantly increase macrophage or astrocyte adhesion on either horizontally or

vertically fixed samples. However, there was a trend ($P > 0.05$) that suggested that an increase in macrophage and astrocyte adhesion might be caused by a decrease or an increase in pressure, respectively on horizontally fixed samples.

3.3.3 Pulsatility-dependent adhesion

The effect of pulsation rate on astrocyte adhesion is shown in Figure 19, Figure 20, and Figure 21. Although inconsistent, clumping of adherent macrophages and astrocytes was observed. A significant difference was observed between macrophage adhesion on horizontally fixed samples under 70 pulses/min and vertically fixed samples under 100 pulses/min. A Kruskal-Wallis H Test was performed on astrocyte adhesion without rejection of the null hypothesis ($P = 0.98$), which implies that the samples came from the same distribution when pulsation rate was varied. Analysis with photometry revealed no significant variation in samples, and the null hypothesis assuming samples came from the same distribution could not be disputed.

3.4 Discussion

The Hydrocephalus Shunt Catheter Bioreactor (HSCB) was used in this study to measure how flow rate, pulsation frequencies, and pressure changes affect adhesion of individual inflammatory cells. Macrophage and astrocyte adhesion on silicone catheters within the HSCB were monitored by measuring the deposition of cells semiquantitatively using confocal microscopy. Altered flow rate and pressure levels did not significantly affect macrophage adhesion. Modified pressure levels and pulsation frequencies did not

significantly affect astrocyte deposition. Of most interest, however, may be the insignificant increase in macrophage adhesion and the statistically significant increase in astrocyte adhesion after exposure to flow conditions compared with those observed after exposure to static culture.

The finding that cell adhesion increases as a function of increased fluid flow is initially quite counterintuitive. Using known determinants that describe velocity and normal shear stress through tubing, as well as continuity equations, flow parameters can be determined that predict flow through catheters for hydrocephalus. However, because cell movement becomes restricted within an occluded catheter, using these calculations to predict the actions of the cells together with fluid behavior becomes quite problematic. To understand the results that yield increased adhesion with increased flow, consideration of Brownian motion, a phenomenon describing the random movement of particles, is helpful. In this case, transmission of thermal excitations caused by cellular collisions in the medium could cause the cells to undergo random walking, or movement in successive random directions, thus changing the distance between cell receptors and their protein ligands that are bound to the catheter surface [102]. A faster transport of cell-containing CSF would decrease contact time between cells and the catheter surface but would increase contact incidence [102]. These mechanisms could explain why our results showed enhanced macrophage and astrocyte adhesion under conditions of flow as compared with static culture conditions. In our opinion, the statistically insignificant change in adhesion seen between 0.25 and 0.3 mL/min conditions is not sufficient to contradict these notions that explain the dramatic enhancement of astrocyte adhesion seen

between static and flow conditions. Our data would predict that adhesion under conditions of normal flow at 0.3 mL/min [11] would not be significantly different under conditions of chronic hydrocephalus where flow rate is decreased to 0.25 mL/min [15]; but, we have no data to indicate whether these relationships would change over longer periods of time.

Another plausible explanation for observing an increase in adhesion under conditions of flow is that the mechanical stress may alter the chemical factors expressed by the cells. Previous findings have shown that mechanical signals can be translated into chemical messages by astrocytes, possibly because of their interconnections within brain parenchyma [165]. Other studies have suggested that clustered $\alpha_5\beta_1$ integrins may support forces during the binding of cells to fibronectin [166]. If $\alpha_5\beta_1$ recruitment is enhanced in astrocytes under conditions of flow, cell adhesion may increase, although to our knowledge this has not been demonstrated. In this study, the cells have been removed from their native state and propelled as individual cells, which may detract from overexpression of chemical messages. However, the concept of enhanced recruitment is still a conceivable explanation for increased cell adhesion under conditions of flow.

In hydrocephalus, the CSF formation rate is strongly associated with ventricular pressure [167-168]. Changes in either CSF flow or ventricular pressure could impact the microenvironment surrounding the ventricular catheter and play a major role in how cells might obstruct CSF shunts; however, while high pressure slightly enhanced astrocyte adhesion on the horizontal catheters, it inhibited macrophage adhesion on horizontal catheters. We speculate that conditions of pressure might increase initial tethering of

protein ligands and cells but are not enough to make a significant impact on overall adhesion after a 20-hour exposure and may actually have an inhibitory effect depending on the specific receptor-ligand interaction. This pattern of adhesion may be comparable to adipose accumulation in hypertensive models of atherosclerosis in which chronic high blood pressure leads to pathologic changes in smaller arteries and arterioles; morphologically, this is observed in vessel wall thickness as lipids accumulate in intimal endothelial cells [169].

Fluctuations in pulsation rate did not significantly impact astrocyte adhesion, and impacted macrophage adhesion only when it was altered concurrently with catheter orientation. Frequencies of 70, 100, and 200 pulses/min were tested to model clinically applicable average CSF pulsation rates seen in adult, pediatric, and neonatal patients. Because such a narrow frequency range was chosen, it is possible that other frequencies outside of this range may yield changes in adhesion, but a full evaluation of pulsation frequency was beyond the scope of this study.

Our results further indicate that there is a trend toward existing surgical grade catheters being more vulnerable to cellular adhesion when they are parallel to the ground, presumably because of the effect of gravity, as astrocyte adhesion on horizontally fixed catheters was generally greater than adhesion on vertically fixed catheters. These data might indicate a need to favor vertical insertion. However, in clinical settings it is often the size and configuration of the enlarged ventricles, as well as the location of the choroid plexus, that dictate the desired insertion pathway.

Qualitative observations support the hypothesis that by controlling environmental cues in the HSCB, factors limiting adhesion are based on the rate of cell transport rather than by the rate of cell adsorption. Thus, the HSCB is quite different from conditions modeled in static cell cultures. These features in combination with data presented here indicate that standard cell culturing techniques are not sufficient to model inflammatory cell adhesion on catheters used in hydrocephalus. These data suggest that the flow parameters encountered *in vivo* (and clinically) may have a more influential role in astrocyte adhesion than was expected from previous studies.

Although use of the HSCB can yield specific data on cell adhesion rate and morphology, the model is not without limitations. Our goal was to obtain a model of adhesion with an emphasis on maintenance of appropriate mechanical factors without the burden of excessively prolonged exposure times. The HSCB can accommodate changes in cell concentration and exposure time if varying conditions are needed for individual experiments.

Current studies in our laboratory involve the use of the HSCB in the study of influential chemical factors that may alter cellular adhesion. Variations in cell type and protein concentration are being tested to continue to model the foreign body response at the catheter–CSF interface at protein concentrations that would mimic the addition of blood products in the ventricular system. As seen clinically [107], the adhesion patterns on silicone are highly variable and can appear in clumps. These patterns were not quantified here but serve as a potential area for future work.

3.5 Conclusions

In this study, the HSCB was used to study how macrophages and astrocytes bind to catheters when adhesion is limited by the rate of cell transport, rather than by the rate of adsorption like in static cultures. By manipulating the system so that clinically applicable CSF flow rates, pressures, and pulsation frequencies are quantified, we gain a physiologic perspective that is not possible in an *in vivo* animal model where these variables are based on the animal's heart rate, choroid plexus size, and level of anesthesia [170]. The data in this study revealed that the only mechanical factor to yield a significant alteration in astrocyte adhesion was fluid flow, while macrophage adhesion was altered by a concurrent change in catheter position and pulsatility. These data suggest that devices used to continuously drain CSF (i.e., shunt catheters and valves) may be more susceptible to inflammatory cell adhesion than are devices inserted into the same cranial space that undergo less continuous flow and pulsatility (i.e., reservoirs).

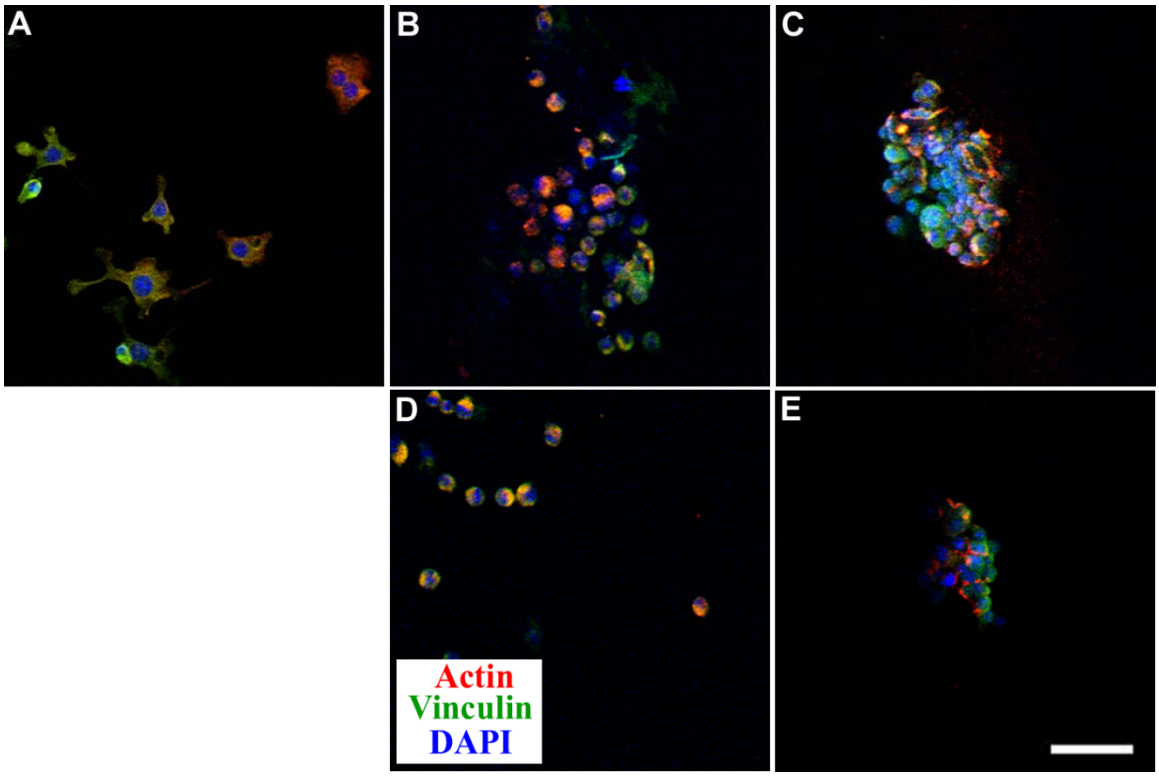

Figure 13 Macrophage attachment to horizontally (A–C) and vertically (D–E) fixed catheters at varying flow rates. Flow rates were 0 mL/min (A, static cultures), 0.25 mL/min (B and D), and 0.30 mL/min (C and E). Static cultures (A) have more pronounced and extended processes as compared to samples exposed to flow. In static cultures, vertically oriented samples are not included in standard practice and have not, therefore, been included in this analysis. Morphologically, cells exposed to static conditions have many more extended processes as compared to cells exposed to flow. Actin and vinculin appear either co-localized (yellow) or dissociated (red and green, respectively) to depict the cytoskeleton and the focal adhesion contacts of the macrophages while DAPI (blue) was used to label the nuclei. Scale bar denotes 50 μm in all panels.

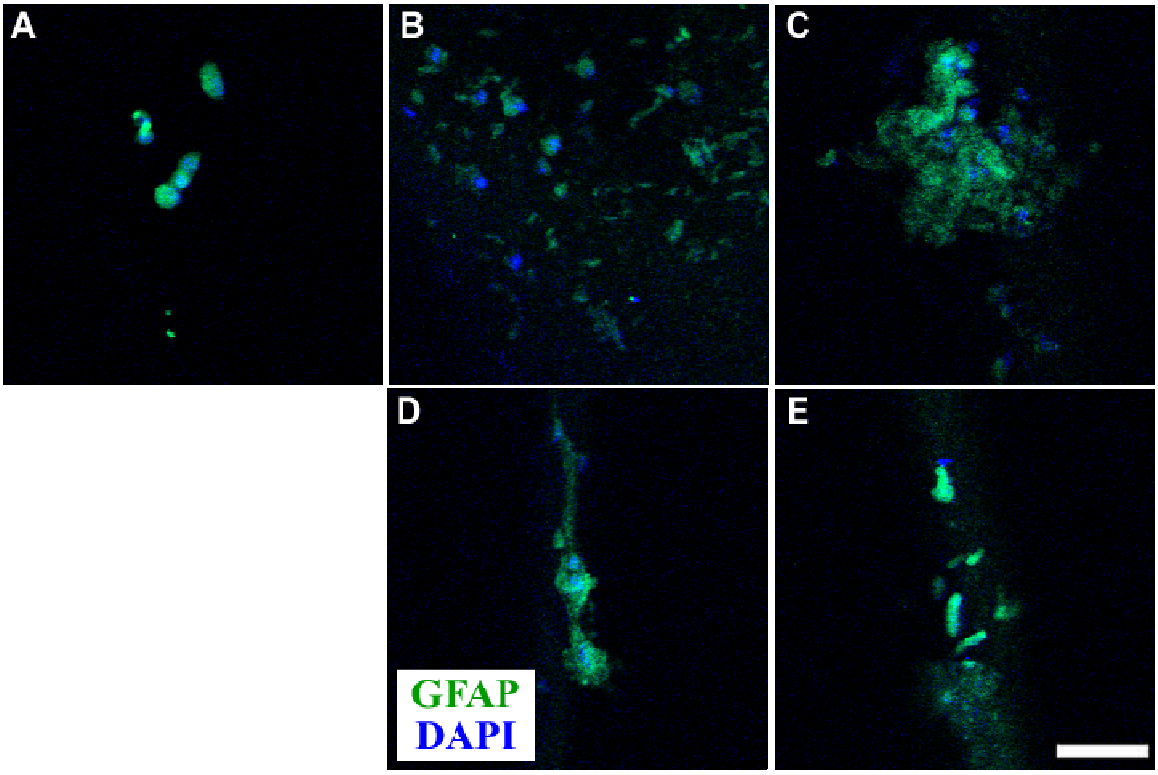

Figure 14 Astrocyte attachment to horizontally (A–C) and vertically (D–E) fixed catheters at varying flow rates. Flow rates were 0 mL/min (A, static cultures), 0.25 mL/min (B and D), and 0.30 mL/min (C and E). As compared with static culture (A), astrocyte adhesion on horizontally fixed catheters appeared elevated at 0.25 mL/min (B) and at 0.3 mL/min (C), although at 0.3 mL/min, clusters of cells were more evident. Adhesion on vertically fixed catheters appeared along the length of each analyzed section yet there was no clear change in concentration. Morphologically, individual cells seem to be relatively round with only minor evidence of process extension. GFAP for astrocytes is shown in green while DAPI for nuclei is in blue. Scale bar denotes 50 μm in all panels.

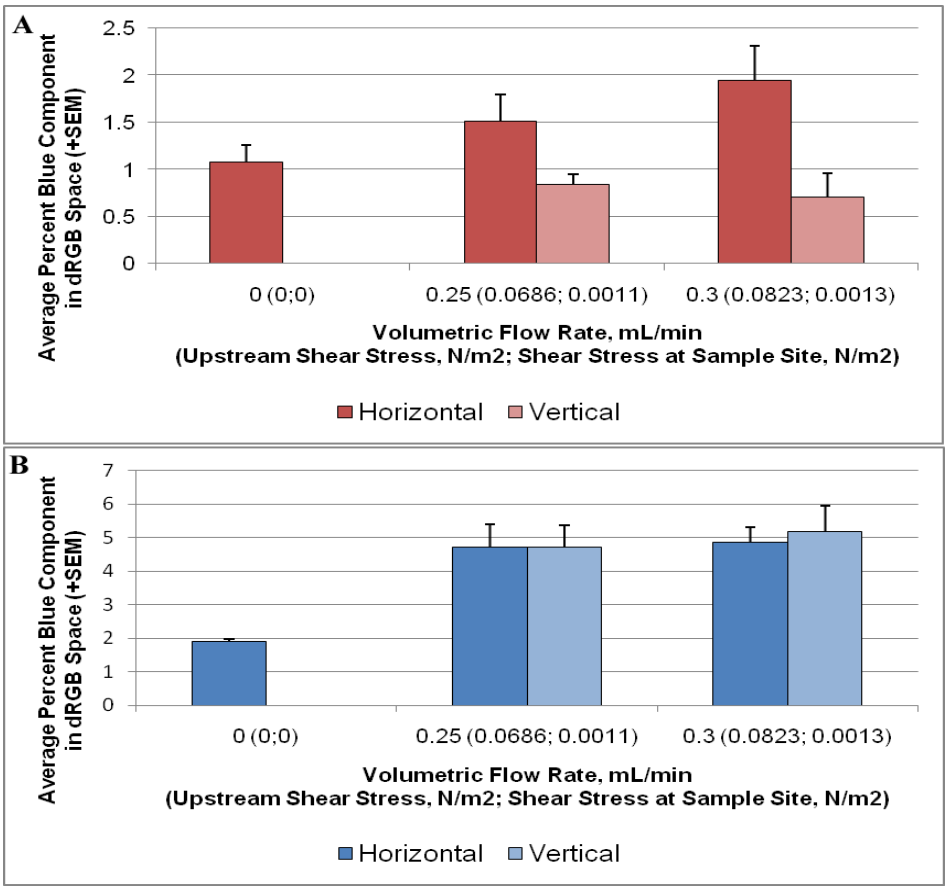

Figure 15 The average blue component in macrophage (A) and astrocyte (B) images. While there was no statistically significant difference in macrophage adhesion, a trend would suggest that adhesion increases with increasing flow rate (and shear stress) when samples were held horizontally. The difference in astrocyte adhesion between the static culture (denoted as 0 mL/min) and samples exposed to 0.25 mL/min flow and 0.3 mL/min, however, is statistically significant as determined using a Kruskal Wallis H Test. In static cultures, vertically oriented samples are not included in standard practice and were therefore excluded for this analysis. No significant differences in adhesion were observed when comparing vertically fixed catheters with either cell type. A sample size of 12 was used in all groups.

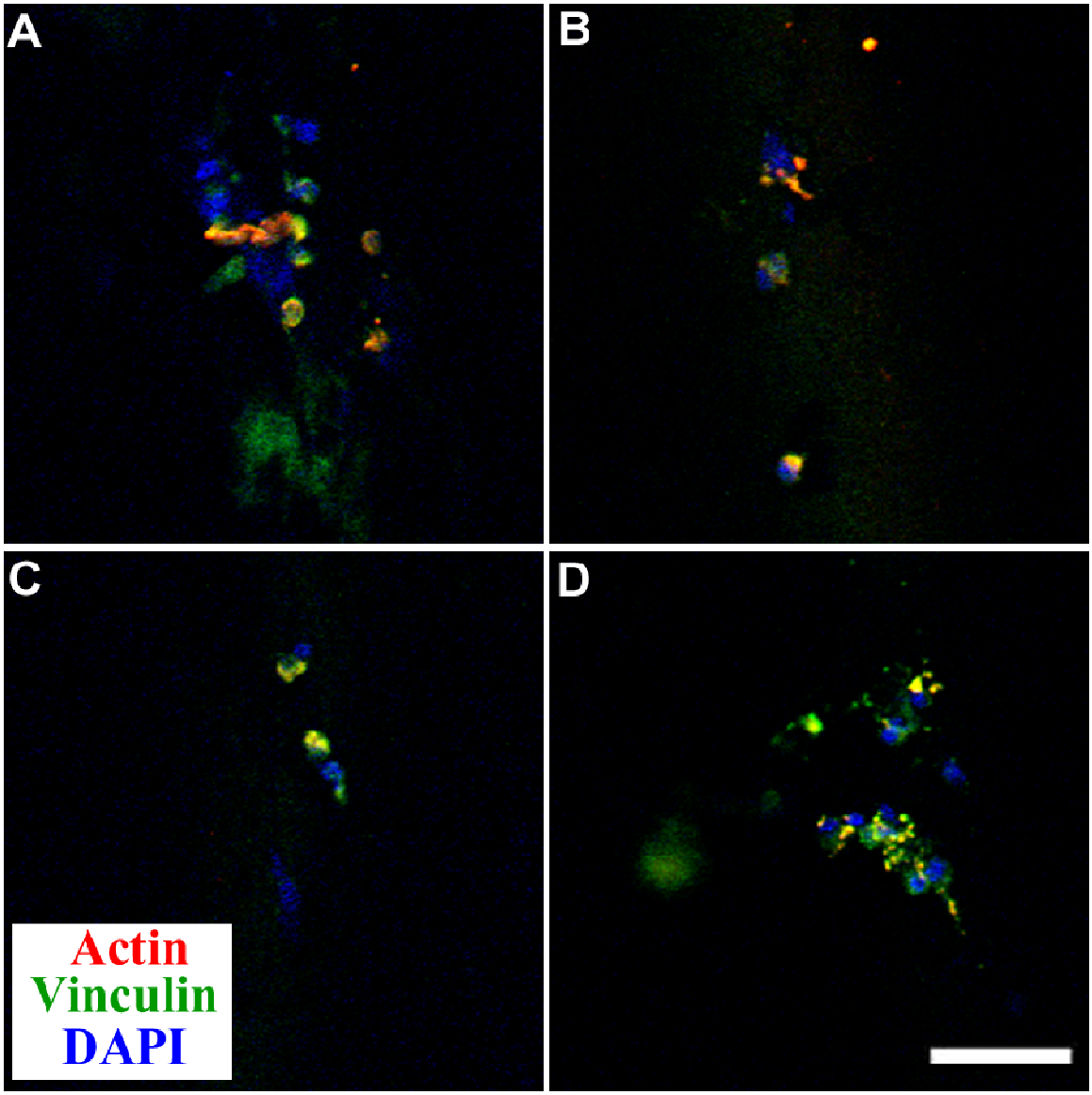

Figure 16 Macrophage attachment to horizontally (A–B) and vertically (C–D) fixed catheters at average luminal pressures of -1.66 mmHg (A and C) and 16.43 mmHg (B and D). Scale bar represents 50 μm.

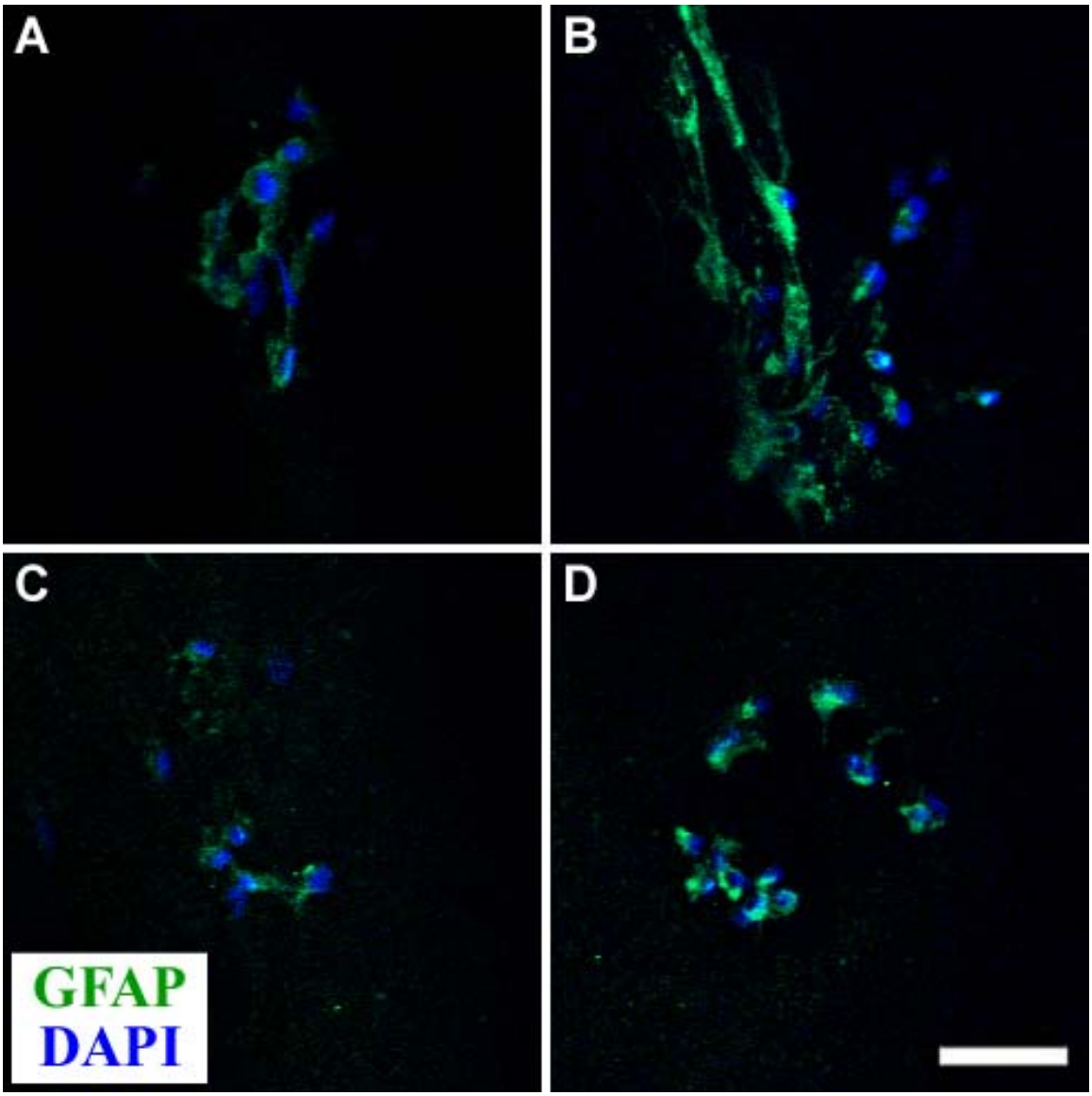

Figure 17 Astrocyte attachment to horizontally (A–B) and vertically (C–D) fixed catheters at average luminal pressures of -1.66 mmHg (A and C) and 16.43 mmHg (B and D). Scale bar represents 50 μm.

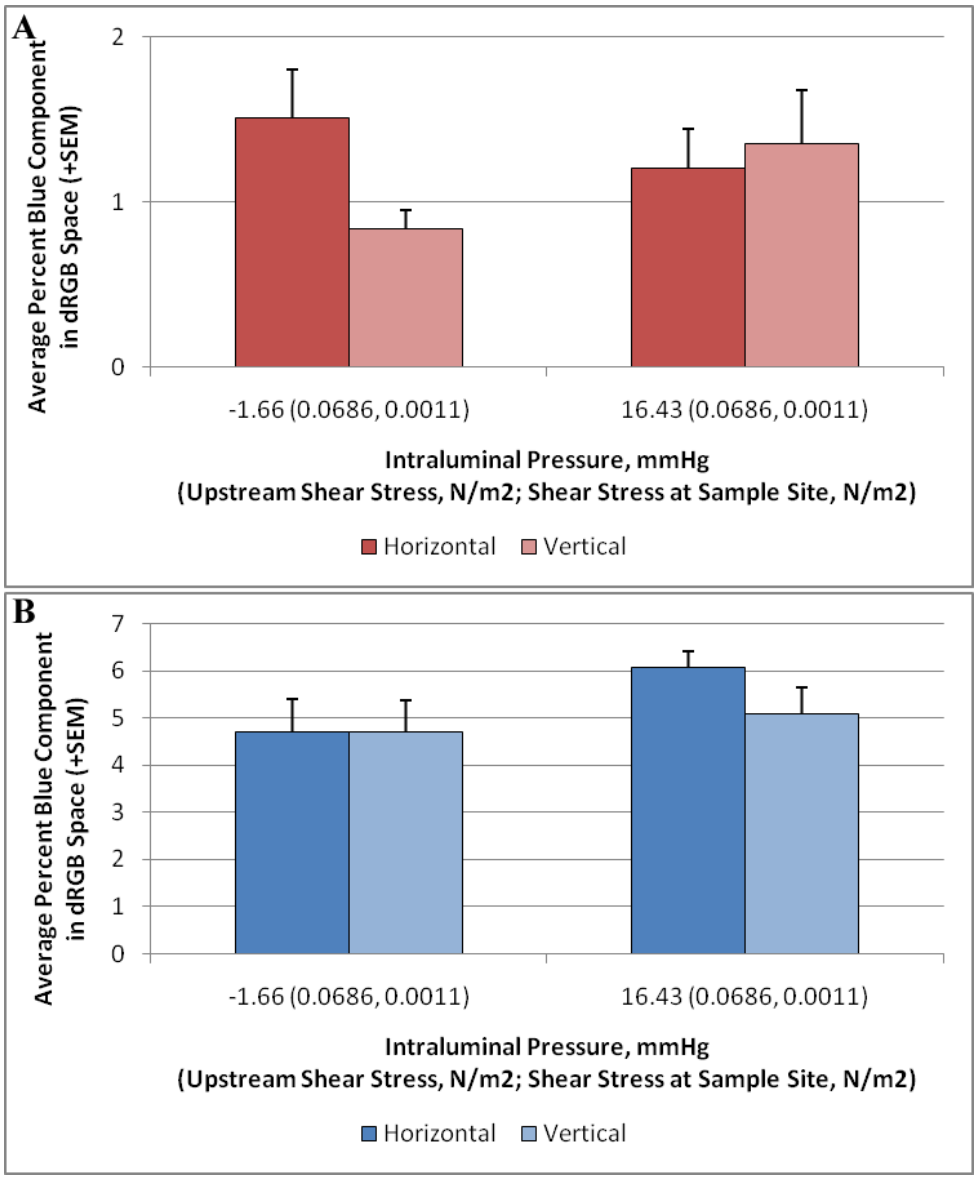

Figure 18 Analysis of the blue DAPI channel for both macrophages (A) and astrocytes (B) revealed no significant difference in adhesion in the presence of low (mean -1.66 mmHg) or high (mean 16.43 mmHg) pressure as determined using a Kruskal Wallis H Test. Trends between low and high pressure in all groups but the horizontal macrophages imply that adhesion increases as the luminal pressure increases. A sample size of 12 was used for each group.

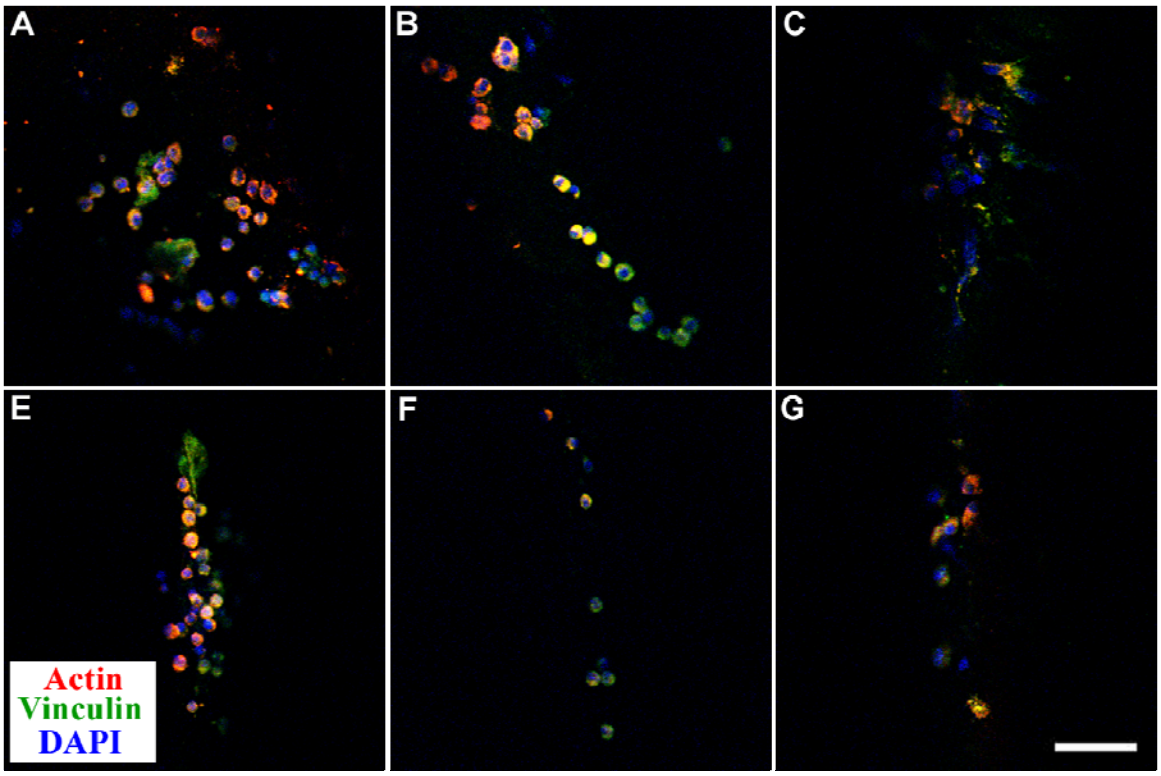

Figure 19 Macrophage attachment to horizontally (A–C) and vertically (D–F) fixed catheters at varying pulsation rates: 70 pulses/min (A and D), 100 pulses/min (B and E), and 200 pulses/min (C and F). Clumping of macrophages can be seen under all conditions. Scale bar denotes 50 μm.

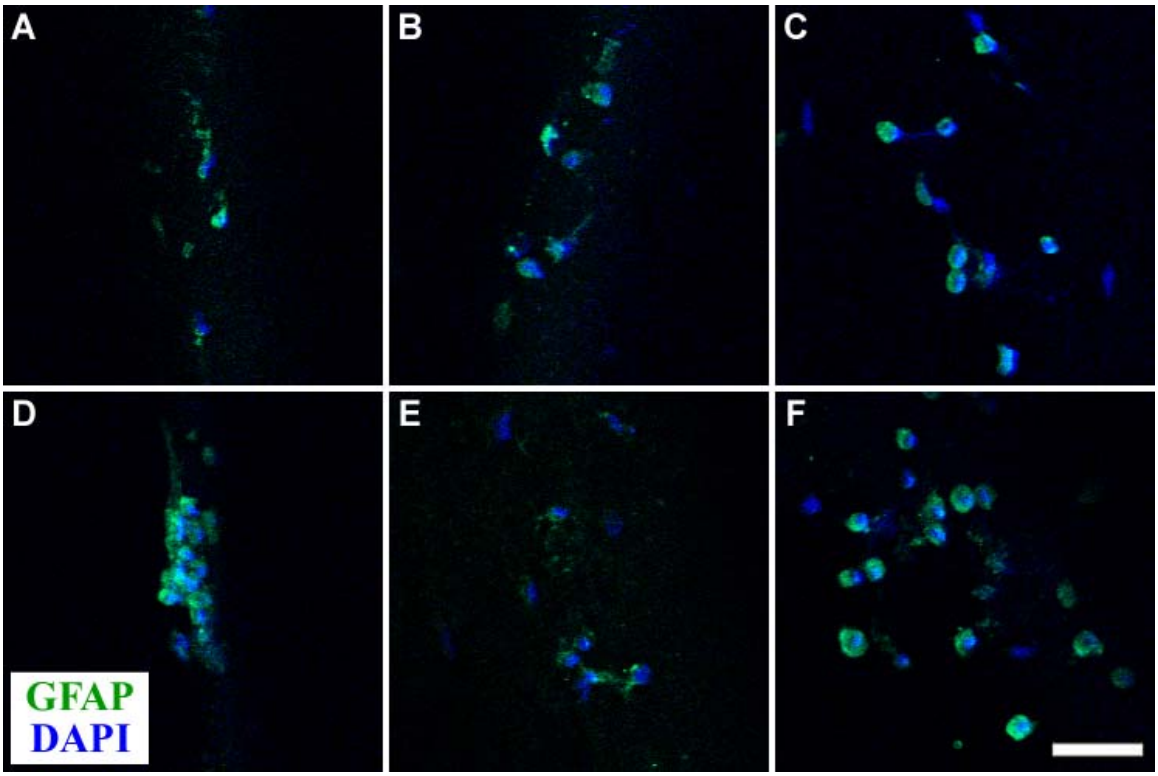

Figure 20 Astrocyte attachment to horizontally (A–C) and vertically (D–F) fixed catheters at varying pulsation rates: 70 pulses/min (A and D), 100 pulses/min (B and E), and 200 pulses/min (C and F). The dramatic yet widely variable distribution of cell clumping can be observed, for example, when comparing panels D and E. Scale bar denotes 50 μm.

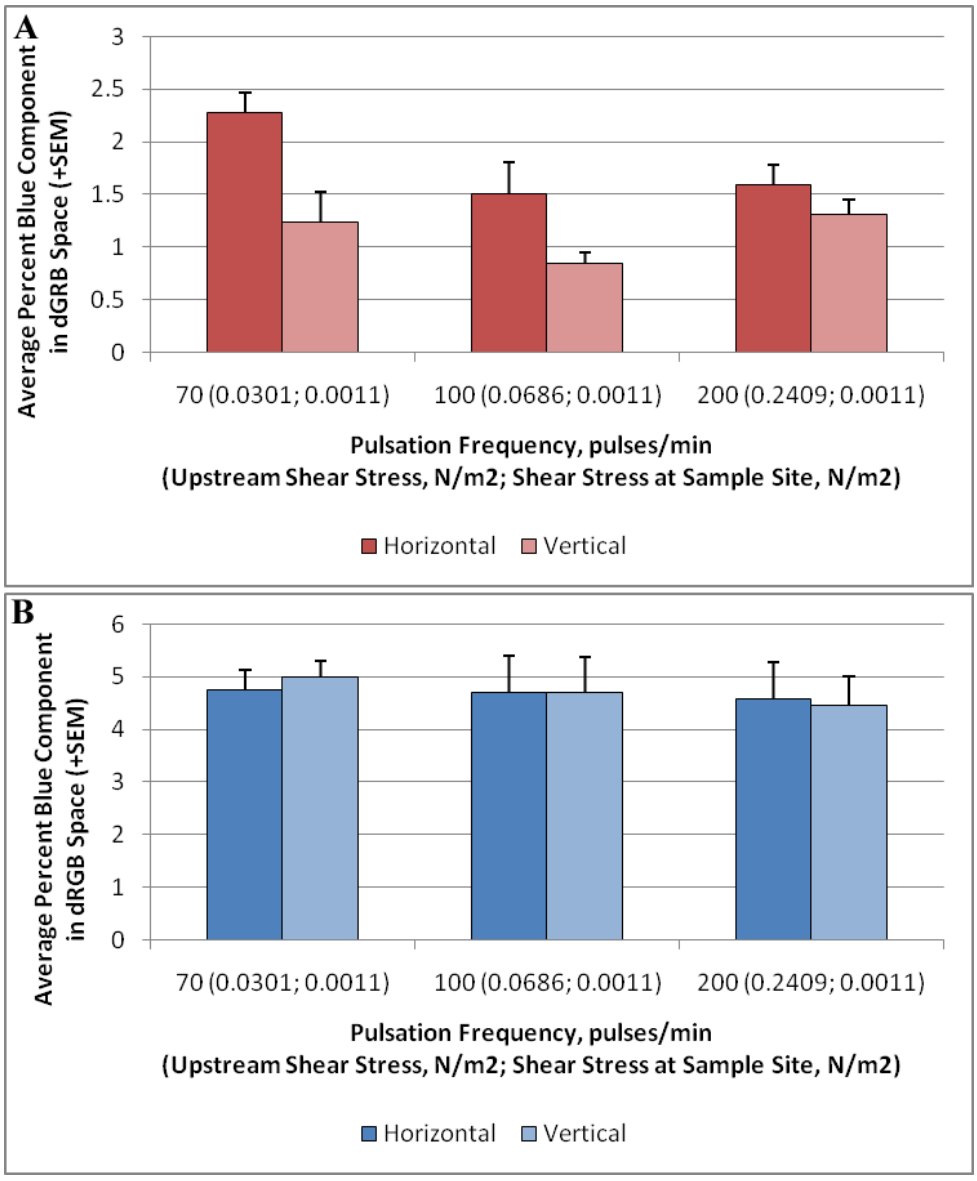

Figure 21 Macrophage (A) and astrocyte (B) adhesion dependency on pulsation rate acquired using analysis of the blue DAPI channel of the fluorescent images. No statistically significant differences were found between samples as determined using a Kruskal Wallis H Test except between macrophage adhesion on horizontal samples at 70 pulses/min and on vertical samples at 100 pulses/min ($P < 0.05$). A sample size of 12 was used for each group.

CHAPTER 4

EFFECTS OF SURFACE WETTABILITY, FLOW, AND PROTEIN CONCENTRATION ON MACROPHAGE AND ASTROCYTE ADHESION IN AN *IN VITRO* MODEL OF CENTRAL NERVOUS SYSTEM CATHETER OBSTRUCTION[2]

4.1 Introduction

Hydrocephalus, a neurological disorder often associated with high intracranial pressure (ICP) and expanding cerebral ventricles, is most often treated by implanting a catheter (shunt system) into the lateral ventricles to drain excess cerebrospinal fluid (CSF). Shunt systems are made of poly(dimethyl)siloxane (PDMS, silicone) because of its high tensile strength, tear resistance, hydrophobicity, and inert nature [75]. In part because of the high hydrophobicity (low surface wettability) of PDMS, its use as a biomaterial is restricted because interactions between PDMS and the body after implantation can include undesired protein adsorption and cell adhesion/scarring [64].

Protein adsorption and cell and tissue adhesion on PDMS shunt tubing have been scrutinized recently because of the extremely high failure rate of shunt systems used to treat hydrocephalus [50, 107, 159]. Within 10 years of implantation, 85% of PDMS

---

[2] Reprinted from Journal of Biomedical Materials Research: Part A, accepted manuscript, Harris, CA; Resau, JH; Hudson, EA; West, RA; Moon, C; Black, AD; McAllister JP "Effects of surface wettability, flow, and protein concentration on macrophage and astrocyte adhesion in an *in vitro* model of central nervous system catheter obstruction."

shunt systems fail [45], and the cause is usually tissue occlusion of the ventricular catheter, most often by microglia, macrophages, and astrocytes. Nevertheless, few attempts to manipulate the surface properties of shunt catheters to inhibit inflammatory cell binding have been reported. Further, the published data are contradictory. Many factors may influence these results, including alterations in the environmental conditions in which the device is implanted. Previous findings suggest that flow influences adhesion [102], and a broad range of literature suggests that surface chemistry influences cell attachment [88, 171]; however, the effect of shunt surface wettability under the flow conditions seen in the cerebral ventricles has not been investigated. We hypothesized that adhesion would increase on a less wettable surface and with increasing flow.

In the medical device industry, the use of hydrophilic surface coatings (with high surface wettability) has gained momentum in the past few decades because of their potential to inhibit nonspecific protein deposition and cell attachment. Mechanically, CSF bulk flow, flow pulsation rate, and flow-induced shear rate alter cell-surface interactions [79, 90, 163, 172], including initial astrocyte binding [140]. Chemically, increasing protein concentration has been shown to increase attachment in neuron–glia cultures [173]. We hypothesize that an increase in protein concentration will increase macrophage and astrocyte attachment. Using a bioreactor specifically designed to simultaneously mimic the bulk flow rate, pulsatile flow rate, flow-induced luminal shear, and protein concentration observed in the cerebral ventricles [140], we used surface hydroxyl groups to render the surface of PDMS hydrophilic and inhibit initial macrophage and astrocyte adhesion.

4.2 Materials and Methods

4.2.1 Macrophage culture and maintenance

Mus musculus IC-21 macrophages derived from SV-40 transformed peritoneal macrophages with phagocytic properties were obtained from ATCC (Manassas, VA). These were originally obtained from a C57BL/6 mouse (ATCC product number TIB-186) and were chosen primarily because of their mature phenotype[142] and characteristic similarity to supraependymal macrophages found bound to CNS implants [143]. After rinsing with Dulbecco's Phosphate Buffered Saline (DPBS, Invitrogen), macrophages were cultured in RPMI-1640 medium with 25 mM 4-(2-hydroxyethyl)-1-piperazineethanesulfonic acid HEPES, 1% penicillin-streptomycin (Sigma, St. Louis, MO), 1% GlutaMAX (Invitrogen, Carlsbad, CA), 1% sodium pyruvate (Invitrogen), and 10% fetal bovine serum (FBS, Sigma). Cells were split at 80% confluence and seeded in T-75 culture flasks, as observed under an inverted microscope. Cells were used after 8 passages following obtainment from ATCC.

4.2.2 Astrocyte extraction, isolation, and maintenance

Astrocytes were chosen primarily because they bind consistently to ventricular catheter explants [49]. Fetal rat astrocytes were extracted using previously described methods [140] approved by the Institutional Animal Care and Use Committee. Briefly, minced brain tissue in PBS, 1 mg/mL DNase with manganese, and 1X Trypsin was centrifuged, resuspended, and filtered through an 80-μm nylon mesh prior to seeding. Adherent astrocytes were separated using a "shake-off" procedure [149]. Flow

cytometry and staining techniques separately confirmed the presence of high glial fibrillary acidic protein (GFAP) in the dissociated cells. RPMI-1640 culture medium with 25 mM HEPES, 1% penicillin-streptomycin, 1% GlutaMAX, and 10% FBS sustained proliferation; the culture was split when confluency reached 80%. Cells were used after 40 passages which could serve as a potential caveat to the study, but GFAP expression did not appear to be altered after continued passages (data not shown).

4.2.3 Cell detachment for passaging and experimental analysis

Similar to previous work completed in our laboratory [140], subsets of macrophages and astrocytes were immersed in a low concentration of albumin-rich medium (0.5% FBS with an albumin additive) for 24 hours before analysis to mimic both the total protein (208.1 mg/L) and the albumin (155 mg/L) concentration of normal CSF prior to cell detachment. A second group of macrophages and astrocytes were immersed in medium with a standard protein concentration (10% FBS), since higher, variable protein concentrations exist in CSF, especially CSF extracted from patients with hydrocephalus [174-175].

Macrophages and astrocytes were detached from cell culture flasks using a 5-min exposure to 1X TrypLE Express (Invitrogen). Once macrophages had been immersed in the enzyme solution for 5 min, mechanical disruption facilitated removal by striking the walls of the flasks sharply. Viable cells were counted on a hemocytometer using the Trypan blue exclusion test and suspended in medium with the low or high protein concentration at a density of 180.175 cells/mm^2 to a final cell suspension of 4.615×10^4

cells/mL (3×10^6 cells total). The cellular solution was added to either the static culture or the bioreactor for testing.

4.2.4 Design of static culture systems, cell attachment, and cell viability

Macrophages and astrocytes were seeded separately onto silicone surfaces in 6-well culture plates. A silicone layer at the bottom of the plates was prepared using the Sylgard 184 Silicone Elastomer Curing Agent and Base (Dow Corning, Midland, MI) at a ratio of 10:1. Approximately 1 mL of the de-gassed combined solution was injected into each well and allowed to cure at a temperature of 60°C for 4 hours before the wells were seeded. A subset of plates were placed in an oxygen plasma chamber under a pressure of 200 mTorr and a power of 50 W for 2 min at room temperature. This process introduced hydroxyl groups and removed methyl groups at the surface [176]. After exposure, plasma-oxidized PDMS (OH-PDMS) was immediately placed in double-distilled, deionized water to temporarily maintain surface wettability. Samples were used within 30 min of preparation. Macrophages and astrocytes in both low- and high-protein solutions were seeded separately. After a 20-hour exposure period at 37°C, cells were fixed in 4% (w/v) paraformaldehyde for 2 hours and visualized with immunofluorescence and analyzed with confocal microscopy.

4.2.5 Design of the hydrocephalus shunt catheter bioreactor and cell viability

A previously published method established by our group to test adhesion on catheters was used in this study to measure inflammatory cell binding [140]. The model

uses a three-channel peristaltic pump (Watson-Marlow 401U/DM3, Cornwall, England) to propel cells through catheter tubing to mimic CSF flow. Since cell adhesion can be measured with a user-defined (and physiological) flow rate, the model can be manipulated to determine the effect of surface modifications in flow conditions similar to those encountered by a clinically implanted shunt system. A flow rate of 0.3 mL/min and pulsation rate of 280 pulses/min were used to imitate pulsatile, ventricular CSF flow under normal conditions [11]. To test the effects of altering the surface wettability with minimal alterations in surface chemistry and topography, hydroxyl groups were introduced onto both external and internal surfaces of medical-grade shunt tubing (native PDMS, Neurosurgery Division of Medtronic, Goleta, CA) by placing samples into an oxygen plasma chamber similarly to samples used in the static culture experiments. Adhesion was measured after a 20-hour exposure period. This time period for attachment was chosen because (a) the concentration of cells in solution approaches zero after 20 hours of exposure to the system, and (b) the first 20 hours captures initiation of the acute inflammatory stage during which inflammatory cell recruitment begins *in vivo* [64].

4.2.6 Surface characterization via static water contact angle measurements

To confirm that surface wettability was increased by our method, a subset of native PDMS and OH-PDMS groups was characterized using water contact angle measurements. Contact angles were obtained using a contact angle goniometer using the sessile drop method. Average advancing and receding water contact angles were

measured after 20-hour exposure to approximately 20 μL of double-distilled, deionized water.

4.2.7 Fluorescent staining procedure

Detailed procedures on cell staining on PDMS can be found in previously published reports from our laboratory [140]. Briefly, astrocytes and macrophages bound to PDMS tubing were immersed in 4% (w/v) paraformaldehyde in PBS for two hours at ambient temperature. Fifteen minutes of exposure to anhydrous methyl alcohol was used to permeabilize the macrophages. Each sample was rinsed and stored overnight at 4°C in 0.1 M PBS. All samples were cut longitudinally to expose the lumen for fluorescent staining. Samples were washed in 0.1% Triton X in 0.1 M PBS to assure cell permeabilization. Macrophages were double stained using 1:300 polyclonal sheep anti-actin (Chemicon) in 0.1 M PBS followed by a 1:100 Cy3-conjugated polyclonal secondary antibody (Chemicon) in 0.1 M PBS to label macrophage actin filaments and 1:300 monoclonal mouse anti-vinculin (Chemicon) in 0.1 M PBS observed with 1:100 FITC-labeled polyclonal goat anti-mouse IgG (H+L) (Chemicon) in 0.1 M PBS to identify focal adhesion plaques. Tubing with bound macrophages was also counterstained with the nuclear dye 4',6-diamidino-2-phenylindole (DAPI) diluted from 1 mg/mL stock to 1:1000 in 0.1 M PBS using established methods. Astrocytes were labeled with monoclonal mouse anti-GFAP (Chemicon) fluorescently labeled with polyclonal goat anti-mouse IgG (H+L) followed by counterstaining of the nuclei using DAPI.

4.2.8 Analysis of cell attachment

After fluorescent staining, a Zeiss 510 confocal microscope was used to acquire spectral epifluorescent images, and Zeiss LSM image analysis software was used for characterizations. Two random spots along each tube half and on each static culture sample were analyzed at 20X magnification (n=12, where tubing halves were grouped and the number of spots equal across groups). Attachment was quantified by the intensity of the blue (DAPI) channel of the confocal images. The average blue component in digital Red-Green-Blue (dRGB) space was determined using the DAPI intensity. Data were reported as a percent of total light emission, with 255 representing brightest light emission.

4.2.9 Statistical analyses

The Anderson Darling normality test was used to reveal whether data sets followed a normal distribution. The Bartlett's test was used to determine the degree of homoscedasticity within data sets. Parametric results were compared using a two-tailed Student's t-test with $\alpha = 0.05$; in the case where two dependent hypotheses were tested simultaneously, the Bonferroni correction set significance at 0.025. Nonparametric results were compared using either a two-tailed Mann-Whitney U Test or the Kruskal-Wallis H Test with a confidence interval of 0.95 ($\alpha = 0.05$). In the cases where the Kruskal-Wallis H Test was used, an unplanned comparison of mean ranks test was applied using least significance in difference rank when the null hypothesis was rejected.

4.3 Results

4.3.1 Water contact angle

Native PDMS had advancing and receding water contact angles of 105.58 ± 5.38° and 71.34 ± 7.88°, respectively. Oxidized PDMS exhibited advancing and receding water contact angles of 27.03 ± 3.74° and 5.00 ± 6.00°, respectively. The advancing and receding water contact angles of PDMS were significantly different than those of OH-PDMS ($P < 0.01$).

4.3.2 Macrophage attachment

As is shown in Table 7 and Figure 22, macrophage binding was generally inhibited on OH-PDMS. Adhesion ($P < 0.05$) on OH-PDMS was significantly lower than on PDMS under flow conditions independent of the solution's protein concentration. Flow appeared to increase macrophage adhesion in all cases except when a high-protein solution was used in combination with OH-PDMS. Protein concentration by itself did not have a significant impact on macrophage attachment, but a trend indicated that a high-protein concentration in solution increased adhesion on PDMS but not on OH-PDMS. Statistical significance ($P < 0.05$) was seen between: (1) adhesion in low protein and flow on PDMS versus adhesion in low protein and flow on OH-PDMS; (2) adhesion in low protein and flow on PDMS versus adhesion in high protein and flow on OH-PDMS; (3) adhesion in high protein and static culture on PDMS versus adhesion in high protein and flow on OH-PDMS; (4) adhesion in high protein and flow on PDMS versus adhesion in high protein and flow on OH-PDMS). Our hypothesis that macrophage

adhesion would increase dependent on a less wettable surface and increasing flow was incorrect, although a nonsignificant trend did imply this relationship.

4.3.3 Astrocyte attachment

The data suggest that surface hydroxyl groups on PDMS inhibit astrocyte adhesion in most cases (Table 7 and Figure 23), although this trend was not statistically significant when analyzed using least significant difference in mean ranks. Flow enhanced adhesion in every case. The difference between the static and flow conditions was significant ($P < 0.05$) when adhesion was analyzed on PDMS surfaces under high-protein conditions. A variance in protein concentration within the astrocyte-suspended solution appeared to increase the difference between static and fluidic cultures but did not significantly alter adhesion when all other conditions were held constant. Our hypothesis that astrocyte adhesion would increase dependent on a less wettable surface and increasing flow was incorrect, although a nonsignificant trend did imply this relationship.

4.3.4 Comparison of macrophage and astrocyte attachment

A statistically significant difference ($P < 0.05$) in attachment of macrophages and astrocytes was found under static conditions and low- and high-protein solutions on PDMS and in high-protein solutions on OH-PDMS. In these cases, macrophage adhesion was greater than astrocyte adhesion except on PDMS surfaces when a low-protein solution was used. In this specific case, astrocyte adhesion was greater than macrophage adhesion. When cells were exposed to flow and a high-protein solution, astrocyte

adhesion was significantly greater than macrophage adhesion ($P < 0.05$), independent of surface type. Under fluidic conditions and a low-protein solution, the difference between macrophage and astrocyte adhesion on PDMS and OH-PDMS was insignificant ($P = 0.22$ and 0.09, respectively).

4.3.5 Cell morphology

Representative confocal images of adherent cells on either PDMS or OH-PDMS under static or fluidic conditions and in a high- or low-protein solution can be seen in Figure 24. It is important to note that the concentration of cells in these images cannot be compared between static and fluidic conditions without normalizing the area. Macrophages and astrocytes adherent on either the PDMS or the OH-PDMS substrate in the flow system appeared to have a rounded morphology. Cellular processes did not appear extended. Clumping of astrocytes was more exaggerated on OH-PDMS under high-protein conditions in static and fluidic culture. Double staining of adherent macrophages provided means for analysis of stress fibers (actin) and point-wise attachment using focal adhesions (vinculin). Under static culture conditions on PDMS, macrophages exhibited extended processes, but these were less pronounced on OH-PDMS, especially when a low concentration of protein was used.

4.4 Discussion

In an effort to understand how surface modifications may alter macrophage and astrocyte adhesion on catheters used to treat hydrocephalus, we examined how the addition of surface hydroxyl groups by plasma oxidation altered adhesion under various adaptations to flow and protein concentrations. We observed that (a) the addition of surface hydroxyl groups inhibited adhesion in most cases but increased adhesion in some cases under static conditions, (b) flow enhanced adhesion with one exception being a decrease in macrophage adhesion on oxidized surfaces under high protein conditions, and (c) adhesion increased with increasing protein concentration except in two cases (macrophage adhesion on oxidized surfaces under flow and astrocyte adhesion on PDMS in static conditions decreased with increasing protein concentration). It was apparent that the degree to which these factors played a role in adhesion varied depending on the cell type. Surface hydroxyl groups had an inhibitory effect on macrophage binding that was generally more pronounced than the effect of flow or protein concentration under the same conditions. With astrocytes, flow increased binding, and the effect was more pronounced than the effect of surface hydroxyl groups or protein concentration under the same conditions. To inhibit both macrophage and astrocyte attachment on shunt systems used in hydrocephalus, it becomes obvious that both the surface chemistry and the flow are important. Future work should incorporate surfaces treatments with added hydroxyl groups as well as modulation of flow through the catheter by adapting the architecture of the shunt system.

Studies of shunt systems are behind those of other devices, including vascular prostheses, heart valves, intraocular implants, hip and joint prostheses, and contact lenses [87], which have already extensively explored material modifications that may inhibit cell attachment. On a hydrophobic surface like PDMS, a biological response can be initiated through an entropic drive for the hydrophobic moieties of proteins in solution to bind onto the implant. In most conditions, this response will be stronger on hydrophobic materials, inducing more cellular activation and spreading than on hydrophilic materials [83]. This response favors tailoring the surface chemistry of biomaterials like PDMS [77-79]. However, the degree of cell attachment is multifactorial and is also dependent on surface-available functional groups [177], roughness [89, 178-179], charge [89], and the environment in which the material is implanted. We chose to study differences in initial cell adhesion between native and plasma-oxidized PDMS to test a wide range of wettability (hydrophobic and hydrophilic extremes) with minimal topographical changes [180].

4.4.1 The effect of plasma oxidation on macrophage and astrocyte attachment

Our results indicate that the addition of surface hydroxyl groups reduces adhesion of macrophages (significantly) and astrocytes (insignificantly) in the acute term under physiological flow, which correlates to data found on modified microfluidic devices [79, 90]. These effects may be due to the fact that surface functionality strongly influences cell integrin binding and specificity through focal adhesion assembly [181]. Macrophages are involved in the acute and chronic inflammatory response to foreign

bodies. Especially in cases of shunt failure, macrophages/microglia have been found focally attached to shunt systems [107, 115]. Macrophages bound to a foreign body in the central nervous system (like the shunt system) act as a precursor to the formation of an astrocytic capsule around the implant [182], so early resolution of the response is ideal.

The addition of surface hydroxyl groups to PDMS surfaces via plasma oxidation did not significantly reduce astrocyte adhesion. Other reports have suggested that the phenotype, morphology, and extracellular matrix protein requirements of fibroblasts adherent to a biomaterial are distinct from adherent monocyte/macrophage cells [183]. There may be a similar heterogeneity between the attachment requirements for astrocytes and macrophages. Both cell types bind via integrin-mediated interactions with adsorbed protein ligands, but the specific interactions are cell type dependent. While these connections can control the function of the cell, which may alter the degree in which the cell moves, proliferates, rearranges its cytoskeleton, or survives [184], it may be simply that attachment of astrocytic end feet are less permissive to changes in the adsorbed protein layer.

4.4.2 The effect of flow on macrophage and astrocyte attachment

The introduction of flow at a flow rate of 0.3 mL/min, the calculated clinical production rate of cerebrospinal fluid [11], increased adhesion of macrophages and astrocytes. The change from a static to a flow environment had a striking (and significant) impact on astrocyte adhesion whereas the effect of flow on macrophage

attachment was apparent but not significant. An important limitation to these results, however, is the geometrical dissimilarity between the static and fluidic cultures. Although calculations were made to insure that the total surface area to which cells were exposed and the cell densities were equivalent, future work should address this issue by altering the static cultures such that cells are seeded directly into catheter lumina. Previous work by our group has shown that flow increases astrocyte adhesion significantly whereas pulsation rate and pressure do not. Together, these studies reveal that flow rate had a stronger influence on astrocyte adhesion in the short term than flow pulsation rate, pressure, protein concentration, and the addition of surface hydroxyl groups on PDMS samples. Most likely, material surface properties dictate protein adsorption and cell adhesion [88], but these properties are also dependent on surrounding conditions. Flow probably modifies receptor-ligand chemical kinetic rate between the bound and unbound state, causing flow-enhanced cell tethering [102]. Mechanical stress has been shown to manipulate the strength of cell surface integrins [166]. It is possible that the difference in response to flow from the macrophage and astrocyte is dependent on the difference in the initial strength or flow-effected strength of the cell's integrins. The finding that flow exacerbates adhesion may also be dependent on the shear rate at the shunt catheter interface. This dependency has been shown with other cell types [102, 172]. Thus, alterations to the catheter dimensions that would alter the flow-induced shear rate may impact adhesion. Our group is currently developing methods to modify these factors.

Classically, there has been a disconnect between results attained from *in vitro* modeling and *in vivo* implantation. Modifications to the surface wettability of recording electrodes have had a dramatic effect *in vitro* but a minimal effect on the surrounding cortical foreign body response *in vivo* [185]. One reason for this may be that the unique protein expression patterns of cultured cells compared to *in vivo* cells influence adhesion and adhesion rate. This is an obvious limitation to *in vitro* work that has not been eliminated in this study. Another reason for an *in vitro* - *in vivo* disconnect is that many *in vitro* models fail to incorporate pertinent mechanical cues presented *in vivo*. Here, we attempt to minimize these differences by incorporating pulsatile flow and found that macrophage adhesion was generally greater than astrocyte adhesion under static conditions but the opposite was true under fluidic conditions (Table 1). These data emphasize the need to study adhesion using a test bed that includes flow.

The results concerning the effect of flow are quite interesting for hydrocephalus research because of the relatively unique environment in which the shunt system is implanted. CSF is produced actively and passively as a blood filtrate from the choroid plexus and from the parenchyma [16]. Changes in cerebral pulsatility, cerebral blood flow, intracranial pressure, and body movement, however, can cause the outflow to be nonconstant over time. For instance, patients with normal pressure hydrocephalus are prone to a decrease in CSF production [186], as are patients with chronic hydrocephalus [15]. Slower or static CSF flow allows toxins and amyloid to accumulate in the brain, contributing to the pathophysiology of this disorder [187-190]. Conceivably, patients

with less flow may be at a lower risk for inflammation-derived occlusion because of the decrease in macrophage and astrocyte attachment in static conditions observed here.

4.4.3 Effect of protein concentration on macrophage and astrocyte attachment

Cell culture medium protein concentration was manipulated in an effort to understand how changes in CSF protein concentration may affect inflammatory cell adhesion on native and oxidized PDMS in the treatment of hydrocephalus. A recent study showed that 23% of shunt systems that were removed because of obstruction or infection were from patients with protein concentration greater than 1.0 g/L [174]. Generally, the high protein concentration enhanced cell adhesion under fluidic conditions, but this trend was not significant. Using PDMS catheters, extrapolation of these acute patterns suggests that patients with a higher concentration of CSF protein may be more likely to have an inflammation-related obstruction. Clinically, it is more likely for patients with abnormal CSF (high protein, many cells) to have an obstruction [191], and although higher CSF protein content by itself does not cause proteins to obstruct catheters [175], an increasing protein concentration may influence cell attachment. This relationship has been shown using culture media where serum influences macrophage [183] and neural-glial [173] adhesion *in vitro*. Because altering the total protein and albumin concentrations in culture media is not identical to alterations in the protein content of CSF, future studies will attempt to compare these results with those obtained when cells are suspended in human CSF.

4.4.4 Impact of conditions on macrophage and astrocyte morphology

Because the morphology varied depending on the presence or lack of flow, using a pulsatile flow system like the bioreactor seems essential in mimicking some of the mechanical factors seen in the ventricular cavity *in vivo.* The morphology of the macrophages changed dramatically with the addition of flow. Under static culture conditions on PDMS, macrophages exhibited extended processes, but these were less pronounced on OH-PDMS, especially when a low concentration of protein was used. Under fluidic conditions, these extended processes were not visible. Actin without vinculin termination may infer cell perturbation by mechanical shear since shear can affect actin and vinculin distribution [192]. The minimal filopodial extension can be interpreted as the cell's lack of effort to spread under fluidic conditions, or the initiation of cell necrosis. The rounded morphology of astrocytes under both static and fluidic conditions might also indicate that the acute 20-hour incubation period was not long enough for cells to extend their processes. Clumping of astrocytes with curious dislocation between the GFAP and cell nuclei may be indicative of nonpermissive surfaces. Previous reports have indicated that astrocytes bound to CNS implants after 8 days of implantation are hypertrophied [182]. After an acute 20-hour exposure to our flow system, astrocytes did not appear enlarged compared with the static culture. Future work prolonging the incubation time of these experiments may allow a comparison between these responses.

4.5 Conclusions

This study is one of the first that attempts to examine the relationship between surface chemistry and cell attachment in a bioreactor that mimics the pulsatile flow mechanics of the cranial cavity. Plasma-oxidized PDMS inhibited macrophage binding compared with native PDMS, while flow significantly exacerbated astrocyte but not macrophage adhesion. The quantity of astrocyte adhesion was greater than macrophage adhesion under fluidic conditions but generally less than macrophage adhesion under static conditions. Thus, to inhibit both macrophage and astrocyte attachment on shunt systems used in hydrocephalus, both the surface chemistry and the flow rate should be modified by long-term surface modifications and alterations in catheter architecture. Surprisingly, protein concentration by itself did not have a significant impact on attachment, although a trend toward increased attachment with greater total protein concentration was apparent. The morphology of adherent cells was affected by flow, but this effect was seen more with macrophages than astrocytes.

Table 7 Average percent blue in dRGB space (± SEM)

	PDMS Low Protein	PDMS High Protein	OH-PDMS Low Protein	OH-PDMS High Protein
Macrophage Static Conditions	1.07 ± 0.19	3.16 ± 0.69	1.20 ± 0.18	1.26 ± 0.14
Macrophage Fluidic Conditions	3.94 ± 0.25	4.07 ± 0.67	1.52 ± 0.40	0.46 ± 0.31
Astrocyte Static Conditions	1.90 ± 0.08	0.27 ± 0.10	0.79 ± 0.10	0.68 ± 0.18
Astrocyte Fluidic Conditions	3.93 ± 1.30	9.94 ± 1.30	3.67 ± 1.08	8.02 ± 3.33

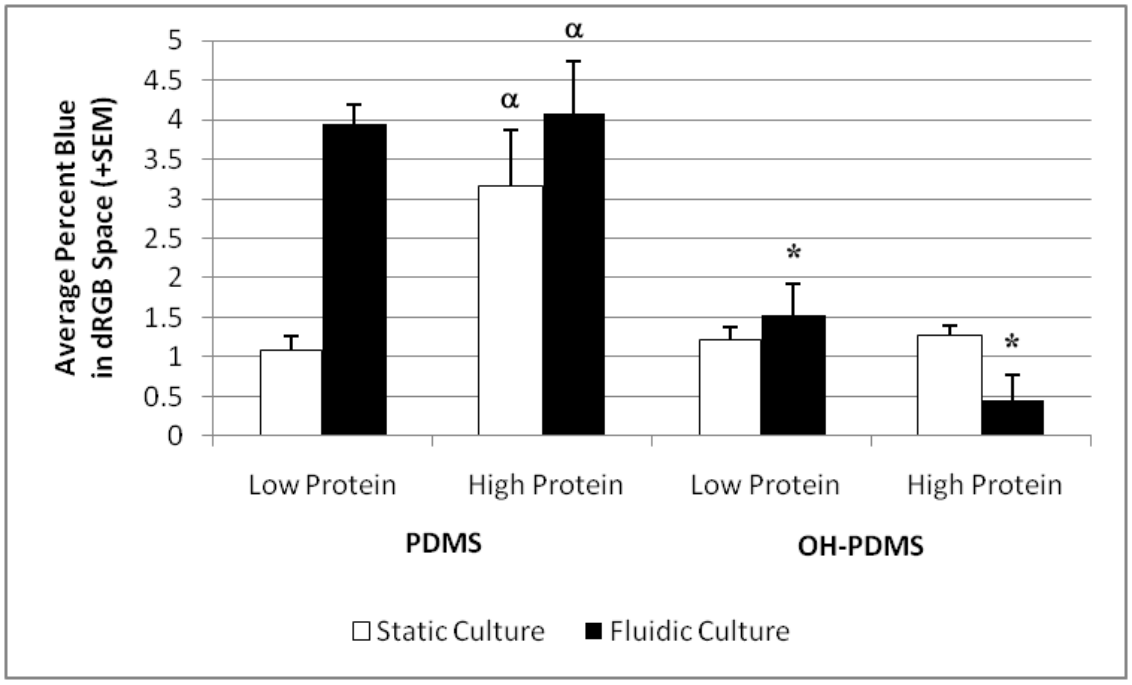

Figure 22 The average percentage of blue in dRGB space as determined by analysis of macrophage DAPI intensity. Although each tested component had an impact on adhesion, the most dramatic difference was caused by the addition of surface hydroxyl groups (OH-PDMS). Statistical significance was determined using a Kruskal Wallis H Test. An asterisk (*) denotes a significant difference ($P < 0.05$) in adhesion compared to adhesion in low protein and flow on PDMS; α denotes a significant difference ($P < 0.05$) in adhesion compared to adhesion in high protein and flow on OH-PDMS. A sample size of 12 was used for each group.

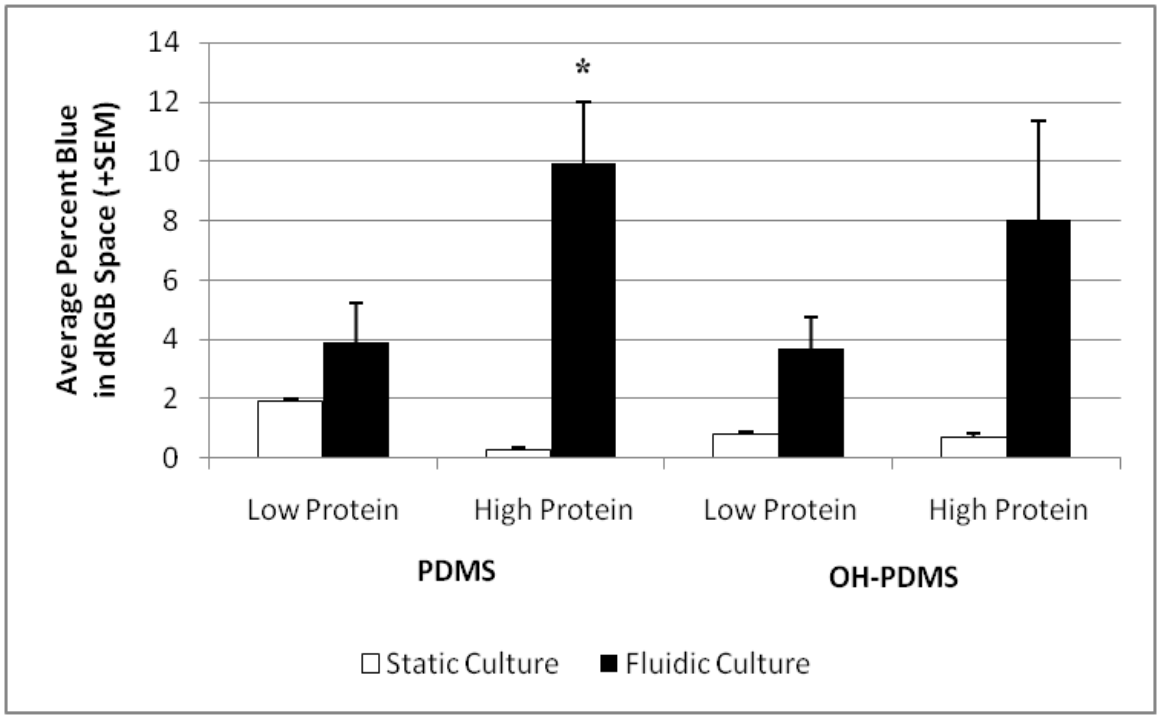

Figure 23 The average percentage of blue in dRGB space as determined by analysis of astrocyte DAPI intensity. A trend in intensity suggests that flow, protein concentration, and the addition of surface hydroxyl groups altered adhesion, but flow had the most apparent impact on astrocytes adhesion. Significance is denoted by an asterisk where * indicates significance compared to adhesion in high protein and static conditions on PDMS as determined using a Kruskal Wallis H Test. A sample size of 12 was used for each group.

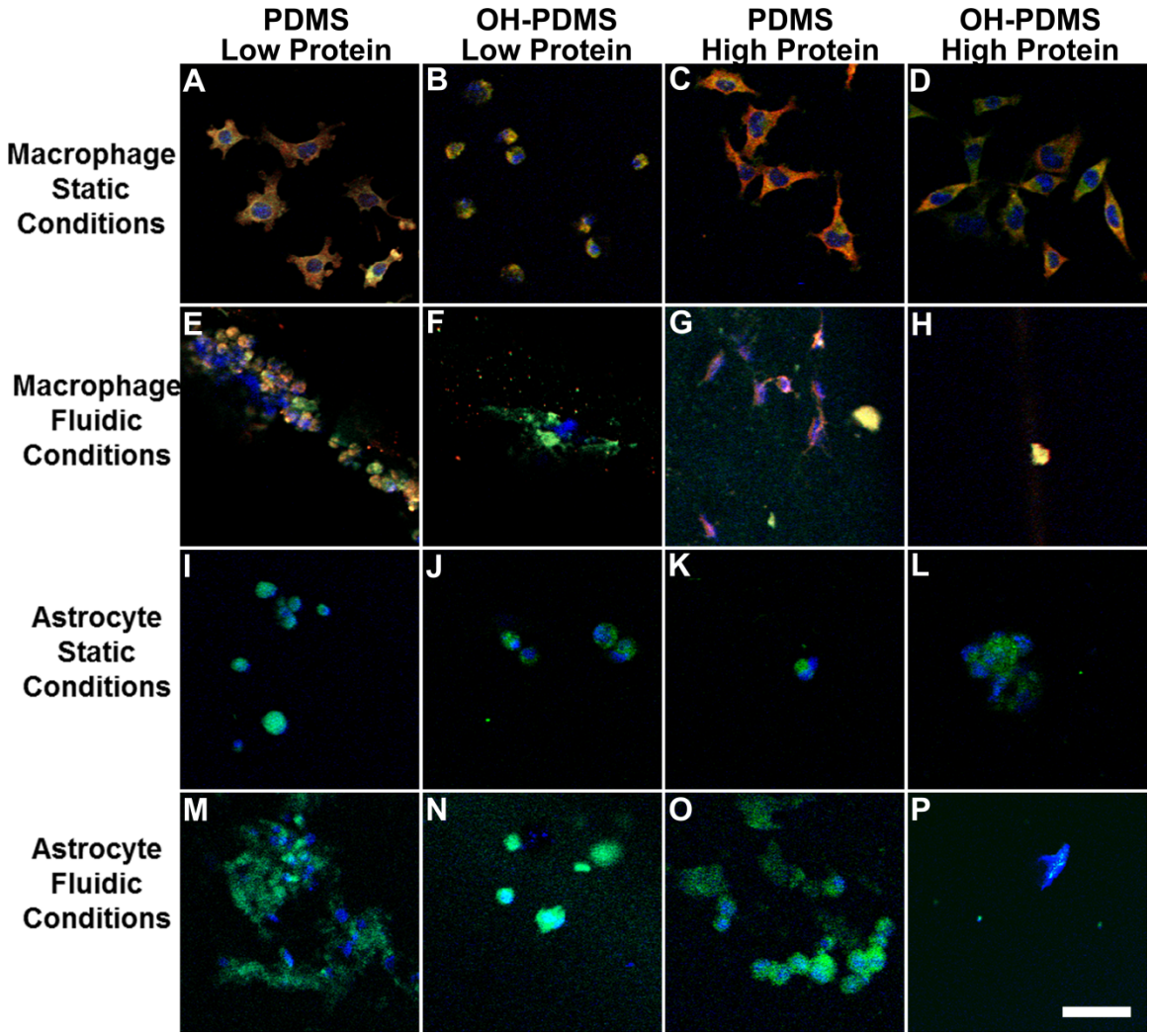

Figure 24 Macrophage (A-H) and astrocyte (I-P) attachment on PDMS and OH-PDMS under the indicated conditions. Morphologically, macrophages appeared to have extended processes in static conditions but retracted processes in flow conditions (compare A and E, C and G, and D and H). Cellular processes of adherent astrocytes did not appear extended. Astrocytes appeared to clump on OH-PDMS under static or flow conditions (compare J and N and L and P). Actin has been fluorescently stained in red (macrophages), vinculin in green (macrophages), GFAP in green (astrocytes), and DAPI in blue (macrophages and astrocytes). Scale bar denotes 50 μm in all panels.

CHAPTER 5

REDUCTION OF PROTEIN ADSORPTION AND MACROPHAGE AND ASTROCYTE ADHESION ON VENTRICULAR CATHETERS BY POLYETHYLENE GLYCOL AND N-ACETYL-L-CYSTEINE[3]

5.1 Introduction

Hydrocephalus, a condition resulting from an imbalance between cerebrospinal fluid (CSF) production and absorption, is a chronic disorder affecting 1 in 500 individuals, particularly children. In most cases of hydrocephalus the cerebral ventricles expand and intracranial pressure (ICP) rises dramatically. Implanting a poly(dimethyl)siloxane (PDMS) catheter into the lateral ventricles allows drainage of CSF from the cranial cavity, lowering the ICP to safe levels. While this type of shunt treatment is usually effective temporarily, revisions are often necessary as current shunt systems are plagued with occlusion-related failure. In a clinical study intended to decipher methods of failure, 61.7% of the 344 patients undergoing first-time shunt placements had failure of the shunt due to obstruction [42]. Previous results using scanning electron microscopy and histological analysis [44, 49, 108, 116] show that a

---

[3] From Journal of Biomedical Materials Research: Part A, submitted manuscript, Harris, CA; Resau, JH; Hudson, EA; West, RA; Moon, C; Black, AD; McAllister JP "Reduction of protein adsorption and macrophage and astrocyte adhesion on ventricular catheters by polyethylene glycol and N-acetyl-L-cysteine."

high percentage of obstructions contain choroid plexus, microglia/macrophages, and astrocyte cells.

There has been a tremendous effort to inhibit protein adsorption and subsequent cell attachment on medical devices [63-64, 85, 193-194] that may elicit responses such as shunt obstruction. Surface treatments are often chosen based on the application of the medical device, the desired reaction, and the underlying material. One surface treatment that has shown great potential to reduce protein adsorption on many medical devices is polyethylene glycol (PEG) [195-198]. For oral and topical applications, polyethylene oxide has been approved by the U.S. Food and Drug Administration; has been investigated as a medical device coating; has been used as a drug carrier; has shown applicability in tissue engineering [199-200], and has been applied to nanotechnology [201]. PEG is a nondegradable hydrophilic polymer and, depending on the deposition method when used as a coating, is stable over time. PEG inhibits proteins with and without cell adhesive ligands [202]. PEG has been shown to inhibit cell adhesion [195], probably because the adsorbed protein layer is critical for subsequent interactions with a variety of cell types.

The mechanisms of inhibition by PEG-modified surfaces depend upon PEG surface density and molecular weight [78]. Often, a decrease in molecular weight of coatings correlates with an increase in surface grafting density and an increase in protein adsorption [195, 203-204]. We hypothesized that these relationships would continue to hold and that macrophages and astrocytes, two cells known to obstruct shunt catheters,

would be inhibited more by high-molecular-weight PEG than by the lower-molecular-weight PEG in a fluidic environment similar to that seen in the cerebral ventricles.

A pharmacologic agent that has recently been used as a surface modifier is N-acetyl-L-cysteine (NAC). NAC is a hydrophilic pharmacologic agent used most often to inhibit mucous overproduction by hydrolyzing glycosaminoglycans through the breakdown of disulfide bonds. Their distinctive sulfhydryl moieties can also interact with and terminate reactive oxygen species in its conversion to glutathione, making NAC a useful supplementary antidote to oxidative stress. NAC sulfhydryl groups can characteristically and nonspecifically reduce cytoplasmic proteins by converting cystine to cysteine. NAC has been successfully bound to stainless steel, and previous data suggest that these coated surfaces deter bacterial biofilm formation [205]. Because cell propensity to bind, grow, differentiate, and proliferate on biomaterials is highly dependent on specific interactions of the adsorbed protein layer ligands and transmembrane integrins, we chose to investigate whether PDMS modified with NAC via adsorption and covalent techniques would inhibit protein adsorption. We hypothesized that NAC would inhibit protein adsorption and macrophage and astrocyte adhesion in a fluidic environment that mimics flow in the cerebral ventricles.

In this work, we tested PEG and NAC surface modifications using our previously published in vitro model incorporating pulsatile flow because it mimics many dynamics of the cerebral ventricles [140]. Because protein adsorption provides a means for facilitating host cell adhesion, we performed a feasibility experiment to explore the use of

the protein attachment inhibitor molecule PEG and the disulfide reducer N-acetyl-L-cysteine (NAC) to inhibit protein adsorption and cell attachment.

5.2 Materials and Methods

5.2.1 Fabrication of PEG and NAC modified PDMS

Medical grade silicone tubing (PDMS) was obtained from Dow Corning (Midland, MI). A subset of tubing used for each modification type was placed in an O_2 Plasmod plasma chamber and held at 200 mTorr to convert surface methyl groups to surface hydroxyl groups, forming oxidized PDMS (OH-PDMS).

PEG604 (2-(methoxy(polyethyleneoxy)propyl)trichlorosilane, Gelest, Covington, KY, 472–604 Da) was immobilized on OH-PDMS by forming an attachment between the silane and the PDMS surface hydroxyl groups by way of chemical vapor deposition. To achieve this, 3 mL of 10% (v/v) of PEG-Cl_3 in deionized water was added to a 50-mL Erlenmeyer flask. Tubes were suspended over the flask and covered using a PDMS sheet and electrical tape. The reaction container was set on a hot plate for 12 hours at 95°C similar to previously established methods [206]. Tubes were then removed and washed in 0.1 M phosphate-buffered saline (PBS).

PEG5K (5000 Da) was immobilized on PDMS using methods similar to those described by Chen and colleagues [207]. OH-PDMS tubes were immersed in a 40% w/v solution of PEG methyl ether (Sigma-Aldrich, St. Louis, MO) in isopropanol. A platinum catalyst (platinum–divinyltetramethyldisiloxane complex) was added at a ratio of 1 drop to 3 mL of PEG solution. The solution was allowed to react with the tubing for

15 hours at room temperature on a rotator before the tubes were removed and washed in 0.1 M PBS.

NAC was immobilized onto the surface of OH-modified PDMS using two methods. In the first method, OH-PDMS was immersed into an NAC-rich solution (4 mg/mL in deionized water) for 24 hours at room temperature to induce physical adsorption (NAC-OH-PDMS) similar to studies where NAC was used to modify the surface of stainless steel [205]. In the second method, OH-PDMS was immersed into an NAC-rich solution (4 mg/mL in deionized water) with N-hydroxysuccinimide (NHS) and 1-ethyl-3-(3-dimethylaminopropyl) carbodiimide) (EDC) additives each at 2.5 mg/mL to activate the carboxylic acid groups of NAC and enhance coupling of the carboxylic acid groups to the hydroxyl groups. The pH of the NAC-rich solution ranged from 2.25 to 2.29 and when EDC and NHS were added, 2.84 to 2.86. In a subset of samples, the pH was increased to 6.0 using 40X PBS to encourage attachment. However, attachment in these conditions was less than optimal so the use of NAC at pH 6.0 was discontinued (unpublished results).

5.2.2 Surface characterization

Water contact angles (the angle created at a solid surface interface from interactions with water and gas) and X-ray photoelectron spectroscopy (XPS) were used to characterize the surface treatments in this study. Contact angles of PDMS, OH-PDMS, and NAC-OH-PDMS were obtained using a contact angle goniometer. Advancing and receding water contact angles were measured using approximately 20 μL of double-

distilled deionized water. Data on the chemical composition for all samples were attained from the National ESCA and Surface Analysis Center for Biomedical Problems (NESAC/BIO) (n=3 with 3 random spots collected per sample). XPS spectra were taken on a Surface Science Instruments S-probe spectrometer equipped with a mono-chromatized Al Kα X-ray and a low-energy electron flood gun. The pressure in the chamber during acquisition was less than 5E-9 Torr. Pass energy was 150 eV and 50 eV for survey spectra and high-resolution scans, respectively. The take-off angle was set at 55°, correlating with a 50 Å sampling depth. Elemental composition calculations were made using the Service Physics ESCAVB Graphics Viewer. Three spots were measured on each sample, and a minimum of three samples were used for analysis.

5.2.3 Modification stability

To determine whether the PEG and NAC modifications remained bound to the PDMS over time, a soak test was performed where samples were soaked in deionized water for 30 days at room temperature. Progressive water contact angles were taken using the contact angle goniometer over this time course.

Because of the novelty of NAC coatings on PDMS, a second method was used to measure the stability of the coatings. A subset of NAC-OH-PDMS and NAC/EDC/NHS-OH-PDMS samples was immersed in 0.1 M PBS. Release of NAC into the PBS solution was measured using the A280 assay at 260 and 280 nm on a ND-1000 NanoDrop Spectrophotometer (Thermo Scientific, Waltham, MA) successively for six days. From

previous analysis of NAC absorbance spectra, NAC peak absorbance is approximately 260 nm.

5.2.4 Protein adsorption assay

To determine the effect of PEG and NAC modifications on protein adsorption, samples were exposed to a flowing protein solution at 0.3 mL/min and 37° for 20 hours. The solution was composed of an equal percent of 100 mg/L fibronectin (Fn, a mammalian extracellular matrix glycoprotein present in CSF that, when adsorbed, can encourage cell attachment [208]) and 400 mg/L albumin (Alb, a protein nonfacilitative to mammalian cell adhesion present in CSF) similar to previously established methods [209]. PDMS and oxidized PDMS (OH-PDMS) controls were also exposed to the flowing protein solution for comparison with modified samples. Following exposure, samples were processed for immunofluorescent staining using 4% (w/v) paraformaldehyde in PBS for two hours. Samples were immediately rinsed and stored in 0.1 M PBS overnight at 4°C. Tubing was cut longitudinally to expose the lumen. Samples were then batch stained with polyclonal rabbit anti-bovine fibronectin (Cedarlane Labs, Burlington, Ontario, CA) and polyclonal goat anti-rabbit IgG conjugated with tetramethyl rhodamine isothiocyanate (TRITC) (Santa Cruz Biotechnology, Santa Cruz, CA) to label fibronectin, and polyclonal sheep anti-bovine albumin conjugated with FITC (Bethyl Labs, Montgomery, TX) to label albumin. Confocal microscopy was performed using a FV1000-XY Confocal Olympus IX81 microscope at 10X for semiquantitative analysis of TRITC and FITC fluorescent

intensities. Data for each condition (n=3) were pooled, a stained negative control was subtracted, and data were analyzed for statistical significance.

5.2.5 Macrophage and astrocyte culture

To determine the degree of adhesion of macrophages and astrocytes, *Mus musculus* IC-21 macrophages and primary rat astrocytes were obtained as described previously [140, 210]. Macrophages were cultured in RPMI-1640 with 25 mM 4-(2-hydroxyethyl)-1-piperazineethanesulfonic acid (HEPES), 1% penicillin–streptomycin (Sigma, St. Louis, MO), 1% GlutaMAX (Sigma, St. Louis, MO), 1% sodium pyruvate (Invitrogen, Carlsbad, CA), and 10% fetal bovine serum (FBS, Sigma, St. Louis, MO); astrocytes were cultured in an identical medium without the addition of sodium pyruvate. Cells were split at 80% confluence and seeded in T-75 Culture Flasks (ISC Bioexpress, Kaysville, UT).

Twenty-four hours before cell passaging for experimental analysis, cells were soaked in a low concentration of albumin-rich medium to acclimatize them to the total protein (208.1 mg/L) and albumin concentration (155 mg/L) of normal CSF. Cells were removed after several washing steps with noncationic Dulbecco's Phosphate Buffer Solution (DPBS, Invitrogen, Carlsbad, CA) by a 5-min exposure to 1X TrypLE Express (Invitrogen, Carlsbad, CA) at 37°C. Macrophage agitation by mechanical perturbation guaranteed suspension. Cells were washed and resuspended through centrifugation at 1200 rpm for 10 min in RPMI-1640. Using the trypan blue exclusion test, viable cells were counted on a hemocytometer. While still in suspension, cells were collected at a

concentration of 4.615E4 cells/ml to equal 3E6 cells total. The concentration of cells coincided with similar studies of catheter obstruction [133].

5.2.6 Hydrocephalus shunt catheter bioreactor setup

Our previously published *in vitro* model developed to study cellular adhesion under pulsatile flow conditions that mimic those of the cerebral ventricles was used in this study [140]. Suspended cells were propelled through this pulsatile flow system and through the PDMS (or modified PDMS) sample tubing at 0.3 mL/min with a pulsation rate of 100 pulses/min for 20 hours. Following exposure, PDMS or modified PDMS tubing was removed and immediately placed in fixative (4% paraformaldehyde). Samples were then longitudinally cut to expose the tubing lumen and the attached cells.

Immunofluorescence was used to identify the cell concentration and morphology of the attached cells using actin (a major protein of the cytoskeleton), vinculin (a cytoskeletal focal adhesion protein at the intracellular face of the plasma membrane that is one of the major mediators linking actin to integrins to permit cell anchorage/spreading), and cell nuclei staining for macrophages and glial fibrillary acidic protein (GFAP) and nuclei staining for astrocytes. Macrophages bound and fixed to PDMS samples were permeabilized in anhydrous methyl alcohol for 15 min. Tubing halves were then batch stained with 1:300 polyclonal sheep anti-actin (Chemicon, Temecula, CA) identified with 1:100 Cy3-conjugated polyclonal secondary antibody (Chemicon). Macrophage focal adhesions were identified using 1:300 monoclonal mouse anti-vinculin (Chemicon) and 1:100 FITC-labeled polyclonal goat anti-mouse IgG

H+L (Chemicon). Astrocytes attached to PDMS or modified PDMS tubing were stained with 1:300 monoclonal mouse anti-GFAP (Chemicon) and observed using 1:100 polyclonal goat anti-mouse IgG H+L (Chemicon). All tubing was counterstained with the nuclear dye 4',6-diamidino-2-phenylindole (DAPI).

5.2.7 Imaging and data collection

PEG- and NAC-modified samples were compared with PDMS and OH-PDMS controls using a Zeiss 510 microscope to obtain spectral epifluorescent images. Zeiss LSM image analysis software was used for characterizations. Quantitative analysis of the percent intensity of DAPI was attained (n=12 with 2 random spots analyzed per tube half, Neurolucida, Micro Bright Field, Williston, VT) by analyzing the blue component of each image in digital Red-Green-Blue (dRGB) space and reporting it as a percent of total light emission, with 255 representing brightest light emission. For each sample, background intensities were subtracted.

5.2.8 Statistical analysis

The Anderson-Darling normality test was used to determine data normalcy. Parametric results were examined using a one-way analysis of variance with α set at 0.05 followed by a post-hoc Scheffe test. Nonparametric results were compared using the Kruskal Wallis H test followed by a least significance difference in mean ranks test with α set at 0.05.

5.3 Results

5.3.1 Generation and analysis PEG and NAC modified PDMS

Increased wettability and decreased water contact angle compared with the PDMS control were clearly evident immediately after modification of PEG and NAC using all methods (Figure 25). Fluctuation between the advancing and receding contact angles implies either some surface non-uniformity, particulate on the measured surface, or inadequate measuring technique. The stability of PEG and NAC appeared relatively constant, with no advancing contact angle reaching the advancing contact angle for PDMS (104.23±1.02°) after 30 days (Figure 26). At 30 days, the advancing water contact angle of PDMS was significantly greater than those of all modified samples, PEG604 was greater than PEG5K, and NAC was greater than NAC/EDC/NHS (P<0.05).

We measured the release of NAC by measuring the decay of the 260-nm peak over time. The additive level of NAC released over time from NAC/EDC/NHS-OH-PDMS was considerably higher than that of NAC-OH-PDMS and plateaued near 4.8 absorbance units/mL (Figure 27). NAC-OH-PDMS did not appear to release NAC. After three days, the difference in inferred NAC release between NAC/EDC/NHS-OH-PDMS and NAC-OH-PDMS was significant (P<0.05). No peaks were found at 280 nm.

XPS was performed with an approximate depth of 50 Å to obtain surface characterization. Low-resolution XPS results are shown in Table 8, and high-resolution results are shown in Table 9. A presence of PEG was evident from a significant (P<0.05) increase in O 1s in both PEG604 and PEG5K samples, a significant decrease in C 1s in the PEG5K samples, and no significant difference in Si 2p (P=0.19 and 0.44,

respectively). The C 1s spectra of these samples revealed a peak at approximately 286.4 eV indicative of a C-O species that was not seen in the PDMS controls. This peak represented a greater percent of the C 1s spectra for the PEG604 sample, but this difference was not significant (P=0.24). The ratio of C-O (286.4 eV) to C-Si (284.3 eV) of PEG604-OH-PDMS (0.27 with experimental error) is nearly twice that of PEG5K-OH-PDMS (0.16 with experimental error). This indicates an increased grafting density [203] of PEG on OH-PDMS when PEG604 is used. NAC-OH-PMDS presented with an increase in O 1s, N 2p, and S 2p and a decrease in Si 2p where NAC/EDC/NHS-OH-PDMS had a significant increase in O 1s (P<0.05), but there was no indication of N 2p or S 2p. The high-resolution C1s spectra revealed a decreased percentage of hydrocarbon peaks or C-Si peaks at 285.0 eV, an increased percentage of C-O or amine species, and an increase in H-O-C=O or amide species relative to the PDMS control (Table 9). There was no significant difference between the C 1s spectra of the NAC modifications (P=0.72 at 286.4 eV and P=0.81 at 288.6 eV).

5.3.2 Modified surfaces decrease albumin and fibronectin adsorption

The inhibition of albumin adsorption in order from greatest to least was NAC > NAC/EDC/NHS > PEG5K > PEG604 (Figure 28). These decreases in albumin adsorption from the PDMS control were significant when surfaces were treated with PEG5K (P<0.01), NAC (P<0.05), and NAC/EDC/NHS (P<0.01). There was no significant difference in albumin adsorption between the PEG604- and PEG5K-modified

samples (P=0.14), nor was there a significant difference in albumin adsorption between the NAC and NAC/EDC/NHS modification methods (P=1.00).

The inhibition of fibronectin adsorption in order from greatest to least was PEG604 > PEG5K > NAC/EDC/NHS > NAC (Figure 28). PDMS had significantly more bound fibronectin than all other samples (P<0.01). Compared with the OH-PDMS control, PEG604-OH-PDMS, PEG5K-OH-PDMS, and NAC/EDC/NHS-OH-PDMS all had significantly less fibronectin adsorption after the 20-hour exposure (P<0.05). Further, PEG604- and PEG5K-modified samples had significantly less fibronectin adsorption than the NAC-modified sample without EDC or NHS (P<0.05). There was no significant difference in fibronectin adsorption between the PEG604- and PEG5K-modified samples (P=1.00), but there was a significant increase in fibronectin adsorption on NAC-OH-PDMS as compared with NAC/EDC/NHS-OH-PDMS (P<0.05).

5.3.3 Modified surfaces decrease macrophage and astrocyte binding

As determined by the average percent of DAPI intensity in the confocal images, the inhibition of macrophage adherence in order from greatest to least was PEG5K > NAC/EDC/NHS > PEG604 > NAC (Figure 29, Figure 30). Using similar methods, the inhibition of astrocyte adherence in order of greatest to least was NAC > PEG5K > NAC/EDC/NHS > PEG604 (Figure 29, Figure 30). That is, immobilized PEG604, PEG5K, NAC, and NAC/EDC/NHS reduced the average level of macrophage adhesion by 53%, 63%, 40%, and 58% (P<0.05 when comparing each case except NAC to PDMS), and reduced the average level of astrocyte adhesion by 47%, 83%, 91%, and

72% (P<0.05 when comparing each case except PEG604 to PDMS), respectively. The degree of macrophage adhesion seemed somewhat linearly dependent on contact angle and therefore surface wettability (R^2 value = 0.742) whereas astrocyte adhesion seemed less linearly dependent (R^2 value = 0.152) on surface wettability with the least amount of adhesion on NAC-OH-PDMS (with contact angle ~58°). Compared with the PDMS control, all modifications significantly reduced macrophage (P<0.05) and astrocyte (P<0.05) adhesion, excluding the difference in macrophage adhesion between NAC and PDMS and the difference in astrocyte adhesion between PEG604 and PDMS. The difference in macrophage adhesion between the PEG604 and PEG5K modifications was insignificant, as was the difference in astrocyte adhesion between the same samples. The difference in macrophage attachment was insignificant between NAC and NAC/EDC/NHS modifications, as was the difference in astrocyte adhesion between NAC samples.

5.4 Discussion

5.3.4 PEG modified PDMS

The significant difference in initial advancing water contact angle between the PEG-modified samples and PDMS together with XPS data showing increased surface C-O on PEG-modified surfaces indicated that modified surfaces are rich with PEG. Neither PEG604- nor PEG5K-modified PDMS contact angles returned to PDMS levels, but the PEG5K-modified PDMS appeared to maintain a lower contact angle over time. The ratio of C-O to C-Si bonds indicated a higher grafting density of PEG using PEG604 than

with PEG5K; however, this is expected because molecular weight and grafting density have been shown to be inversely proportional [203-204]. The difference in mean initial advancing and receding water contact angle between PEG604-OH-PDMS (7.2) and PEG5K-OH-PDMS (29.8) also alludes to less uniformity (and decreased grafting density) on PEG5K-modified PDMS.

Both PEG604-OH-PDMS and PEG5K-OH-PDMS decreased albumin adsorption compared with PDMS, by 55% and 90%, respectively, but this trend was only significant at the P.05 level when PEG5K-OH-PDMS was compared with PDMS. The decrease in albumin adsorption on higher-molecular-weight PEG5K also corresponds to previously published results [204]. While albumin lacks motifs recognizable by host cells, enhanced adsorption may provide a gateway for bacterial colonization and biofilm formation, so an inhibition of albumin was preferred. Fibronectin adsorption was decreased by 98% on both PEG samples compared with PDMS, and macrophage adhesion was significantly decreased on both PEG modifications. However, there was a clear (but not significant) difference in the astrocyte response that correlated to the Fn response to both surfaces, suggesting that PEG5K inhibited more than PEG604. We can speculate that the increase in molecular weight permitted increased chain mobility. This increase in mobility may have been less conducive to astrocyte adhesion because astrocytes are particularly sensitive to mechanical stresses [165] or it may simply have been that the proinflammatory response of astrocytes on PEG5K is less than the proinflammatory response of astrocytes on PEG604. These analyses indicate an area of future work.

We conclude from the experiments with PEG that 1) PEG can be immobilized on oxidized PDMS and these modifications are relatively stable over time; 2) PEG-modified samples decrease initial protein adsorption and cell binding; and 3) PEG5K is preferential to PEG604 to inhibit inflammatory-derived adhesion in a fluidic and pulsatile environment. Together with data indicating that PEG attenuates the acute macrophage/microglia response and the long-term astrocyte response [211], we speculate that PEG immobilization onto shunt catheters may provide an effective alternative to PDMS shunt catheters that commonly occlude with macrophages/microglia and astrocytes.

5.3.5 NAC modified PDMS

The advancing and receding water contact angle of NAC-modified PDMS with and without EDC and NHS was significantly lower than that of PDMS. From low-resolution XPS analysis and deconvolution of the C1s spectra, we can infer a presence of NAC on the surface of PDMS both by the existence of sulfur on NAC-OH-PDMS surfaces and by the enhanced C-O (at 286.4 eV) and O-C=O/amide species (at 288.6 eV) on both NAC-OH-PDMS and NAC/EDC/NHS-OH-PDMS. The ratio of mean O-C=O/amide species to C-Si can allude to the NAC grafting density on NAC-OH-PDMS (0.0526 with experimental error) and NAC/EDC/NHS-OH-PDMS (0.0418 with experimental error). These data imply that the concentration of NAC is low and similar between NAC-OH-PDMS and NAC/EDC/NHS-OH-PDMS after exposure.

Water contact angle measurements after a 30-day incubation in distilled water revealed that NAC-modified PDMS surfaces maintained significantly lower wettability (and increased hydrophilicity) compared with PDMS over time. However, absorbance spectra revealed that NAC was released from NAC/EDC/NHS-OH-PDMS but not from NAC-OH-PDMS. Assuming that NAC/EDC/NHS-OH-PDMS releases NAC despite maintenance of hydrophilicity over time, we can speculate that released NAC can non-specifically inhibit macrophage attachment upon release. It may be that released NAC can reduce the disulfide groups of adsorbed proteins and also of attaching cell integrins in a cell-type–dependent manner. However, a major concern related to the release of NAC is that prolonged attachment may be needed on shunt catheters that are implanted in patients for long periods of time.

Both methods of NAC immobilization on PDMS decreased albumin adsorption, fibronectin adsorption, and astrocyte adhesion significantly ($P<0.05$) compared with the PDMS control. The relative degree of astrocyte adhesion on NAC modified surfaces also correlated to the relative Fn response to both surfaces. Additionally, a trend indicated that NAC inhibited macrophage adhesion which was significant ($P< 0.05$) when PDMS was compared to NAC/EDC/NHS-OH-PDMS but not to NAC-OH-PDMS. The mechanisms of NAC protein and cell inhibition on PDMS are still speculative and are probably multi-factorial. NAC bound or in solution can reduce bacterial growth *in vitro* [205]. After traumatic brain injury, NAC in solution has been shown to decrease cytokines present under proinflammatory conditions [212], decrease nuclear factor kappa B (NF-κB), interleukin-1 beta (IL-1β), tissue necrosis factor-alpha (TNF-α), and inter-cellular adhesion molecule-1 (ICAM-1) [212], and block induction of TNF-α, IL-1β,

interferon-gamma (IFN-γ), and inducible nitric oxide synthase (iNOS) [213]. Whether NAC is released (in solution) or is bound to PDMS, it may modify acute protein adsorption and cell adhesion by hiding or modifying cell adhesion ligands. In this study, the antibody used in immunofluorescent analysis of fibronectin targeted the cell adhesion ligand arginine–glycine–aspartic Acid (RGD). The 75% mean reduction in RGD on NAC-OH-PDMS and 97% NAC/EDC/NHS-OH-PDMS surfaces compared with PDMS suggests that NAC may either passively inhibit adsorption because of its hydrophilic nature or actively cause a scission or change in protein folding that hides the cell adhesion ligands. If this process is active, then chronic cell adhesion may also be inhibited because of the seemingly permanent changes in the adsorbed protein layer. The effects of NAC on chronic adhesion have not been reported and are a source of future work.

We conclude from these experiments with NAC that 1) NAC can be immobilized on oxidized PDMS where the hydrophilicity is stable over time but components of NAC are released from NAC/EDC/NHS-OH-PDMS; 2) NAC-modified samples decrease initial protein adsorption and cell binding; and 3) bound NAC (NAC-OH-PDMS) inhibits astrocyte binding more than surface-attached and releasing NAC (NAC/EDC/NHS-OH-PDMS), although these relationships are not significantly different. Because a trend indicates that NAC/EDC/NHS-OH-PDMS inhibits fibronectin adsorption and macrophage binding more than NAC-OH-PDMS, NAC/EDC/NHS-OH-PDMS may combat inflammatory cell obstruction in the short term more adequately than NAC-OH-PDMS, but the release of NAC from NAC/EDC/NHS-OH-PDMS

together with the enhanced inhibition of astrocyte adhesion on NAC-OH-PDMS may implicate NAC-OH-PDMS as the preferred NAC modification for long-term applicability.

PEG and NAC are two polymers that may inhibit protein adsorption, cell adhesion, and subsequent inflammatory cell obstruction of shunt catheters used in the treatment of hydrocephalus. Both are hydrophilic, with an initial mean advancing water contact angle ranging from 33 to 65°. While cell adhesion involves an array of factors, it is certainly dependent on surface chemistry as well as the conditions in which the catheter is implanted *in vivo.* A trend in our previous work suggests that hydrophilic surfaces inhibit macrophage adhesion more so than astrocyte adhesion in the acute term depending on flow conditions that mimic those in the cerebral ventricles [210]. The data presented here support our previous work by suggesting that, while both macrophage and astrocyte adhesion is inhibited on hydrophilic surfaces, macrophage adhesion is more linearly dependent on surface wettability than is astrocyte adhesion. Likely, the inhibition seen on PEG and NAC modified surfaces results from a combination of the surface wettability, the flow conditions, and the unique properties of PEG (e.g. steric hindrance) and NAC (e.g. disulfide reduction).

The only marketed hydrophilic surface coating used in the treatment of hydrocephalus, the poly(vinylpyrrolidone)-grafted catheter, was developed for increased lubricity but was shown to induce abscess formation *in vivo* [128]. Despite the success of other hydrophilic surface coatings *in vivo,* hydrophilic modifications have not been used to inhibit inflammatory adhesion in the treatment of hydrocephalus. The extensive history and success of PEG-modified medical devices make PEG a logical candidate to

inhibit inflammatory cells that occlude catheters. The unique properties of NAC also make it an interesting candidate to inhibit adhesion because of its novelty, biocompatibility, and bacterial inhibition. Although PEG and NAC did have a dramatic effect on adsorption and binding compared with PDMS, the two binding strategies of PEG and the two of NAC used in this study did not produce any significant differences in acute albumin adsorption when they were compared with each other. Both PEG modifications had significantly less surface-adsorbed fibronectin than did NAC-OH-PDMS ($P<0.05$), but because macrophage and astrocyte adhesion was not significantly different between the PEG modifications and NAC-OH-PDMS, we cannot say that NAC-OH-PDMS should be ruled out. In fact, the data reveal a trend that suggests that NAC-OH-PDMS decreased astrocyte adhesion more than the other modification strategies.

5.5 Conclusions

In a bioreactor mimicking fluid flow within the cerebral ventricles, PDMS shunt tubing was modified with PEG and NAC to decrease macrophage and astrocyte adhesion that occludes catheters. The inhibition of albumin adsorption in order of greatest to least was NAC > NAC/EDC/NHS > PEG5K > PEG604 and the inhibition of fibronectin adsorption in the same hierarchy was PEG604 > PEG5K > NAC/EDC/NHS > NAC. The inhibition of macrophage adherence in order of greatest to least was PEG5K > NAC/EDC/NHS > PEG604 > NAC and the inhibition of astrocyte adherence in the same ordering system was NAC > PEG5K > NAC/EDC/NHS > PEG604. Because of a significant decrease in both macrophage and astrocyte adhesion on PEG5K-OH-PDMS

compared with PDMS and on NAC/EDC/NHS-OH-PDMS compared with PDMS, these surface treatments have potential to inhibit macrophage and astrocyte dependent occlusion of catheters used to treat hydrocephalus.

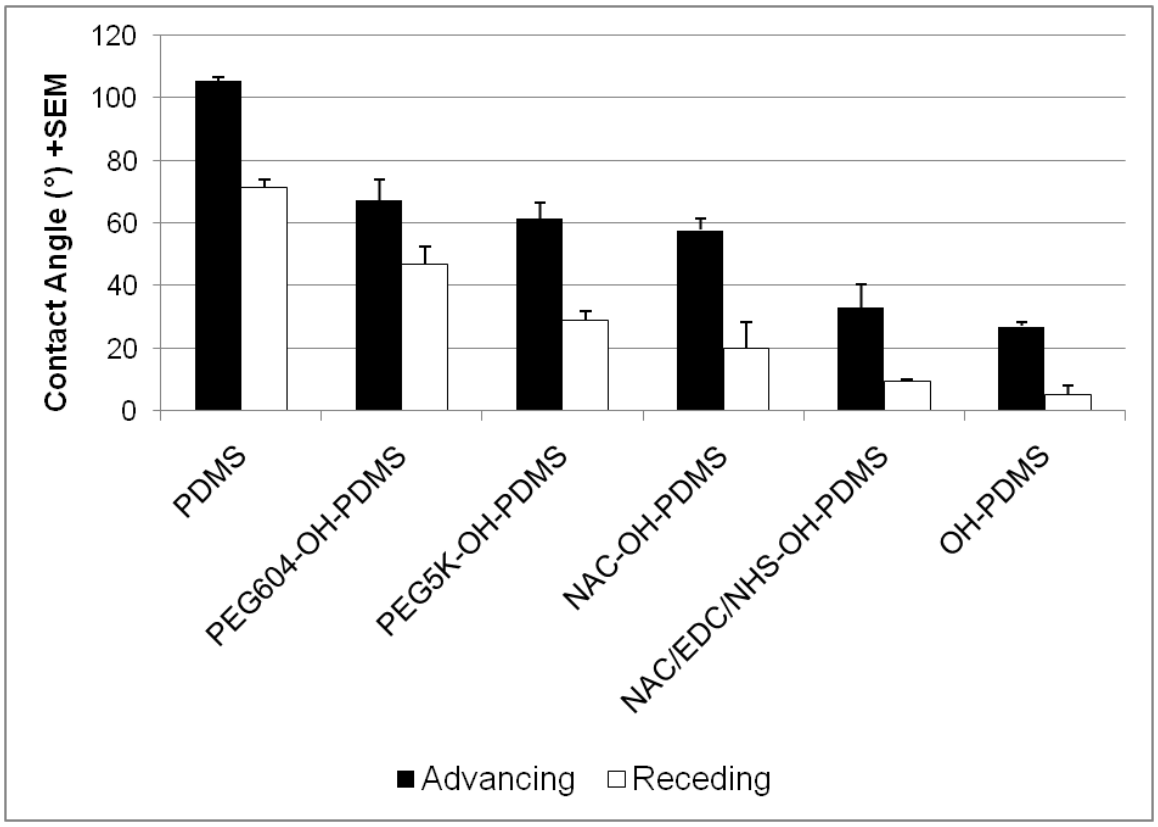

Figure 25 Water contact angle measurements on PDMS, PEG and NAC modified PDMS, and OH-PDMS shown in order of decreasing hydrophobicity from left to right immediatley proceeding modification. As determined using a one-way ANOVA, decreases in advancing angles from PDMS are significant ($P < 0.05$) with every modification, and decreases in receding angles from PDMS are significant ($P < 0.05$) with every modification but PEG604-OH-PDMS ($P = 0.13$). A sample size of 5 was used in each case. All statistically significant differences are outlined in the text.

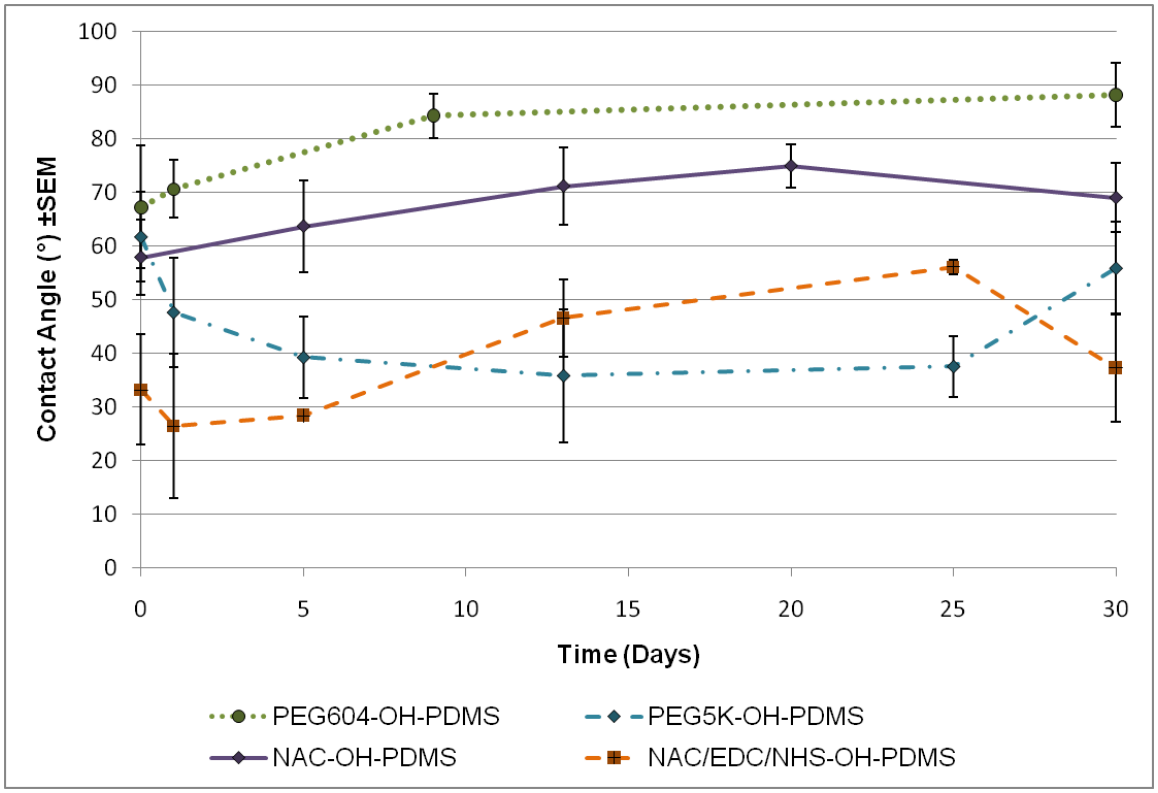

Figure 26 Advancing water contact angle measurements over time on PEG604-OH-PDMS (dotted line), PEG5K-OH-PDMS (dashed and dotted line), NAC-OH-PDMS (solid line), and NAC/EDC/NHS-OH-PDMS (dashed line). No contact angle reached the advancing contact angle of the PDMScontrol (104.23 ± 1.02°) after 30 days. All statistically significant differences were determined using a one-way ANOVA and are outlined in the text.

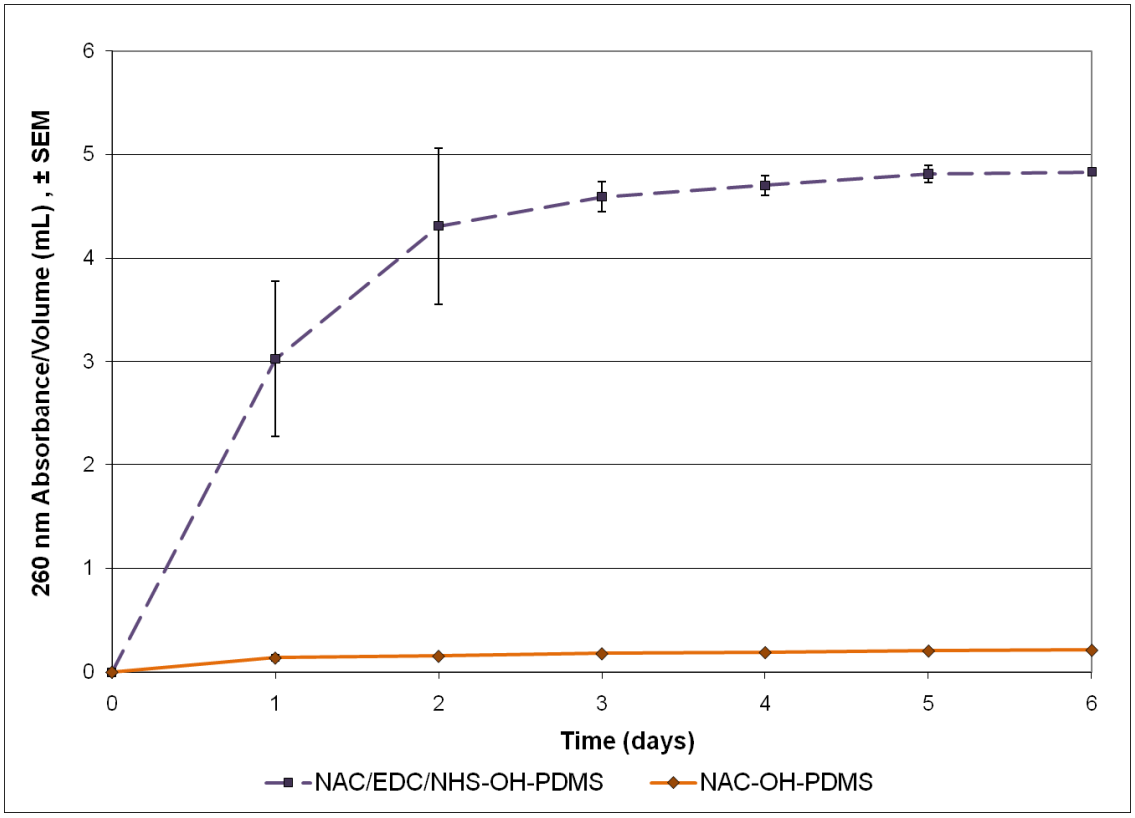

Figure 27 Mean absorbance at 260 nm over time to depict NAC release from PDMS over time. There is a clear difference between release from NAC-OH-PDMS and NAC/EDC/NHS-OH-PDMS where NAC/EDC/NHS-OH-PDMS shows release of some or all NAC components from its surface. All statistically significant differences were determined using a one-way ANOVA and are outlined in the text.

Table 8 Low resolution XPS atomic concentration results (percent ± STDV)

	C 1s (%)	O 1s(%)	Si 2p(%)	N 2p(%)	S 2p(%)
PDMS	48.9 ± 1.0	24.5 ± 0.6	26.7 ± 0.4	N/d	N/d
PEG604-OH-PDMS	43.8 ± 2.8	31.2 ± 1.2	25.0 ± 1.1	N/d	N/d
PEG5K-OH-PDMS	30.2 ± 4.0	42.0 ± 4.3	27.9 ± 0.6	N/d	N/d
NAC-OH-PDMS	51.2 ± 0.6	27.3 ± 0.2	17.1 ± 0.6	1.8 ± 0.3	2.6 ± 0.4
NAC/EDC/NHS-OH-PDMS	43.6 ± 3.0	31.9 ± 1.9	23.0 ± 1.0	1.2 ± 0.2	N/d

Table 9 High resolution XPS Carbon Spectra (percent ± STDV)

	284.3 eV (C-C/C-H/C-Si)	**286.4 eV (C-O/amine)**	**288.6 eV (O-C=O/amide)**
PDMS	98.6 ± 2.5	0 ± 0	0 ± 0
PEG604-OH-PDMS	78.6 ± 6.1	21.4 ± 6.1	0 ± 0
PEG5K-OH-PDMS	80.5 ± 10.0	13.0 ± 6.1	0 ± 0
NAC-OH-PDMS	83.6 ± 5.5	10.9 ± 1.9	4.4 ± 5.4
NAC/EDC/NHS-OH-PDMS	86.1 ± 2.7	10.3 ± 1.7	3.6 ± 1.5

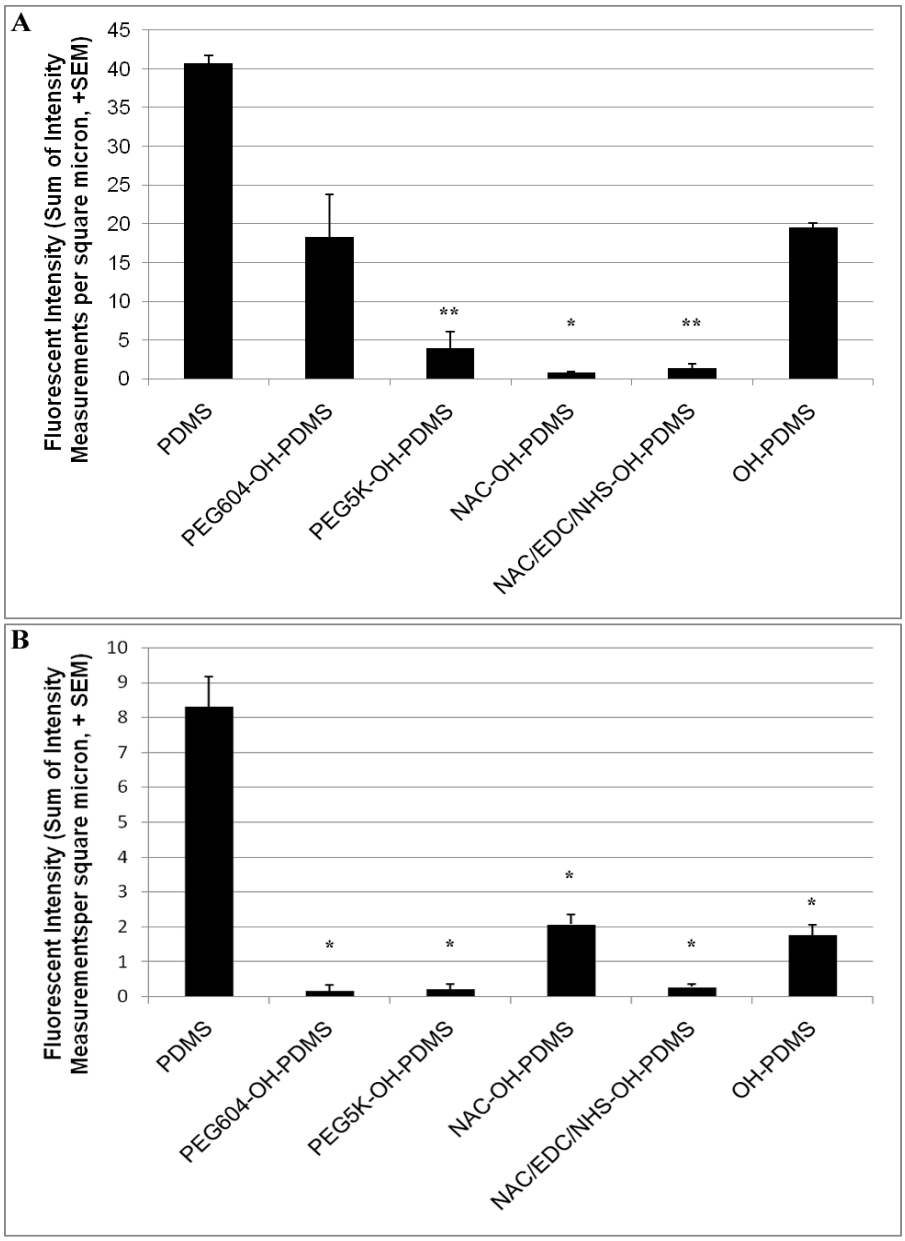

Figure 28 Mean Fluorescent Intensities per square micron of FITC labeled albumin (A) and RITC labeled fibronectin (B). Please note the difference in y-axis maxima. Asterisks denote significance of either $P < 0.05$ (*) or $P < 0.01$ (**) compared to PDMS. A minimum sample size of three was used for each group with two spots of analyses averaged per sample. Significance was determined using a Kruskal Wallis H Test.

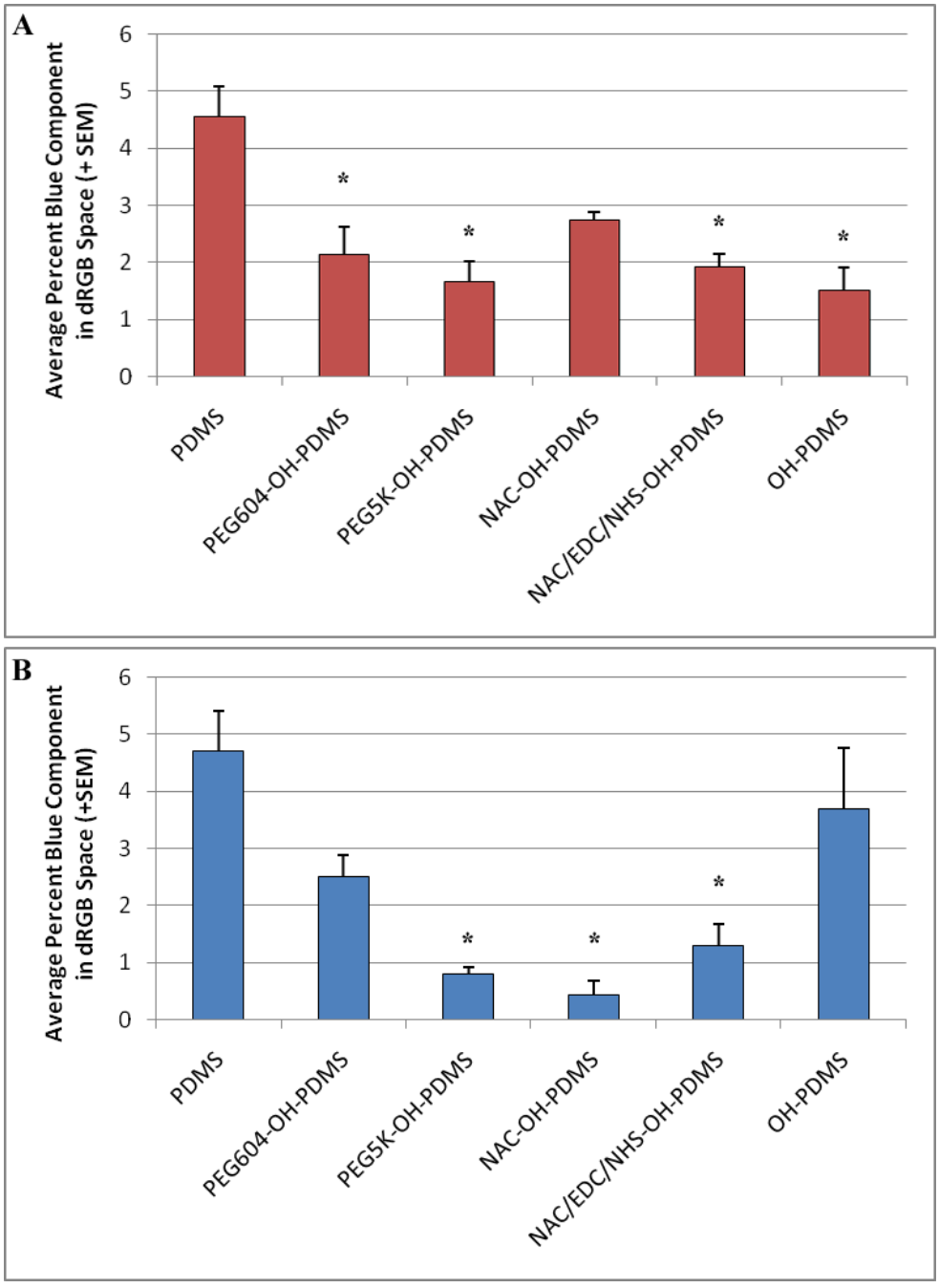

Figure 29 The average percentage of blue in dRGB space as determined by analysis of macrophage (A) and astrocyte (B) DAPI intensity. Asterisks (*) denote significance of $P < 0.05$ compared to PDMS for each respective cell type from a Kruskal Wallis H Test.

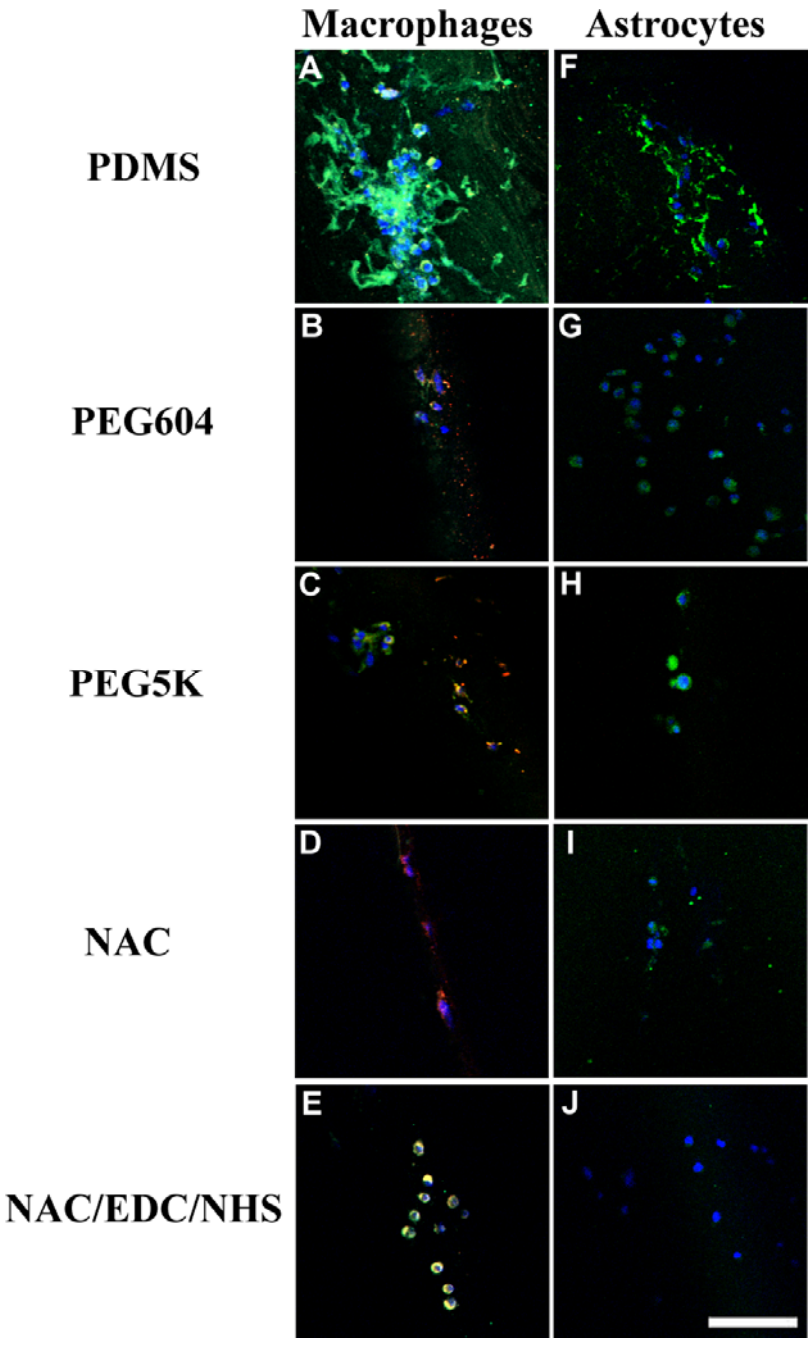

Figure 30 Macrophages (A–E) and astrocytes (F–J) bound to PDMS controls and modified PDMS. Actin (red) and vinculin (green) were used to depict macrophages while GFAP (green) was used to define astrocytes. DAPI (blue) was used to label the cell nuclei in all images. Scale bar denotes 50 μm in all panels.

CHAPTER 6

EFFECTS OF VENTRICULAR CATHETER ARCHITECTURE ON MACROPHAGE AND ASTROCYTE ADHESION[4]

6.1 Introduction

Since 1955, the shunt system has been used to treat hydrocephalus by draining cerebrospinal fluid (CSF) from the cerebral ventricles, but its substantial failure rate has caused neurosurgeons and engineers to question its design. The ventricular catheter of the shunt system is made of poly(dimethyl)siloxane (PDMS) and typically includes 32 500-μm-diameter holes spaced approximately 500 μm apart in four rows [214]. These drainage holes are often occluded by parenchyma infiltration, choroid plexus tissue migration, and inflammatory cell accumulation [44, 49, 53, 108, 116], but manufacturers have only slightly altered the number of holes and their placement over the last 56 years [130]. There are no publicly available records indicating why the number of holes, the size of each hole, and the distance between holes was chosen. Historically, the general consensus has been that the number and size of holes was chosen to facilitate adequate flow from the ventricular space, but recent studies have suggested that perhaps fewer holes are required to reach adequate CSF flow from the ventricles [116, 120].

---

[4] Reprinted from Child's Nervous System, accepted manuscript, Harris, CA; McAllister JP "Does Drainage Hole Size Influence Adhesion on Ventricular Catheters?" Copyright (2011), with permission from Springer. The final publication is available at springerlink.com.

Surprisingly, to our knowledge, there is only one study on ventricular catheters that has attempted to vary drainage hole size [131]. In 2003, Lin et al. postulated that a graduated decrease in hole diameter from the catheter tip would alter the mass flow rate distribution and theoretically reduce the likelihood of occlusion [131], but the latter was not tested. Importantly, modifying the size of the drainage holes changes the shear through the holes, a factor known to influence cell adhesion [102]. The current study expands upon previous work by observing whether adhesion of macrophages and astrocytes, two inflammatory cell types commonly found on obstructed catheters, is dependent on the size of the ventricular catheter drainage holes. We hypothesized that increasing the hole size would decrease macrophage and astrocyte binding onto ventricular catheters.

6.2 Materials and Methods

6.2.1 Material design

To study the effect of the drainage hole size of the ventricular catheter, we designed PDMS samples with holes that varied from 282 to 975 μm in diameter. The number of holes was calculated such that the bulk flow rate (0.25 mL/min or approximately 4.2×10^{-9} m^3/s) and total hole surface area (6.3×10^{-6} m^2) were equal across all samples. The placement of the drainage holes across samples was designed to mimic the current clinical catheter by maintaining the distance between each hole (approximately 500 μm) and the number of hole rows (four). Two fabrication techniques were analyzed to attain drainage holes in PDMS: stereotactically guided punched holes

and hole production using photolithography and Bosch-like deep reactive ion etching (DRIE). Table 10 shows sample group number assignments and their calculated parameters. Shear stress has been calculated assuming that the volumetric flow rate through each hole and the hole diameter remain constant. These shear stress values can be interpreted only as approximate values, however, because the volumetric flow rate through each hole has not been measured in this study and probably varies depending on (1) its proximity to the catheter tip [131], and (2) the measurement location within or immediately surrounding the hole.

6.2.2 Punched holes in PDMS (groups one and two)

In an industrial setting, holes in current clinical catheters are fabricated in PDMS tubing with a sealed tip using a set of blunt-ended needles [215]. The needle set punctures each side of the catheter wall, creating holes. Needles are removed, the catheter is rotated 90º, and the process is repeated such that four rows of holes are created, each with a 90º offset. Holes in adjacent rows are also positioned in the interval between the neighboring holes.

Similarly, holes were mechanically punched in our laboratory using a set of blunt-ended needles (Nordson EFD, Providence, RI). Commercially available catheter tubing without pre-existing 500 μm holes (Medtronic, Inc, Goleda, CA) was cut into 4-cm lengths. At one end of each catheter segment, 1 drop of PDMS Sylgard 184 (1 part catalyst: 10 parts base by weight, Dow Corning, Midland, MI) was injected and allowed to cure for 30 min at 150ºC. To assure that the silicone plug was cured and had sealed

the lumen, distilled water was injected into the opposite end. Catheter segments were then individually placed in a stereotactic frame and punched with blunt-ended needles. The smallest holes (with average hole diameter of 282 μm) were punched into the PDMS tubing using a 32 gauge blunt needle, one of the smallest sizes manufactured. To attain smaller size holes, wire punches were attempted. Samples produced using wire punches produced less than optimal cutting profiles and were therefore discarded. The PDMS surface area and the total hole surface area of each catheter segment equaled the PDMS surface area and total hole surface area of the clinical hardware (4.7×10^{-4} m^2 and 6.3×10^{-6} m^2, respectively, Table 10).

6.2.3 Lithographic discs (group three)

An alternative strategy to create holes in PDMS was attempted using a combined lithography/DRIE fabrication method. First, the design pattern was drawn in AutoCAD 2011 (Autodesk, Inc, San Rafael, CA) with 32 500-μm-diameter holes spaced 500 μm apart in four rows. Using this design, a chromium-on-glass mask was fabricated with a ±1.0-μm tolerance (Photo Sciences, St. Torrance, CA). Separately, 200-μm chromium layers were deposited on 4-inch-diameter silicon (Si) <100> wafers (p-type) obtained from the Nanofabrication Laboratory at the University of Utah. These wafers were then placed on a 150°C hotplate for 5 min before spin-coating with thick positive photoresist (AZ® 9260, AZ Electronic Materials, Branchburg, NJ) at 1000 rpm for 1 min. Wafers were allowed to sit untouched for 10 min after photoresist deposition to reduce the risk of bubble formation and were then transferred to a hotplate to bake at 105°C for 5 min. A

3-cm inner-diameter rubber ring was placed around each mask pattern, and photolithography was performed using a hard contact aligner for 4 repetitive 17-s exposures set 30 s apart to transpose the mask pattern onto the chromium-coated wafer. A 25% concentration of AZ 400K Developer (AZ Electronic Materials) in water then removed excess photoresist (5 min) and a chromium etch exposed the negative space on the Si wafer (5-min exposure). The wafer was washed with water, dried with nitrogen gas, and etched with oxygen plasma for 5 min. A 2-step DRIE process was used to etch away negative space and attain vertical Si pillars. A total of 650 SF_6 and C_4F_8 cycles at a rate of 0.435 μm/cycle were used. The wafer was again etched with oxygen plasma for 5 min. Release agent tridecafluoro-1,1,2,2,-tetrahydrooctyl1-1-trichlrosilane (13F) was vapor-deposited on the wafers under vacuum for 2 hours [216]. A surface profilometer (KLA-Tencor P-10 Profiler, Milpitas, CA) was used to measure the etch depth of the wafer. The final PDMS sample was created by depositing 1 mL of degassed Sylgard 184 (1 part catalyst to 14.3 parts base by weight, Dow Corning) onto the modified Si wafer. This catalyst-to-base ratio was used to increase the ultimate tensile strength of the PDMS [217] to more closely represent commercial PDMS catheters with a thickness of approximately 1 mm. Prior to curing, excess PDMS was removed using a 4-inch squeegee. PDMS was cured for 10 min at 150°C [218] before it was lifted from the wafer. The result was a reverse mold replication of the Si wafer columns to attain PDMS sheets with 500-μm holes. The PDMS was punched into 13-mm-diameter discs to attain a PDMS surface area of 1.5×10^{-4} m^2. The thickness of the PDMS discs was measured using a surface profilometer. Samples were assigned to Group 3 (Table 10).

6.2.4 Material surface analysis

Scanning electron microscopy (SEM) was performed using a Quanta 600 under high vacuum in the Surface Analysis Division of the Nanofabrication Laboratory at the University of Utah. Images were acquired using a backscatter detector at both 40X and 400X magnification. An optical profilometer (Zygo Corporation, Middlefield, CT) was used to detect reflected light using a 40-μm bipolar (10-s) scan length and attain root mean square (RMS) average roughness values. Samples were cut laterally such that the wall of the hole was exposed. Fringes were nulled by adjusting the roll/pitch. Values were averaged across the longitudinal plane of the hole wall to determine the effect of the cutting edge of the punch. Because optimal profilometry was not ideal for Group 3 lithographic discs (they were not impregnated with barium as Groups 1 and 2), atomic force microscopy was attempted to attain an RMS average roughness value of the hole wall. The attempt failed because the force to acquire the image deformed the soft hole lumen, and thus average roughness data were not obtained for Group 3 samples.

6.2.5 Macrophage and astrocyte adhesion assay

Mouse IC-21 peritoneal macrophages and rat primary astrocytes were attained and cultured using previously described methods [140, 210]. Briefly, macrophages were obtained from ATCC (SV-40 transformed peritoneal IC-21 macrophages, ATCC product number TIB-186) and cultured in RPMI-1640 medium with 25 mM 4-(2-hydroxyethyl)-1-piperazineethanesulfonic acid (HEPES, Sigma, St. Louis, MO), 1% penicillin-streptomycin (Sigma), 1% GlutaMAX (Sigma), 1% sodium pyruvate (Invitrogen,

Carlsbad, CA), and 10% fetal bovine serum (FBS, Sigma). Astrocytes were obtained through an extraction and shake-off process and cultured in RPMI-1640 medium with 25 mM HEPES, 1% penicillin-streptomycin, 1% GlutaMAX, and 10% FBS. Both cultures were seeded in T-75 Culture Flasks (ISC Bioexpress, Kaysville, UT) and were split at 80% confluence. To mimic both the total protein (208.1 mg/L) and the albumin (155 mg/L) concentration of cerebrospinal fluid, a subset of macrophages and astrocytes intended for analysis were immersed in a low concentration of albumin-rich medium (0.5% FBS with an albumin additive) for 24 hours before being detached and added to a cell adhesion assay.

6.2.6 Cell detachment for passaging and experimental analysis

A 5-min exposure to 1X TrypLE Express (Invitrogen) caused macrophages and astrocytes to detach from cell culture flasks. Once macrophages had been immersed in the enzyme solution for 5 min, physical dislodgement by striking the walls of the flasks sharply facilitated cell removal. Viable cells were counted on a hemocytometer using the Trypan blue exclusion test and suspended in the low protein medium at a final cell suspension of 4.615×10^4 cells/mL (3×10^6 cells total). The cellular solution was then added to a cell adhesion assay (a flow system termed the Hydrocephalus Shunt Catheter Bioreactor).

6.2.7 Hydrocephalus Shunt Catheter Bioreactor

A previously published method established by our group to test adhesion on catheters [140]was manipulated in this study to measure macrophage and astrocyte adhesion after alterations in PDMS drainage hole size. To mimic pulsatile flow conditions within the cerebral ventricles, the model uses a three-channel peristaltic pump (Watson-Marlow 401U/DM3, Cornwall, England). In the published model, cells were propelled through the lumen of catheter tubing where adhesion was recorded. In the current experiments, the system was slightly modified to encase a PDMS catheter or disc with drainage holes: PDMS catheters (groups 1 and 2) were suspended in plastic 1-mL syringes with the cannula removed (BD, Franklin Lakes, NJ); PDMS discs (Group 3) were positioned in polytetrafluoroethylene (PTFE) 13-mm syringe filter holders (Swinney Syringe Holder, Sterlitech, Kent, WA). From a suspension flask, the system propels a macrophage or astrocyte cell suspension toward the PDMS sample, through the holes of the sample, and out through either the lumen of the catheter or the back side of the disc (Figure 31). A flow rate of 0.25 mL/min and a pulsation rate of 100 pulses/min were used in this study to imitate pulsatile, ventricular CSF flow under chronic hydrocephalus conditions [15]. Adhesion was measured in and around the drainage holes after a 20-hour exposure period.

6.2.8 Fluorescent staining procedure

After the 20-hour exposure period, samples were removed and fixed with 4% (w/v) paraformaldehyde. To assure that Group 3 discs were properly immersed in

fixative, polytetrafluoroethylene (PTFE) rings were used. To identify the cell nuclei of cells fixed to the samples, immunofluorescence was employed. Each sample was rinsed and stored overnight at 4°C in 0.1 M PBS. For permeabilization, samples were incubated in 0.1% Triton X in 0.1 M PBS for 10 min. Fifteen minutes of exposure to anhydrous methyl alcohol confirmed permeabilization of the macrophages. Samples were stained with the nuclear dye 4',6-diamidino-2-phenylindole (DAPI) diluted from 1 mg/mL stock to 1:1000 in 0.1 M PBS using established methods.

6.2.9 Analysis of cell attachment

After fluorescent staining, a Leica microscope was used to obtain epifluorescent images of the exterior surface of the catheter. Serial images were acquired from the catheter tip to the opposite end to (1) determine the total cell adhesion around all of the holes and (2) categorize data based on the position of the hole in relation to the catheter tip. Catheters were then rotated approximately 90° and reimaged so that adhesion could be categorized based on the catheter orientation in the flow system (top, bottom, sides of catheter). With all image acquisition, the camera settings were fixed to an exposure of 702.5 ms. A sample size of six catheters was used for each experimental group with analysis including examination of adhesion around every hole.

For analysis, DAPI channel images were loaded into ImageJ (National Institute of Health, Bethesda, MD) [219] and converted to 16-bit images before the contrast was enhanced with saturated pixels set at 0.5%. The ellipse tool was used to construct circular area selections around each hole such that PDMS surface area to be analyzed was

equal across all groups. The background was subtracted using a rolling ball radius of 25 pixels. Next, selected particles were analyzed where the threshold was adjusted to include only cell nuclei. Advantages to this method are that only pertinent (in focus) cell nuclei were analyzed without background problems, information on the percent area covered by cell nuclei could be acquired directly rather than through inferences based on intensity, and data were not dependent on the identification of the hole edge.

To compare adhesion across groups with more focus on the area surrounding each hole, a second analysis technique was performed. A custom software package was built to compute the average color in user-defined areas, including areas meant to distinguish holes, concentric rings surrounding the holes, and the image background. The average blue component in digital Red-Green-Blue (dRGB) space was determined using the DAPI channel from the epifluorescent acquired images. A normalized background was removed and data were reported as a percent from 0 to 255, with 255 representing brightest light emission. Although analysis using nuclei area is preferred in this study because of the aforementioned advantages, this additional measurement provides cell density data in fixed distances from the hole edge.

6.2.10 Statistical analyses

Acquired data were analyzed for normalcy using the Anderson-Darling normality test. Parametric results were analyzed using either a two-tailed Student's t-test or a one-way analysis of variance (ANOVA) with $\alpha = 0.05$. A post-hoc Scheffé test was performed when the null hypothesis (no differences in the group means) was rejected.

Nonparametric data were evaluated using either a two-tailed Mann-Whitney U Test or the Kruskal-Wallis H Test with a confidence interval of 0.95 ($\alpha = 0.05$). Kruskal-Wallis H Tests were followed by unplanned comparison of mean rank tests using least significant difference rank when samples came from different distributions.

6.3 Results

6.3.1 Fabrication

Light microscopy confirmed that holes were successfully created in all groups. The punching method in Groups 1 and 2 created a larger hole diameter at the punch entry site than the diameter of the punch exit site (visual tapering is noted in Figure 32).

The Si wafer prepared for PDMS cast molding of Group 3 lithographic discs can be seen in Figure 33. DRIE processing caused a slight decrease in pillar diameter approaching the wafer surface of approximately 49 μm. Pillar height with the 13F release agent was 279.20 ± 0.66 μm. Subsequent PDMS discs had height (thickness) of 267.77 ± 18.00 μm. Because of the decrease in pillar diameter, the diameter of the Group 3 holes varied by approximately 50 μm.

6.3.2 Comparison of fabrication methods

Fabrication methods across groups were compared by analyzing macroscopic (using SEM, Figure 32) and microscopic (using optical profilometry, Table 11) roughness as well as macrophage and astrocyte adhesion on 500-μm samples. Macroscopic analysis suggested that Group 2 holes had a linear textured surface. This

was not apparent in Group 1 or Group 3 samples and was likely due to imperfections in the punch. Analysis of the RMS roughness measurements between Groups 1 and 2 revealed no significant difference in microscopic roughness.

Adhesion results used to compare fabrication methods can be seen in Figure 34 and Figure 35. There was a significant difference ($P < 0.05$) in the degree of macrophage attachment on the Group 3 discs compared to both the Group 1 and 2 catheters, but there was no significant difference in adhesion of macrophages on Group 1 and 2 catheters. There were no significant differences in total astrocyte adhesion. When adhesion was analyzed with respect to the distance from each hole edge, macrophage adhesion was significantly greater ($P < 0.05$) on the Group 3 discs than on the Group 1 or 2 catheters (at all distances away from the hole edge) but there was no significant difference in macrophage adhesion between Groups 1 and 2. Astrocyte adhesion on Group 1 and 2 catheters appeared to increase with increasing distance away from the hole until it plateaued at approximately 150 μm whereas adhesion on the lithographic discs decreased around 100 μm and did not appear to follow the same trend with respect to distance away from the hole wall. At all intervals away from the hole edge but 50 μm, astrocyte adhesion was significantly greater ($P < 0.05$) on Group 2 catheters than on Group 1 or Group 3 samples.

6.3.3 Comparison of hole size

Fabricated catheters used to analyze variance in hole size can be viewed in Figure 36. Measured hole diameters and RMS roughness values are shown in Table 11. There

were no statistically significant differences in RMS roughness values, except when 754-μm samples were compared with 975-μm samples: 754-μm samples had a significantly smaller RMS value than did the 975-μm samples ($P < 0.05$).

The average total area the macrophage nuclei occupied on the catheter followed a trend from least to most adherent as hole diameters decreased, $975 < 754 \approx 500 < 282$; the average total astrocyte adhesion from least to most adherent followed a trend as hole diameters changed, $975 < 500 < 754 < 282$ (Figure 37, Figure 38). A linear regression analysis with R^2 values of 0.63 for macrophage adhesion and 0.84 for astrocyte adhesion implied a trend of decreasing adhesion with increasing hole diameter. None of the differences in adhesion were significant, however, except for the differences in astrocyte adhesion on 282- and 754-μm samples compared with astrocyte adhesion on 975-μm samples ($P < 0.05$). On 754-μm samples, the difference between macrophage and astrocyte attachment was significant ($P < 0.05$).

Macrophage and astrocyte adhesion appeared to occur predominantly on the top of the catheter (remembering that the catheter was horizontally fixed in the flow system as seen in Figure 31). On the top of the catheter, there were significantly more macrophage nuclei on 282-μm samples than on 500-, 754-, or 975-μm samples ($P < 0.05$), but there was also a significant difference in macrophage adhesion between 754-μm samples and 975-μm samples ($P < 0.05$, Figure 39). Astrocyte adhesion on 975-μm samples was significantly less than astrocyte adhesion on 282- and 754-μm samples. On the bottom of the catheter, there were no significant differences in macrophage adhesion and a significant difference in astrocyte adhesion between only 754-μm samples and 975-

μm samples. Hole diameter did not create any significant differences in macrophage or astrocyte adhesion on the sides of the samples.

There were no obvious trends suggesting that adhesion was dependent on the proximity of the hole to the catheter tip (Figure 40). This finding was confirmed using a one-way ANOVA, which revealed no statistically significant differences in adhesion on 282-, 500-, 754-, or 975-μm samples between the first, second, third, or fourth quarter of the holes. Closest to the tip, there was a significant difference in adhesion on 282-μm samples compared with 500-μm samples (macrophages), 754-μm samples (astrocytes), and 975-μm samples (astrocytes and macrophages). Adhesion in the latter half of the catheter (more distal to the catheter tip) was significantly greater on 282-μm samples compared with 500-, 754-, and 975-μm samples, independent of cell type.

6.4 Discussion

6.4.1 Fabrication method

Fabrication methods were varied among Groups 1–3 in an attempt to find a model method to analyze how modifications to hole size impact cell adhesion. Group 2 samples consisted of punched tubing with a sealed tip. Holes were accurately placed when stereotactically guided. The overall geometry of Group 2 samples was similar to that of Group 1 controls used clinically. Fabrication was simple and created tapered holes with RMS roughness values that were not significantly different from RMS roughness values of Group 1 holes. An important limitation to using Group 2 samples, however, was the inherent macroscopic roughness of the fabricated hole walls.

Adhesion may be dependent on the visible grooves caused by imperfections in the punch. Future work should explore other fabrication methods to reduce this factor. Perhaps the use of a sharp biopsy cutter would minimize these artifacts.

Lithography and DRIE were used to create a mold on which Group 3 PDMS discs could be cast. These methods required the sample to be flat, although samples could conceivably be fixed around tubing after fabrication. Fabrication was quite extensive and required labor-intensive trial and error. Once complete, samples were not macroscopically rough, and hole walls were not tapered like those obtained with a mechanical punch. Samples had a fixed distance between each hole with a much smaller deviation than Group 2 samples. To create pillars in the Si mold that could withstand an injection and removal of PDMS, the pillars had to be fabricated with a minimal height (to decrease thinning of the pillar at the pillar base). This inhibited the attainable thickness of the PDMS disc, which decreased the calculated ultimate tensile strength (data not shown). The ultimate tensile strength was increased by altering the PDMS base: catalyst ratio, but the deformation of the PDMS under flow conditions may have been altered compared with deformation of thick PDMS catheter walls. Additionally, a release agent was required to facilitate removal of the PDMS from the mold that may have added release agent residuals on the PDMS. Finally, Group 3 samples were not impregnated with barium as was the shunt material for Groups 1 and 2.

Extensive alternative strategies were tried in an attempt to fabricate Group 3 discs with a diameter less than 500 μm and with increased thickness. Conventional lithography can fabricate structures on the nano-scale, but separation of PDMS from the

Si wafer often tore the PDMS and/or broke the Si pillars. To eliminate the shear caused by lifting the PDMS away from the Si wafer, we attempted to dissolve the Si wafer using potassium hydroxide (KOH), but despite attempts to alter the Si etching rate, the KOH attacked the PDMS, leaving it rougher and mesh-like. The ratio of SF_6 to C_4F_8 cycles in the DRIE process was also modified to decrease grass (surface roughness) and to attain more vertical walls, with little success. Another strategy included the use of a gold release layer between the Si and the PDMS that would permit the release of the PDMS without damaging the micron-size holes. This, too, tore the PDMS. Attempts to increase the thickness of the PDMS layer caused the Si pillars to fracture more regularly, and a decrease in PDMS thickness often caused the PDMS to tear upon removal. Although there is still room for perfection in the final protocol, we were able to attain relatively thick PDMS samples with near-vertical hole walls for samples with hole diameter of greater than or equal to 500 μm.

Adhesion across fabrication types was compared by analyzing 500-μm hole diameter samples after macrophage and astrocyte exposure in the flow system. There was a striking elevation of macrophages on Group 3 discs which was not evident when astrocyte adhesion was analyzed. Perhaps this relationship was due to residual release agent on the PDMS surface; however, previous studies have suggested that macrophages bind to 13F (here used as a release agent) similarly to -OH functionalized surfaces [220]. Therefore, this probably does not explain the difference in macrophage adhesion (Figure 34), because data acquired in Chapter 4 suggest that macrophage adhesion tends to decrease on -OH functionalized PDMS (Figure 22) under similar conditions. This large

deviation in macrophage adhesion on Group 3 discs contributed to our decision to vary hole size using Group 2 samples.

After all pros and cons to both methods were analyzed, the Group 2 punching method was chosen to analyze how alterations in hole size influence macrophage and astrocyte adhesion. Not only were the holes morphologically similar to those in the Group 1 controls, but the catheter geometry was analogous to that of the controls. This created an environment in which appropriate flow vector fields would be applied to the sample and adhesion could be analyzed with dependencies on catheter orientation. Adhesion close to Group 1 holes also appeared to follow a pattern more similar to adhesion on Group 2 samples rather than to Group 3 samples.

6.4.2 Drainage hole size

The degree of cell adhesion (from least to greatest) increased as hole size declined $975 < 754 \approx 500 < 282$ (μm) for macrophages and $975 < 500 < 754 < 282$ (μm) for astrocytes. Adhesion was greatest around 282-μm holes, where there was a relatively high calculated shear stress of 0.0134 N/m^2 (assuming an even flow distribution across holes). Previous findings on leukocyte adhesion suggest that increases in shear stress below 0.1 N/m^2 will enhance adhesion [102], and our previous results on flow through catheter lumina indicate that an increase in flow (and therefore shear) at these levels increases astrocyte adhesion [140]. Although we did not test leukocyte adhesion and acknowledge that findings may be cell-type dependent, we can speculate that elevated shear stress played a role in increasing macrophage and astrocyte adhesion on samples

with decreasing hole diameters. In our opinion, the relatively small increase in average astrocyte adhesion on 754-μm samples compared with 500-μm samples is not sufficient to contradict this thinking.

Analysis of the data using linear regression suggested that the relationship between astrocyte adhesion and hole size was more linear than the relationship between macrophage adhesion and hole size. It has been proposed that shear stress alters the kinetics of the receptor–ligand interactions that induce binding [103]. Perhaps the kinetics of macrophage receptor–ligand interactions are more threshold dependent than those of astrocytes, where elevated shear stress (albeit below 0.1 N/m^2) does not exacerbate adhesion until shear exceeds a particular threshold (in this case between 0.0134 and 0.0075 N/m^2). Another plausible explanation is that identical shear stresses may pull differently on macrophages than on astrocytes because of the difference in cell size.

In the only other study to date that has observed the effect of hole size, Lin et al. reported that flow and blockage are greatest in the holes farthest from the catheter tip and speculated that this was due to uneven flow distribution through the holes [131]. Our results implied no clear dependencies between adhesion and proximity to the catheter tip but rather a dependency on how the holes were oriented in the flow system. This leads us to believe that one or more of the following are true: (1) flow distribution is not the only factor in adhesion and may be influenced by gravity; (2) obstruction that occurs distal to the catheter tip *in vivo* may be caused by other factors, including holes being positioned outside of the ventricle [116]; (3) our model does not adequately mimic

chronic, multifaceted, obstruction. Future work should explore these phenomena in more detail.

Lin et al. expanded their work by varying hole sizes such that the diameter decreased distal to the catheter tip [131]. This was done in an effort to increase resistance to flow. While the results of the study by Lin et al. suggested that flow could be changed by varying the hole size, we note that the proposed decrease in hole size would increase shear stress. By using the flow distributions from the study by Lin et al., we calculated shear stress along the catheter. This approach revealed that shear stress through all the adapted holes would be higher (0.0613 N/m^2 most distal to the tip and 0.0013 N/m^2 most proximal to the tip) than through the holes of standard catheters (0.0361 N/m^2 most distal to the tip and 0.0006 N/m^2 most proximal to the tip). If we assume that an increase in shear stress brought on by either an increase in flow rate [140] or a decrease in hole diameter (present study) increases adhesion, then a preferred catheter prototype should attempt to decrease shear stress through all of its holes. A 975-μm hole diameter produces the lowest shear stress of the tested samples (0.0039 N/m^2 if flow is evenly distributed, 0.0078 N/m^2 distal to the tip and 0.0008 N/m^2 proximal to the tip if flow is distributed based on hole location). Macrophage and astrocyte adhesion had a strong dependency on hole size (and presumably shear stress), and therefore these relationships must be considered in future studies. From a practical perspective, if a continued effort indicates that a large hole size is preferred, the design must be such that an electrocautery probe cannot pass through the catheter and enter the ventricular space.

Although porous materials contain holes with diameters of a much smaller scale and often of a different morphological structure, we can draw some similar conclusions on hole size. Previous work investigating porous materials implanted subcutaneously reveal that components of the foreign body reaction are dictated by the pore (hole) size [100-101]. A decreased pore size has been shown to increase mature collagenous tissue [101]. Similarly, astrocytes, which probably bind to the shunt catheter with the formation of the collagenous sheath, increase with decreasing hole size in this study. There may be no correlation in the mechanisms that cause these interactions, however, as the diameter of the holes and of the pores vary approximately 100-fold and the environment in which the materials are implanted is also considerably different.

An important limitation to this work is the degree of sample roughness. Others have shown that adhesion is dependent on surface roughness [89], so it is likely that surface roughness played some role in macrophage and astrocyte adhesion in this study. Despite the fact that the only significant difference in microscopic RMS roughness values was between the 754- and 975-μm samples, we are currently investigating further alternative strategies to modify hole size independent of surface roughness.

6.5 Conclusions

Two catheter drainage hole fabrication methods were attempted to manipulate the average hole diameter and relate it to macrophage and astrocyte adhesion. Based on results of electron microscopy, optical profilometry, and analysis of macrophage and astrocyte adhesion, it was determined that punched holes should be used to compare

differences in hole size. With this method, hole size can be manipulated easily and was found to directly impact cell adhesion around the holes of catheters. The trend in overall adhesion from least to most adherent appeared to follow 975 < 754 ≈ 500 < 282-μm hole diameter for macrophages and 975 < 500 < 754 < 282 for astrocytes, perhaps because of a dependency on shear stress. Further work must be performed, perhaps in a more chronic environment, to understand how these parameters alter obstruction.

Table 10 Sample group assignments

Group Number	Sample Type	Hole Diameter (µm)	Shear Stress per Hole (N/m^2)[5]	Hole Number
1 (control)	Industry Punched tube	500	0.0075	32
2	Punched tube	282	0.0134	101
		500	0.0075	32
		754	0.0050	14
		975	0.0039	8
3	Lithographic disc	500	0.0075	32

[5] Values assume an equal flow distribution through holes

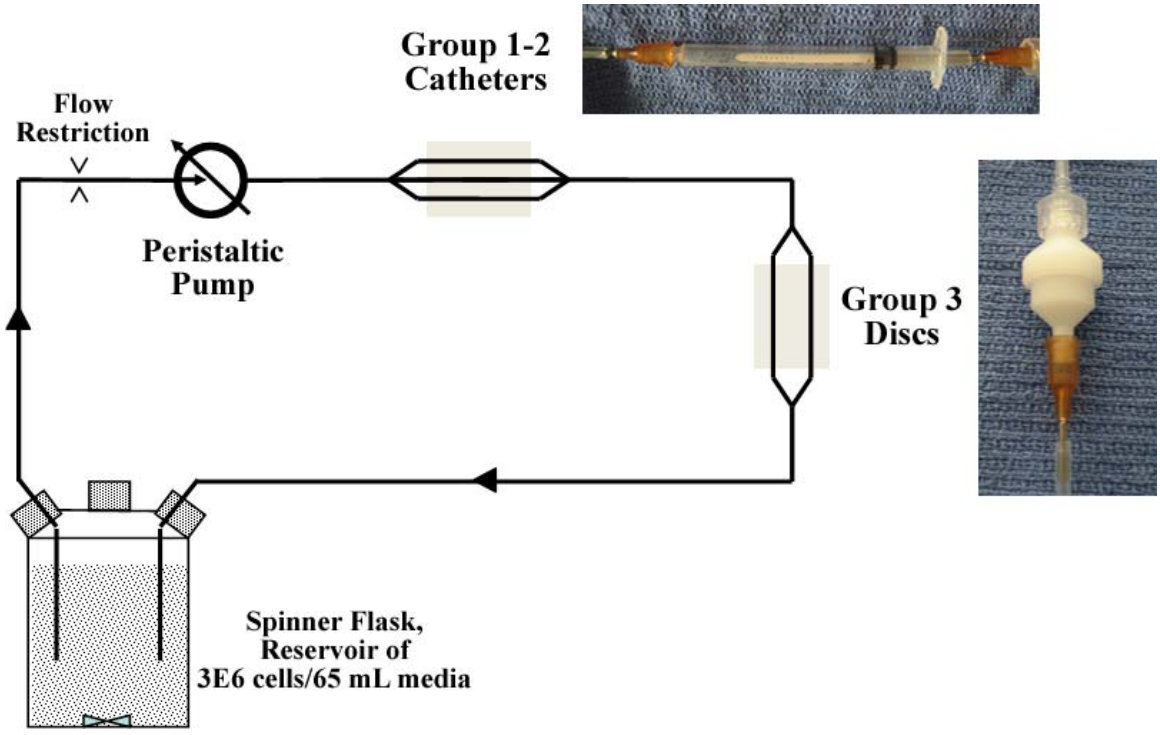

Figure 31 Diagram of the modified Hydrocephalus Shunt Catheter Bioreactor to measure the dependence of macrophage and astrocyte adhesion on the size of the drainage holes. A peristaltic pump was used to propel a cellular suspension from the solution reservoir (denoted "Spinner Flask"), through PDMS transport tubing (solid black line), through a point of flow restriction (small-diameter tubing to attain physiological flow and pulsation rates), through PDMS samples (PDMS catheters for Groups 1–2 or PDMS discs for Group 3), and back to the cellular solution reservoir. Note that groups were run separately; the schematic shows groups 1–2 and 3 in line for illustration purposes only.

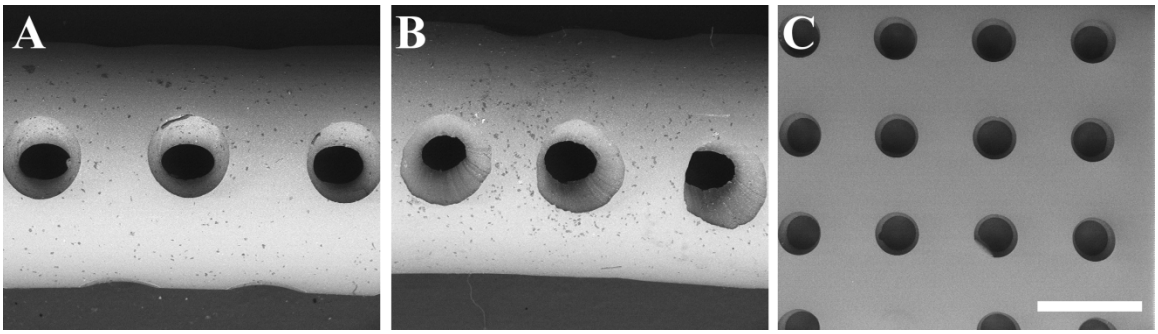

Figure 32 Scanning electron microscopy of 500-µm-diameter samples in each group revealed macroscopic grooves in the hole architecture in Group 2 (B) but not in Groups 1 (A) or 3 (C). Although RMS values were unattainable on the Group 3 samples, there was no statistically significant difference in microscopic RMS values in Groups 1 or 2. Groups 1 and 2 have apparent tapering of the hole walls, presumably because of the punch fabrication method. Microfractures were not visible around the holes. Scale bar denotes 1000 µm for all panels.

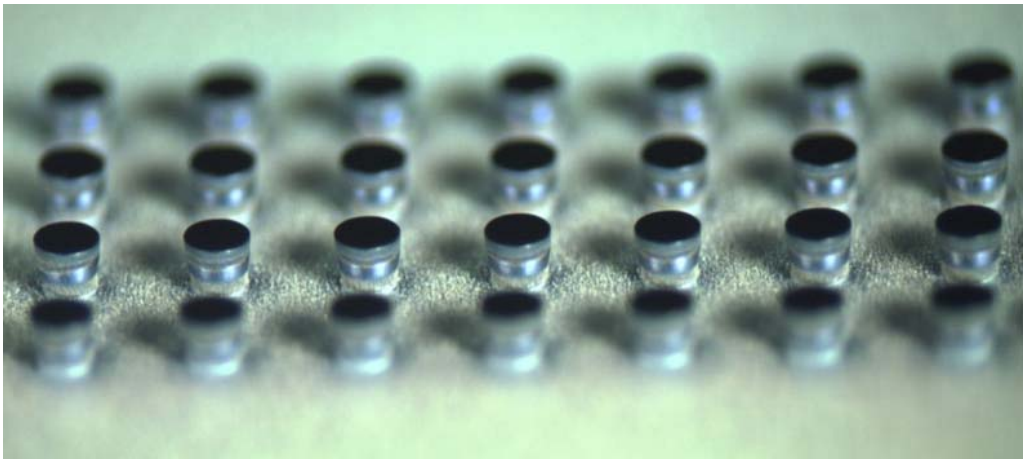

Figure 33 Pillars in a representative silicon wafer prepared for subsequent PDMS cast molding.

Table 11 Comparison of fabrication methods ± STDV

Group Number	Hole Diameter Measurements (µm)	Roughness Average (RMS)
1 (control)	500 ± 2.4	1.12 ± 0.5
2	281.7 ± 35.5	1.10 ± 0.4
	460.0 ± 44.7	0.93 ± 0.2
	753.8 ± 12.4	0.88 ± 0.3
	975.05 ± 35.4	1.48 ± 0.2
3	443.8 ± 7.9	N/A

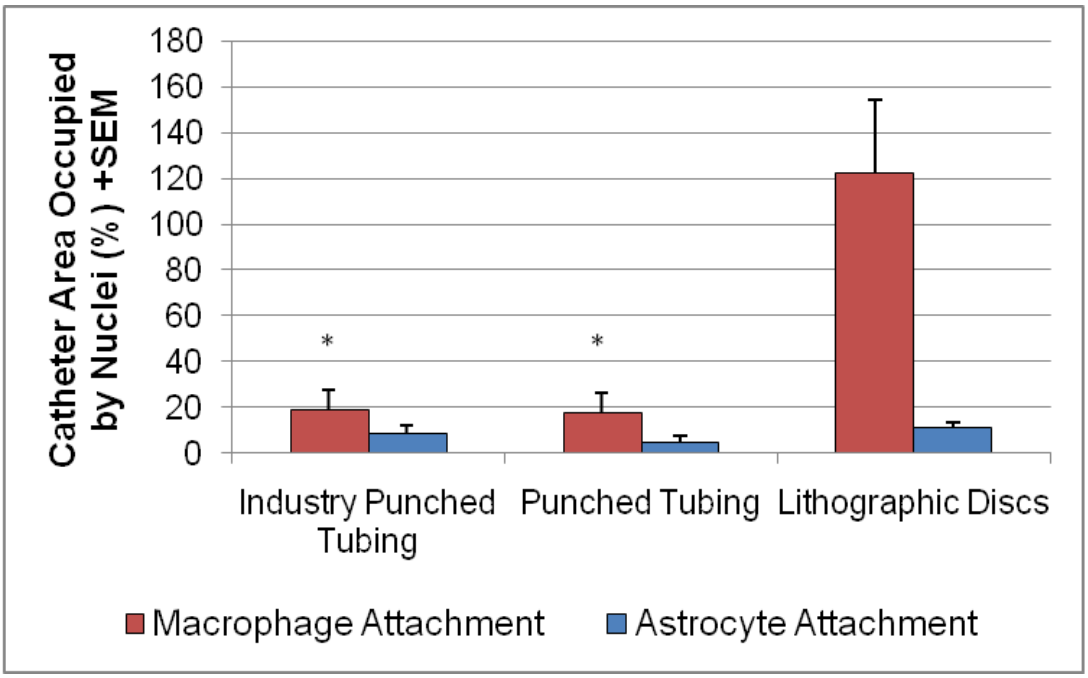

Figure 34 Differences in fabrication methods were analyzed by measuring the total nuclei area. The asterisks (*) represent a significant difference in adhesion compared to macrophage adhesion on the lithographic discs as determined using a one-way ANOVA.

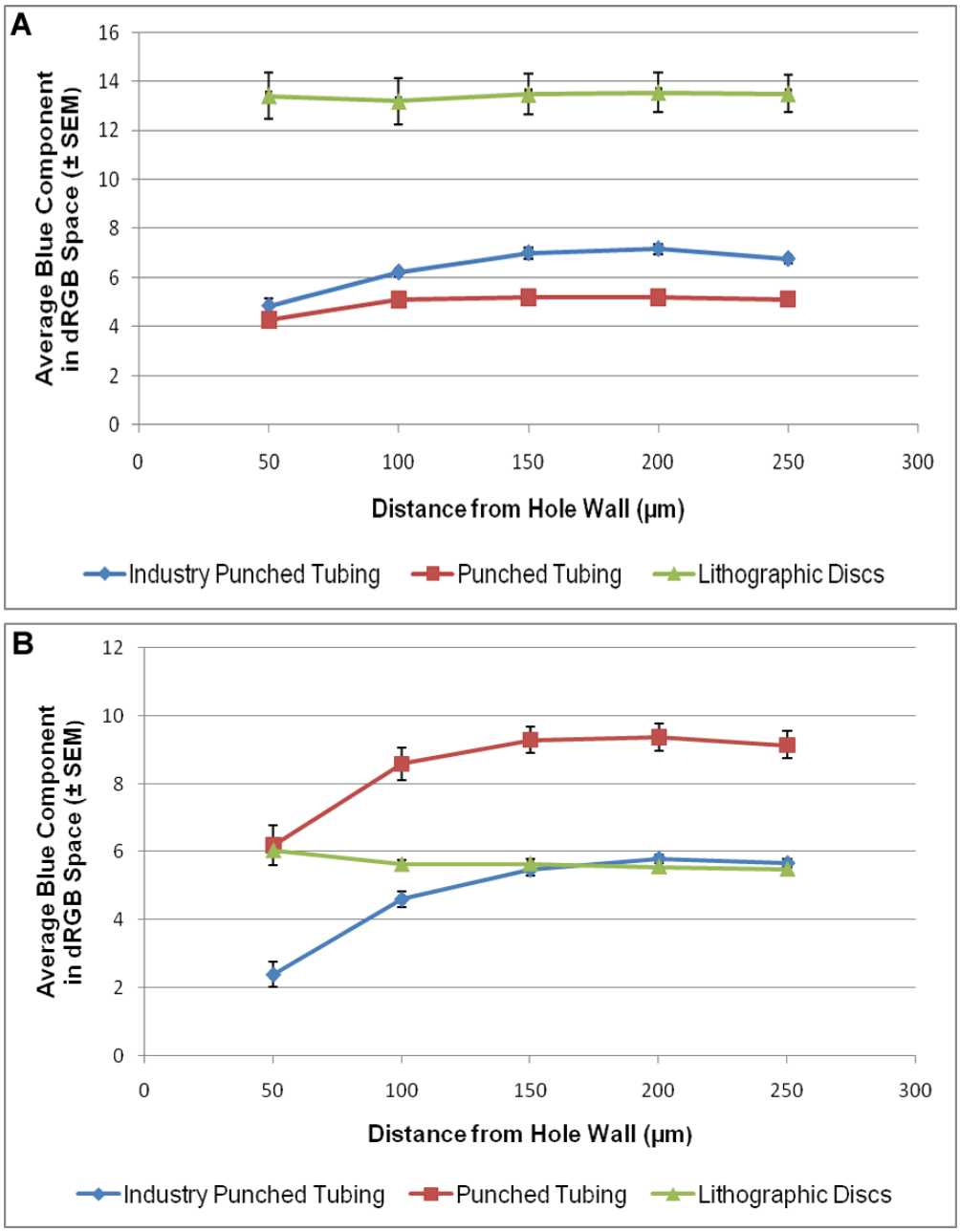

Figure 35 Differences in fabrication methods were analyzed by measuring the macrophage (A) and astrocyte (B) DAPI intensity around the holes. All statistically significant differences are outlined in the text as determined using a one-way ANOVA.

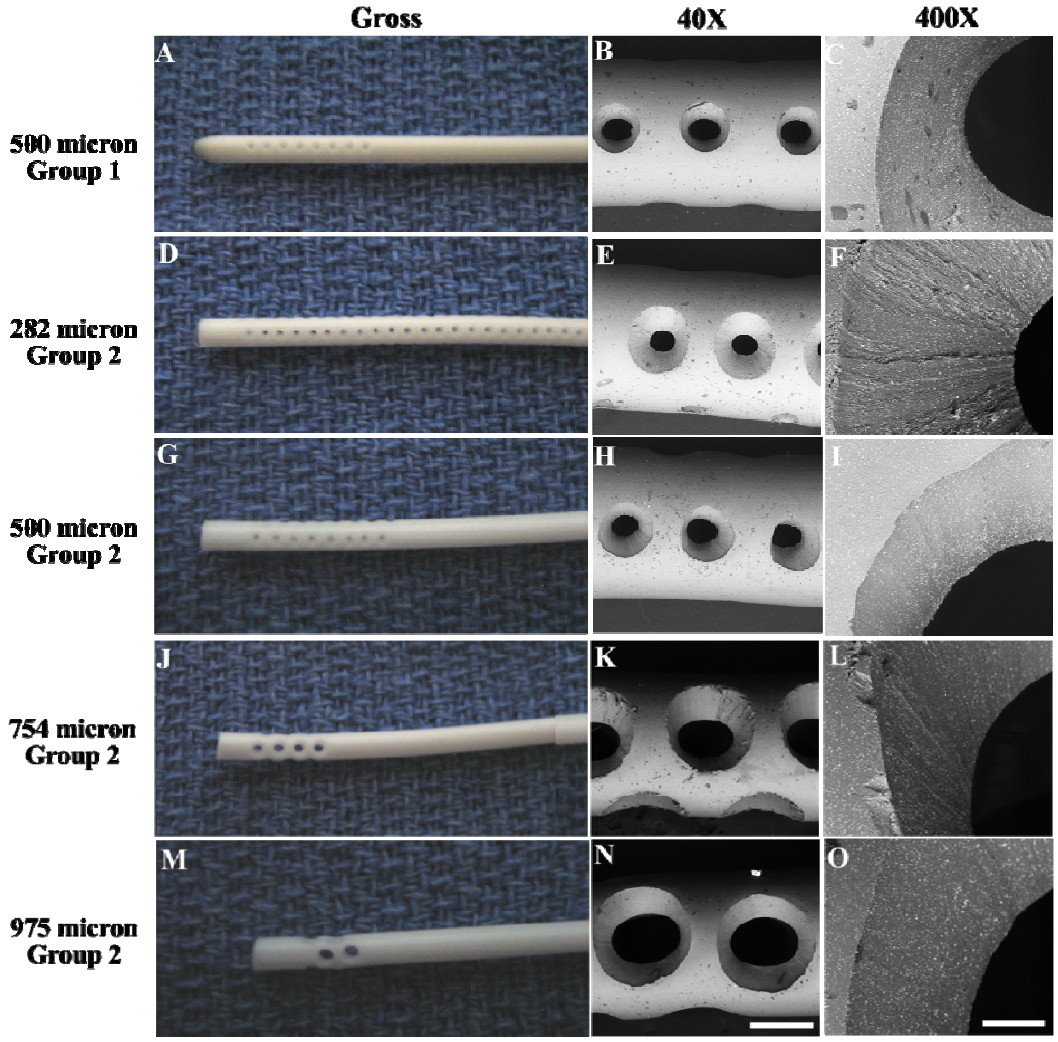

Figure 36 Gross (A, D, G, J, M) and scanning electron (B, C, E, F, H, I, K, L, N, O) microscopy images depicting the total hole surface area and the surface morphology of Groups 1 and 2. The distance between holes was fixed to 500 μm from the most exterior hole edge (489.6 ± 92.4 μm). Roughness on a macroscopic scale appears large but relatively consistent. Impregnated barium (white particulate) and imperfections (dark particulate) in the PDMS and on the PDMS surface can also be noted. The scale bar in N represents 1000 μm at 40X (B, E, H, K, and N); the scale bar in O represents 100 μm at 400X (C, F, I, L, and O).

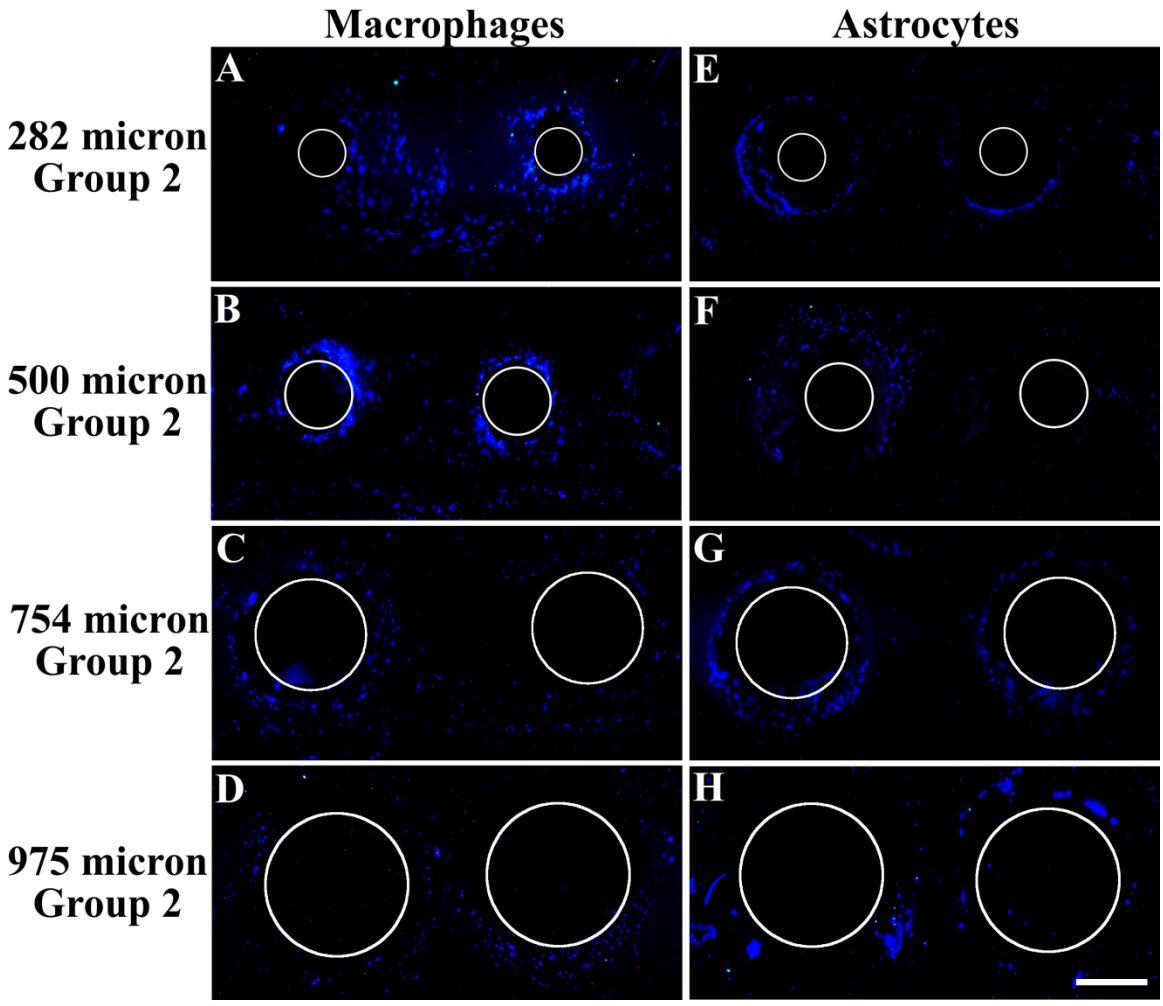

Figure 37 Adhesion of macrophages (A–D) and astrocytes (E–H) as a function of hole size. Cells aggregated around the holes. White circles denote the smallest diameter of each hole bearing in mind the tapering of the hole walls. DAPI was used to label the nuclei. Scale bar denotes 500 μm.

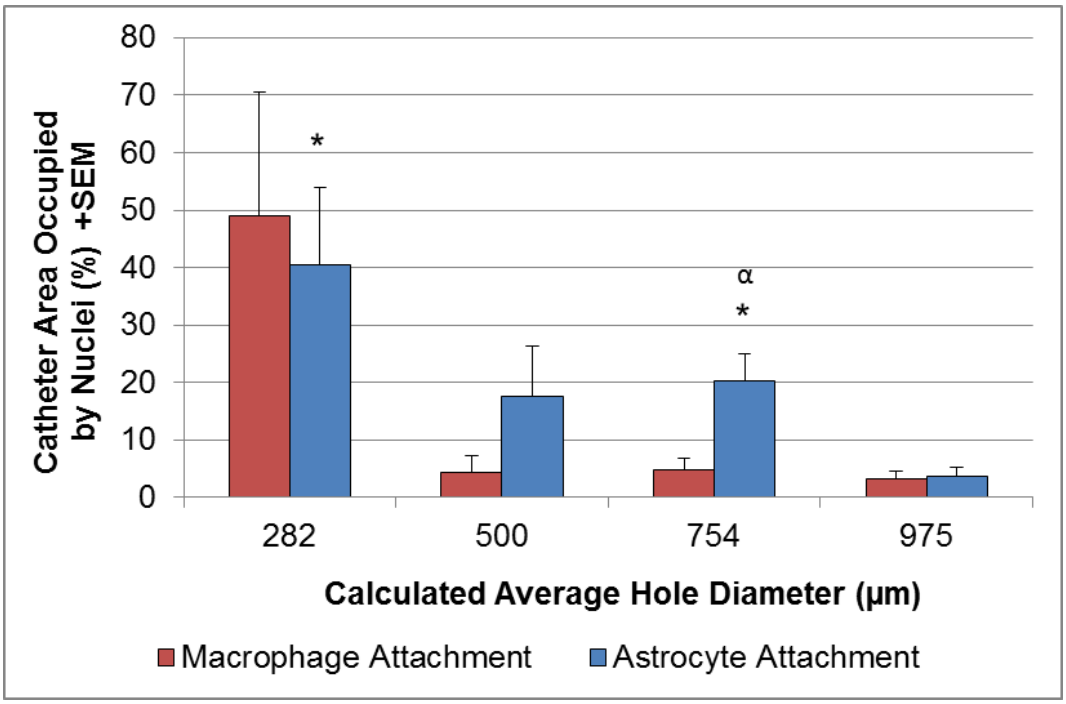

Figure 38 Area occupied by cells around all holes. Asterisks (*) denote a significant difference of the marked sample compared to astrocyte adhesion on 975 µm sample; alpha (α) represents a significant difference between macrophage and astrocyte attachment on 754-µm samples as determined using a one-way ANOVA.

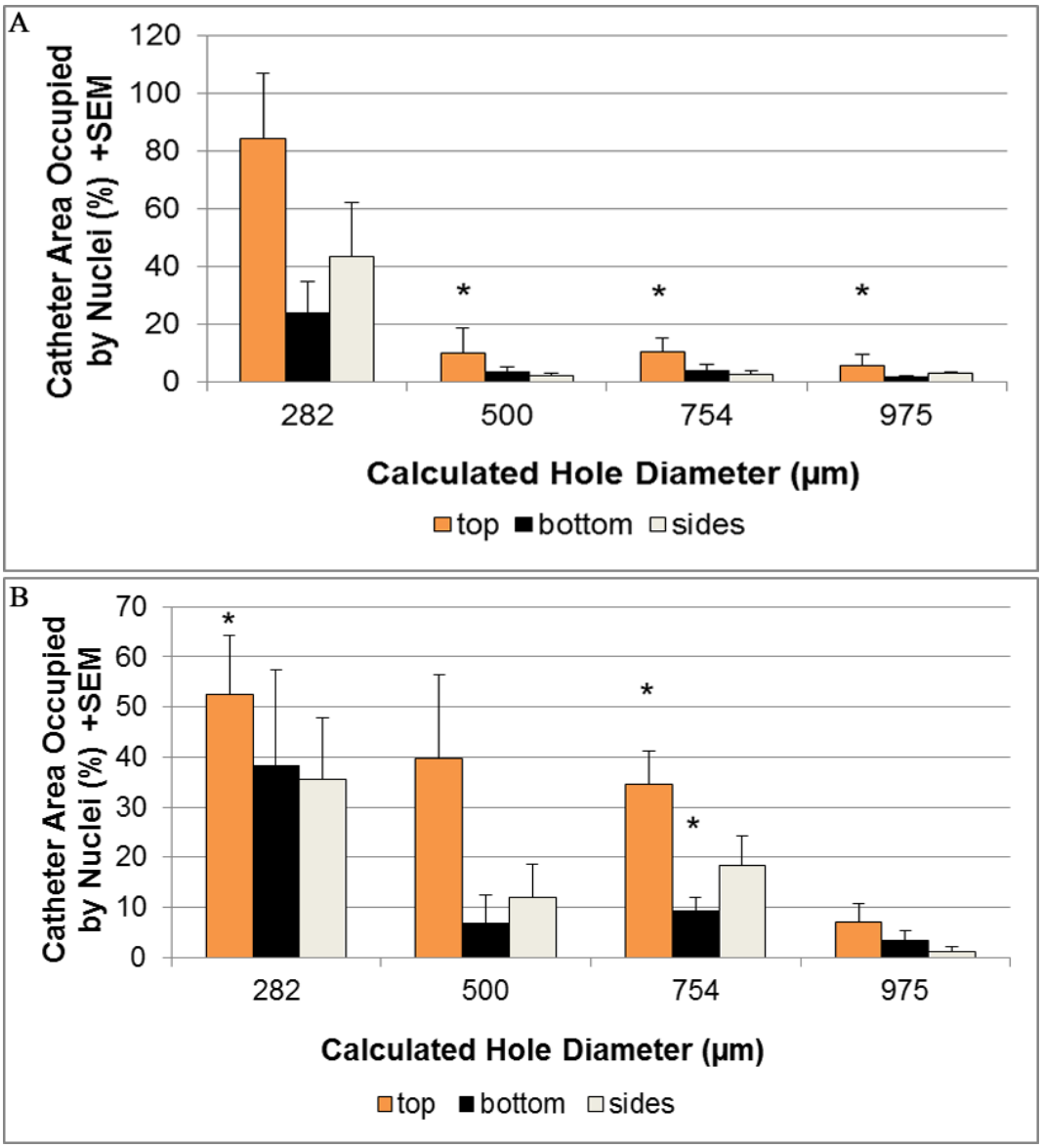

Figure 39 Macrophage (A) and astrocyte (B) adhesion as a function of hole diameter and the orientation in which the catheter was positioned in the flow system. In (A), the asterisks (*) denote significance of the marked sample compared to adhesion on 282 µm samples; in (B), asterisks represent a significant difference in adhesion compared with the 975-µm samples. Significance was determined using a one-way ANOVA.

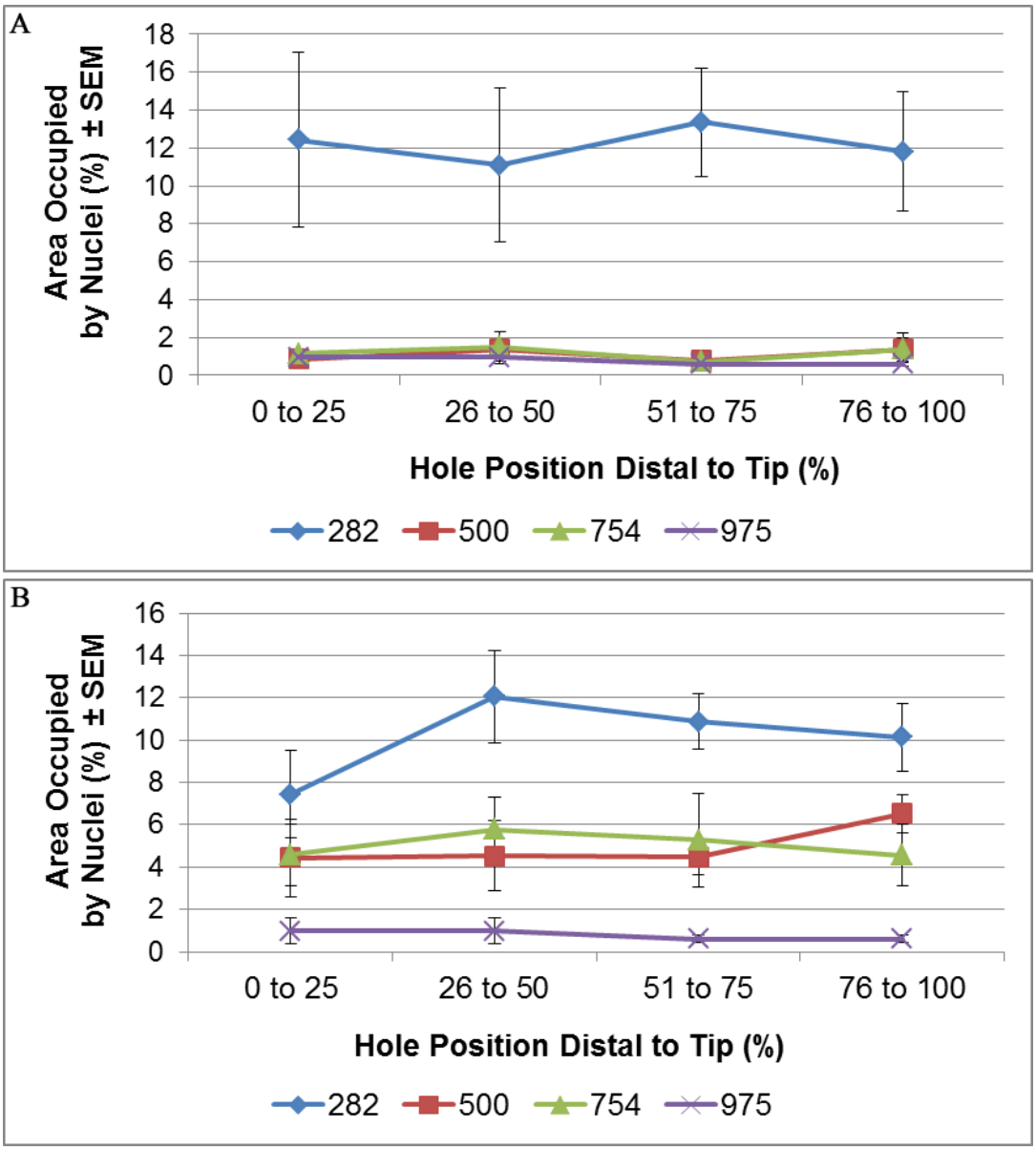

Figure 40 Macrophage (A) and astrocyte (B) adhesion dependent on the proximity to the catheter tip. The position relative to the tip is expressed as a percentage, where 0% represents adhesion closest to the tip and 100% denotes adhesion farthest from the tip. All statistically significant differences were determined using a one-way ANOVA and are outlined in the text.

CHAPTER 7

SUMMARY, CONCLUSIONS, AND FUTURE WORK

7.1 *In Vitro* Flow Model for Macrophage and Astrocyte Adhesion

Hydrocephalus is a debilitating disorder, in part because the most common treatment, shunting, has an extremely high failure rate. From a detailed review of the literature, it becomes obvious that shunt failure is often correlated with an inflammatory response in which macrophages, glial tissue, and giant cells envelope the catheter exterior [48], migrate through the holes [44, 48], and/or invade the catheter lumen [44, 110].

Despite efforts to define causation, the mechanisms that influence the degree of inflammatory-derived shunt obstruction are not well understood. In this dissertation an *in vitro* model was developed as a tool to help answer some of these questions in a controlled hypothesis-driven environment. The model was meant to mimic adhesion of macrophages and astrocytes suspended in CSF in an acute 20 hour time period. The model helped us to not only begin to understand key aspects of macrophage and astrocyte binding to silicone shunts, but it provided a test bed in which modifications to current catheter design could be examined.

7.2 The Effect of Mechanical Cues

7.2.1 Pressure and Pulsation Frequency

There appeared to be no significant impact on macrophage and astrocyte adhesion due to either alterations of pressure or pulsation rate by themselves in a physiological range. We speculate that conditions of pressure might increase initial tethering of protein ligands and cells but are not enough to make a significant impact on overall adhesion after an acute exposure and may actually have an inhibitory effect depending on specific receptor-ligand interactions. Pulsatile flow compared to oscillatory flow impacts cytoskeletal reorganization of cells and decreases nuclear factor kappa-light-chain-enhancer of activated B cells (NFκB, involved in inflammation) [163], but macrophage and astrocyte adhesion did not appear to be dependent on alterations to the pulsation frequency.

7.2.2 Shear stress and flow rate

An obvious trend from this work suggests that adhesion of macrophages and astrocytes is dependent on calculated shear stress caused by either changes in total flow rate through the catheter lumen (Chapter 3) or in flux through each catheter hole as a result of changes in hole diameter (Chapter 6). These findings coincide with implications from Lin et al. [131] who suggested that obstruction occurs where a majority of the flow occurs. If we assume that adhesion is a function of measured shear stress just as adhesion appears to be dependent on calculated shear stress, we find that our data coincide with the literature where adhesion increases with increasing shear until shear

surpasses a certain level [102]. In our studies, data would suggest that adhesion generally increased with increasing shear stress with shear ranging from 0.0039 to 0.0134 N/m^2 (Chapter 3, Chapter 6) but not when a relatively large shear stress of 0.2409 N/m^2 was tested (Chapter 2, where the luminal diameter was decreased to increase shear). Another explanation for these nonconforming data in Chapter 2 is the possibility that cells in a small diameter lumen with an arbitrary length behave differently than they do in a larger diameter lumen. This is plausible since a recent study suggested that the reaction to a chronically implanted catheter is dependent on the length of the catheter [221].

7.3 The Effect of Chemical Cues on Adhesion

7.3.1 Protein concentration

Generally, a higher protein concentration enhanced macrophage and astrocyte adhesion under fluidic conditions, but this trend was not significant. Using PDMS catheters, extrapolation of these acute patterns may suggest that patients with a higher concentration of CSF protein may be more likely to have an inflammatory-related obstruction than patients with lower CSF protein levels, but this was not tested.

7.3.2 Surface chemistry

Altering the surface chemistry with surface hydroxyl groups often decreased macrophage and astrocyte adhesion (Chapter 4). These data suggest that, at least in the acute term, modifying the surface with hydroxyl groups minimizes adhesion and leads us

to question whether other hydrophilic surfaces inhibit adhesion in a similar environment. Chapter 5 results showed that macrophage and astrocyte adhesion was inhibited by the addition of polyethylene glycol (PEG) and N-Acetyl-L-Cysteine (NAC), two hydrophilic surface coatings that appeared to be relatively stable on PDMS catheters dependent on modification methods. The extensive history and success of PEG-modified medical devices make PEG a logical candidate to inhibit inflammatory cells that occlude catheters. The unique properties of NAC also make it an interesting candidate to inhibit adhesion because of its novelty, biocompatibility, and bacterial inhibition.

7.4 Comparison of Macrophage and Astrocyte Attachment

As referred to in Chapter 1, both macrophages and astrocytes are often components of inflammatory-derived shunt obstruction and therefore inhibition of both is likely to be essential to reduce shunt failure rate. Macrophages and astrocytes appeared to respond differently to physiological mechanical and chemical cues. Generally, mechanical cues appeared to have a more pronounced effect on astrocyte adhesion than macrophage adhesion, but mechanical cues seemed to alter macrophage morphology more than astrocyte morphology (Chapter 4). Furthermore, astrocyte adhesion appeared to be greater than macrophage adhesion with a few exceptions related to shear (Chapter 6). Previous findings have shown that astrocytes translate mechanical signals into chemical messages [165] and that monocyte interactions are weaker than those of other cell types under flow conditions [222]. Conceivably, if macrophage interactions are weaker than astrocyte interactions with PDMS under flow conditions, astrocyte adhesion

may appear more influenced by mechanical signals and may be greater than macrophage adhesion. Perhaps under high and low shear stress extremes, the kinetics of macrophage receptor-ligand interactions vary so that adhesion surpasses astrocyte adhesion.

7.5 The Impact of These Studies on Future Work

A clear conclusion from these results is that a combination of mechanical and chemical cues promote or inhibit macrophage and astrocyte attachment to shunt systems. In this author's opinion, flow and/or shear stress and surface chemistry are important mediators in inflammatory cell adhesion to ventricular catheters. Perhaps if mechanical and chemical cues are modified by alterations in catheter architecture (for instance, increasing drainage hole diameter) and by long term surface modifications (for instance, using PEG surface coatings), a shunt system can be produced that is less likely to occlude from inflammatory cell adhesion and accumulation. Of course, not all relationships could be tested in this work and future work *in vitro* and *in vivo* must validate these statements. Others have proposed ways in which these relationships factor into adhesion. For example, it has been suggested that adhesion to dialysis membranes is dependent on pore size as well as surface chemistry [223]. Similarly, results from Chapter 6 imply that adhesion appears to be dependent on hole size (since hole size changes shear stress through the holes) and Chapters 4 – 5 show a dependence on surface chemistry. Results from Chapters 2 – 3 generally show similar patterns that imply dependence on mechanical and chemical cues.

Certainly activation of macrophages and astrocytes in the cortical gray matter, in the periventricular white matter, in the CSF, or bound to the catheter itself may have a resounding effect on adhesion. Activation of cells was beyond the scope of this study, but it remains an important aspect for understanding the mechanisms of obstruction, especially because gliosis is a well-known component of the pathophysiology of hydrocephalus. Certainly flow, pressure, pulsation rate, protein concentration, cell concentration, and surface chemistry can manipulate soluble and insoluble mediators that may influence cell activity. For instance, upregulation of the cytokine TNF-α [24] from hydrocephalic insult (perhaps due to changes in any of the above factors) and initial shunting could be a key regulator in macrophage and or astrocyte adhesion. Certainly the activity of this and other proinflammatory cytokines and proteins have been shown to be key players in the foreign body response [23, 60, 64, 224]. These interactions must be studied in future work; in the short term, the role of proinflammatory cytokines must be studied and manipulated in the flow system such that it properly mimics acute macrophage and astrocyte adhesion *in vivo*. Proliferation of these cells may also play a key role in understanding obstruction.

The flow system developed, tested, used, and amended in this body of work was primarily meant to improve current *in vitro* testing with the long term objective being to develop a model in which univariable testing leads to shunt improvements. While the system improved modeling compared to static *in vitro* systems and also was more applicable to hydrocephalus compared to other fluidic *in vitro* models, it is not without limitations. Like all other *in vitro* systems, the Hydrocephalus Shunt Catheter Bioreactor

lacks systemic cues. In future studies, results from the flow system should be compared to *in vivo* work. Although Chapter 2 shows why each component of the system was used, a positive attribute to the system is that most of the components can be altered to fit user needs. Adjusting the cell concentration and the types of cells are important future directions that may help us understand inflammatory derived shunt obstruction.

The most dramatic difference in adhesion due to mechanical cues was an alteration in adhesion due to shear stress. Results from this body of work can be used in future hypothesis driven studies to help identify the cause of inflammatory derived shunt obstruction. In most cases, a decreased shear stress decreases initial macrophage and astrocyte binding. These data can be expanded in numerous ways including future work that could relate these findings to CSF stagnancy at certain times of a patient's life or during particular activities that may alter CSF production rate. Results could further be expanded to understand why devices used to continuously drain CSF (i.e., shunt catheters and valves) may be more susceptible to inflammatory cell adhesion than are devices inserted into the same cranial space that undergo less continuous flow and pulsatility (i.e., reservoirs).

Results implicating a role of shear stress in macrophage and astrocyte adhesion can also be used in future work to develop strategies to inhibit obstruction. While other studies including *in vivo* analysis to support these findings in the acute and chronic term are needed, we begin to speculate if pharmaceutical agents such as diuretic mannitol, which decreases CSF production and flow rate [225] and has been used to treat increased intracranial pressure [226], may also decrease shunt failure by creating an environment

less conducive to macrophage and astrocyte adhesion. Alternatively, these results can be used to manipulate the catheter architecture so that changes in hole size (Chapter 6), hole number (future work), or perhaps luminal diameter (future work) may influence adhesion because of inherent changes to shear stress.

Modifications to the surface chemistry can easily be expanded in the flow system and also *in vivo* to test other surface coatings and to test the long term applicability of the proposed NAC and PEG modifications. There has been a trend over the last decade to tailor surfaces to actively target and dissuade cells from attaching [194]. These concepts can be employed in future studies for the improvement of shunt systems. However, surface wettability is certainly not the only component of a surface that influences adhesion. Future work should expand not only on surface wettability but on roughness and charge to correlate these results to those acquired with other medical devices.

Importantly, results acquired in this body of work may be used in future hypothesis driven studies to help inhibit inflammatory-derived obstruction. Because the obstruction rate of shunt systems is incredibly high, modifications need to be tested with alacrity to improve shunt design.

REFERENCES

[1] Rekate H. The definition and classification of hydrocephalus: a personal recommendation to stimulate debate. Cerebrospinal Fluid Research. 2008;5.

[2] McAllister JP, II, Chovan P. Neonatal hydrocephalus. Mechanisms and consequences. Neurosurgery Clinics of North America. 1998;9:73-93.

[3] Harris N, McAllister J, Conaughty J, Jones H. The effect of inherited hydrocephalus and shunt treatment on cortical pyramidal cell dendrites in the infant H-Tx rat. Experimental Neurology. 1996;141:269-79.

[4] Fernell E, Hagberg B, Hagberg G, von W. Epidemiology of infantile hydrocephalus in Sweden. III. Origin in preterm infants. Acta Paediatr Scand. 1987;76:418-23.

[5] Fishman R. Cerebrospinal fluid in diseases of the nervous system. Philadelphia: Saunders Company; 1992.

[6] Emery J, Staschak M. The size and form of the Cerebral Aqueduct in children. Brain. 1972;95:591-8.

[7] Irani D. Cerebrospinal fluid in clinical practice. Philadelphia: Saunders Company; 2009.

[8] Welch K. The principles of physiology of the cerebrospinal fluid in relation to hydrocephalus including normal pressure hydrocephalus. Advances in Neurology. 1975;13:247-332.

[9] Johnston M. The importance of lymphatics in cerebrospinal fluid transport. Lymphat Res Biol. 2003;1:41-4 discussion 5.

[10] Oldendorf W. Cerebrospinal fluid formation and circulation. Prog Nucl Med. 1972;1:336-58.

[11] Wagshul M, Chen J, Egnor M, McCormack E, Roche P. Amplitude and phase of cerebrospinal fluid pulsations: experimental studies and review of the literature. J Neurosurg. 2006;104:810-9.

[12] Laterra J, Keep RF, Betz A, Goldstein G. Blood-brain-cerebrospinal fluid barriers. In: Siegel G, Agranoff B, Albers R, Fisher S, Uhler M, editors. Basic neurochemistry: molecular, cellular and medical aspects. 6 ed. Philadelphia: Lippincott-Raven; 1999. p. 671.

[13] Spector R, Johanson C. Vitamin transport and homeostasis in mammalian brain: focus on vitamins B and E. J Neurochem. 2007;103:425-38.

[14] Saunders N, Habgood M, Dziegielewska K. Barrier mechanisms in the brain, I. Adult brain. Clin Exp Pharmacol Physiol. 1999;26:11-9.

[15] Silverberg G, Huhn S, Jaffe R, Chang S, Saul T, Heit G, et al. Downregulation of cerebrospinal fluid production in patients with chronic hydrocephalus. J Neurosurg. 2002;97:1271-5.

[16] Czosnyka M, Czosnyka Z, Momjian S, Pickard J. Cerebrospinal fluid dynamics. Physiol Meas. 2004;25:R51-76.

[17] Del Bigio MR, McAllister JP, II, Choux M, DiRocco R, Hockley AD, Walker ML. Pathophysiology of Hydrocephalus. Pediatric Neurosurgery. Philadelphia: Churchill Livingstone; 1999. p. 217-36.

[18] Miller JM, McAllister JP. Reduction of astrogliosis and microgliosis by cerebrospinal fluid shunting in experimental hydrocephalus. Cerebrospinal Fluid Res. 2007;4:5.

[19] Del Bigio M, Wilson M, Enno T. Chronic hydrocephalus in rats and humans: white matter loss and behavior changes. Ann Neurol. 2003;53:337-46.

[20] Del Bigio M. Cellular damage and prevention in childhood hydrocephalus. Brain Pathol. 2004;14:317-24.

[21] Wood P. Roles of CNS macrophages in neurodegeneration. In: Wood P, editor. Neuroinflammation: mechanisms and management. Totowa, NJ: Humana Press, Inc; 1998.

[22] Hanisch U. Microglia as a source and target of cytokines. Glia. 2002;40:140-55.

[23] Leung B, Biran R, Underwood C, Tresco P. Characterization of microglial attachment and cytokine release on biomaterials of differing surface chemistry. Biomaterials. 2008;29:3289-97.

[24] McAllister JP, Forsyth J, Deren K. Global neuroinflammation patterns in experimental neonatal hydrocephalus. Cerebrospinal Fluid Res. 2009;27:Suppl 2: S12.

[25] Bergsneider M, Egnor M, Johnston M, Kranz D, Madsen J, McAllister JP, et al. What we don't (but should) know about hydrocephalus. J Neurosurg. 2006;104:157-9.

[26] Kehler U, regelsberger J, Gliemroth J, Westphal M. Outcome prediction of third ventriculostomy: a proposed hydrocephalus grading system. Minim Invasive Neurosurg. 2006;49:238-43.

[27] Farin A, Aryan H, Ozgur B, Parsa A, Levy M. Endoscopic third ventriculostomy. Journal of Clinical Neuroscience. 2006;13:763-70.

[28] Mohnaty A, Biswas A, Satish S, Vollmer D. Efficacy of endoscopic third ventriculostomy in fourth ventricular outlet obstruction. Neurosurgery 2008;63:905-13.

[29] Koch-Wiewrodt D, Wagner W. Success and failure of endoscopic third ventriculostomy in young infants: are there different age distributions? Childs Nerv Syst. 2006;22:1537-41.

[30] Robinson S, Kaufman B, Park T. Outcome analysis of initial neonatal shunts: does the valve make a difference? Pediatr Neurosurgery. 2002;37:287-94.

[31] Walker M. Looking at hydrocephalus: where are we now, where are we going? Child's Nervous System. 2005;21:524-7.

[32] Walker M. Treatment of hydrocephalus: mere survival is not enough. Clin Neurosurgery. 2005;52:279-82.

[33] The stats on hydrocephalus. 2009:http://www.hydroassoc.org/media/stats.

[34] Simon T, Riva-Cambrin J, Srivastava R, Bratton S, Dean J, Kestle J. Hospital care for children with hydrocephalus in the United States: utilization, charges, comorbidities, and deaths. J Neurosurg Pediatrics. 2008;1:131-7.

[35] Simon T, Hall M, Riva-Cambrin J, Albert J, Jeffries H, Lafleur B, et al. Infection rates following initial cerebrospinal fluid shunt placement across pediatric hospitals in the United States. Clinical article. J Neurosurg Pediatrics. 2009;4:156-65.

[36] Kestle J, Garton H, Whitehead W, Drake J, Kulkarni A, Cochrane D, et al. Management of shunt infections: a multicenter pilot study. J Neurosurg 2006;105:177-81.

[37] Bayston R, Milner R. Antimicrobial activity of silicone rubber used in hydrocephalus shunts, after impregnation with antimicrobial substances. J Clin Pathol. 1981;34:1057-62.

[38] Kan P, Kestle J. Lack of efficacy of antibiotic-impregnated shunt systems in preventing shunt infections in children. Childs Nerv Syst. 2007;23:773-7.

[39] Baru J, Bloom D, Muraszko K, Koop C. John Holter's shunt. J Am Col Surg. 2001;192:79-85.

[40] Williams M, McAllister J, Walker M, Kranz D, Bergsneider M, Del Bigio M, et al. Priorities for hydrocephalus research: report from a National Institutes of Health-sponsored workshop. J Neurosurg. 2007;107:345-57.

[41] Serlo W, Fernell E, Heikkinen E, Anderson H, von Wendt L. Functions and complications of shunts in different etiologies of childhood hydrocephalus. Childs Nerv Syst. 1990;6:92-4.

[42] Browd S, Ragel B, Gottfried O, Kestle J. Failure of cerebrospinal fluid shunts: part I: Obstruction and mechanical failure. Pediatr Neurol. 2006;34:83-92.

[43] Del Bigio M, Fedoroff S. Short-term response of brain tissue to cerebrospinal fluid shunts in vivo and in vitro. J Biomed Mater Res. 1992;26:979-87.

[44] Schoener W. Evaluation of shunt failures by compliance analysis and inspection of shunt valves and shunt materials, using microscopic or scanning electron microscopic techniques. In: Matsumoto S, Tamaki N, editors. Hydrocephalus: pathogenesis and treatment. Tokyo: Springer Verlag; 1991. p. 452-72.

[45] Enchev Y, Oi S. Historical trends of neuroendoscopic surgical techniques in the treatment of hydrocephalus. Neurosurg Rev. 2008;31:249-62.

[46] Sainte-Rose C, Piatt J, Renier D, Pierre-Kahn A, Hirsch J, Hoffman H, et al. Mechanical contributions in shunts. Pediatr Neurosurgery. 1991-992;17:2-9.

[47] Mwachaka P, Obonyo N, Mutiso B, Ranketi S, Mwang'ombe N. Ventriculoperitoneal shunt complications: a three-year retrospective study in a Kenyan national teaching and referral hospital. Pediatr Neurosurgery. 2010;46:1-5.

[48] Del Bigio M. Biological reactions to cerebrospinal fluid shunt devices: a review of the cellular pathology. Neurosurgery. 1998;42:319-25.

[49] Sekhar L, Moossy J, Guthkelch A. Malfunctioning ventriculoperitoneal shunts. Clinical and pathological features. J Neurosurg. 1982;56:411-6.

[50] Gower D, Watson D, Harper D. e-PTFE ventricular shunt catheters. Neurosurgery. 1992;31:1132-5.

[51] Snow R, Kossovsky N. Hypersensitivity reaction associated with sterile ventriculoperitoneal shunt malfunction. Surg Neurol. 1989;31:209-14.

[52] Tung H, Raffel C, McComb J. Ventricular cerebrospinal fluid eosinophilia in children with ventriculoperitoneal shunts. J Neurosurg. 1991;75:541-4.

[53] Bigner S, Elmore P, Dee A, Johnston W. The cytopathology of reactions to ventricular shunts. Acta Cytol. 1985;29:391-6.

[54] Fournier E, Passirani C, Montero-Menei C, Benoit J. Biocompatibility of implantable synthetic polymeric drug carriers: focus on brain biocompatibility. Biomaterials. 2003;24:3311-31.

[55] Kim Y, Hitchcock R, Bridge M, Tresco P. Chronic response of adult rat brain tissue to implants anchored to the skull. Biomaterials. 2004;25:2229-37.

[56] Castejon O. Transmission electron microscope study of human hydrocephalic cerebral cortex. Journal of Submicroscopic Cytology & Pathology. 1994;26:29-39.

[57] Wikkelso C, Blomstrand C. Cerebrospinal fluid proteins and cells in normal-pressure hydrocephalus. J Neurol. 1982;228:171-80.

[58] Luttikhuizen D, Harmsen M, Van Luyn M. Cellular and molecular dynamics in the foreign body reaction. Tissue Eng. 2006;12:1955-70.

[59] Aderem A, Underhill D. Mechanisms of phagocytosis in macrophages. Annu Rev Immunol. 1999;17:593-623.

[60] Biran R, Martin D, Tresco P. Neuronal cell loss accompanies the brain tissue response to chronically implanted silicon microelectrode arrays. Experimental Neurology. 2005;195:115-26.

[61] Mosher D. Adhesive proteins and their cellular receptors. Cardiovascular Pathology. 1993;2:149-55.

[62] Hynes R. Integrins: versatility, modulation, and signaling in cell adhesion. Cell. 1992;69:11-25.

[63] Morehead J, Holt G. Soft-tissue response to synthetic biomaterials. Otolaryngologic clinics of North America1994. p. 195-201.

[64] Anderson J, Rodriguez A, Chang D. Foreign body reaction to biomaterials. Semin Immunol. 2008;20:86-100.

[65] Anderson J. Inflammatory response to implants. ASAIO J. 1988;34:101-7.

[66] Scheltes J, Heikens M, Pistecky P, van Andel C, Borst C. Assessment of patented coronary end-to-side anastomotic devices using micromechanical bonding. Ann Thorac Surg. 2000;70:218-21.

[67] Lovely T, McAllister J, Miller D, Lamperti A, Wolfson B. Effects of hydrocephalus and surgical decompression on cortical norepinephrine levels in neonatal cats. Neurosurgery. 1989;24:43-52.

[68] McAllister J, Maugans T, Shah M, Truex Jr. R. Neuronal effects of experimentally induced hydrocephalus in newborn rats. J Neurosurg. 1985;63:776-83.

[69] Shiu Y, Weiss J, Hoying J, Iwamoto M, Joung I, Quam C. The role of mechanical stresses in angiogenesis. Crit Rev Biomed Eng. 2005;33:431-510.

[70] Corum L, Hlady V. Screening platelet-surface interactions using negative surface charge gradients. Biomaterials. 2010;31:3148-55.

[71] Bacabac R, Smit T, Cowin S, Van Loon J, Nieuwstadt F, Heethaar R, et al. Dynamic shear stress in parallel-plate flow chambers. J Biomech. 2005;38:159-67.

[72] Albright A, Adelson P, Pollack I. In: Brandenburg B, editor. Principles and practice of pediatric neurosurgery. New York: Thieme Medical Publishers, Inc.; 2008. p. 136.

[73] Frisch E. Silicones in artificial organs. Polymeric materials and artificial organs1984. p. 63-97.

[74] Yamamoto S, Ohno K, Aoyagi M, Ichinose S, Hirakawa K. Calcific deposits on degraded shunt catheters: long-term follow-up of V-P shunts and late complications. Childs Nerv Syst. 2002;18:19-25.

[75] Kalousdian S, Karlan M, Williams M. Silicone elastomer cerebrospinal fluid shunt systems. Neurosurgery. 1998;42:887-92.

[76] Boop F, Chadduck W. Silastic duraplasty in pediatric patients. Neurosurgery. 1991;29:785-7.

[77] Habal M. The biologic basis for the clinical application of the silicones. A correlate to their biocompatibility. Arch Surg. 1984;119:843-8.

[78] Chen H, Brook M, Sheardown H. Silicone elastomers for reduced protein adsorption. Biomaterials. 2004;25:2273-82.

[79] Peterson S, McDonald A, Gourley P, Sasaki D. Poly(dimethylsiloxane) thin films as biocompatible coatings for microfluidic devices: cell culture and flow studies with glial cells. J Biomed Mater Res A. 2005;72:10-8.

[80] Hlady V, Buijs J. Protein adsorption on solid surfaces. Current Opinion in Biotechnology. 1996;7:72-7.

[81] Andrade J, Hlady V. Protein adsorption and materials biocompatibility: a tutorial review and suggested hypotheses Biopolymers/Non-Exclusion HPLC: Springer Berlin / Heidelberg; 1986. p. 1-63.

[82] Andrade J, Gregonis D, Smith L. Physicochemical aspects of polymer surfaces. New York: Plenum Press; 1981.

[83] Saltzman W. Cell interactions with polymers. Principles of tissue engineering. Second ed. San Diego: Academic Press; 2000.

[84] Xue Y, Liu X, Sun J. PU/PTFE-stimulated monocyte-derived soluble factors induced inflammatory activation in endothelial cells. Toxicology in Vitro. 2010;24:404-10.

[85] Poncin-Epaillard F, Legeay G. Surface engineering of biomaterials with plasma techniques. J Biomater Sci Polymer Edition. 2003;14:1005-28.

[86] Curtis A, Forrester J, McInnes C, Lawrie F. Adhesion of cells to polystyrene surfaces. The Journal of Cell Biology. 1983;97:1500-6.

[87] Ratner B. Biomaterials science: overview and opportunities with special reference to organic and polymeric glow discharge plasma treatments. In: D'Agostino R, Favia P, Fracassi F, editors. Plasma Processing of Polymers. Botson: Kluwer Academic Publishers; 1996. p. 453-64.

[88] Webb K, Hlady V, Tresco P. Relative importance of surface wettability and charged functional groups on NIH 3T3 fibroblast attachment, spreading, and cytoskeletal organization. J Biomed Mater Res. 1998;41:422-30.

[89] Hallab N, Bundy K, O'Connor K, Clark R, Moses R. Cell adhesion to biomaterials: correlations between surface charge, surface roughness, adsorbed protein, and cell morphology. J Long Term Eff Med Implants. 1995;5:209-31.

[90] Cox J, Curry M, Skirboll S, Gourley P, Sasaki D. Surface passivation of a microfluidic device to glial cell adhesion: a comparison of hydrophobic and hydrophilic SAM coatings. Biomaterials. 2002;23:929-35.

[91] Wong T, Lee L, Liu R, Yeh S, Chang T, Ho D, et al. Hydrogel ventriculoperitoneal shunt for the treatment of hydrocephalus in children. In: Matsumoto S, Tamaki N, editors. Hydrocephalus: pathogenesis and treatment. Tokyo: Springer-Verlag; 1991. p. 438-49.

[92] Kopecek J, Jiyuan Y. Hydrogels as smart biomaterials. Polymer International. 2007;56:1078-98(21).

[93] Montheard J, Chatzopoulos M, Chappard D. 2-Hydroxyethyl methacrylate (HEMA): chemical properties and applications in biomedical fields. Polymer reviews. 1992;32:1-34.

[94] Winer J, Janmey P, McCormick M, Funaki M. Bone marrow-derived human mesenchymal stem cells become quiescent on soft substrates but remain responsive to chemical or mechanical stimuli. Tissue Eng Part A. 2009;15:147-54.

[95] Parsons J, Horwitz A, Schwartz M. Cell adhesion: integrating cytoskeletal dynamics and cellular tension. Nat Rev Mol Cell Biol. 2010;11:633-43.

[96] Singhal R, Janzig D, Wahlstrand C, Skime R, Olson P, Scott E, et al. Implantable medical device with lubricious material. United States Patent Office. 2007;United States Patent # 11/526514

[97] Defife K, Hagen K, Clapper D, Andersen J. Photochemically immobilized polymer coatings: effects on protein adsorption, cell adhesion, and leukocyte activation. J Biomater Sci Polymer Edition. 1999;10:1063-74.

[98] Rouxhet L, Duhoux F, Borecky O, Legras R, Schneider Y. Adsorption of albumin, collagen, and fibronectin on the surface of poly(hydroxybutyrate-hydroxyvalerate) (PHB/HV) and poly(e-caprolactone) (PCL) films modified by an alkaline hydrolysis and of poly(ethylene terephtalate) (PET) track-etched membranes. J Biomater Sci Polymer Edition. 1998;9:1279-304.

[99] Tung K, Chang Y, Chuang C. Effect of pore morphology on fluid flow through track-etched polycarbonate membrane. Tamkang Journal of Science and Engineering. 2001;4:127-32.

[100] Campbell C, Von Recum A. Microtopography and soft tissue response. Journal of Investigative Surgery. 1989;2:51-74.

[101] Klinge U, Klosterhalfen B, Birkenhauer V, Junge K, Conze J, Schumpelick V. Impact of polymer pore size on the interface scar formation in a rat model. Journal of Surgical Research. 2002;103:208-14.

[102] Zhu C, Yago T, Lou J, Zarnitsyna V, McEver R. Mechanisms for flow-enhanced cell adhesion. Ann Biomed Eng. 2008;36:604-21.

[103] Long M, Lu S, Sun G. Kinetics of receptor-ligand interactions in immune responses. Cell Mol Immunol. 2006;3:79-86.

[104] Cerebrospinal fluid (CSF) flow and chiari malformation. 2011;2011:www.pressenter.com/~wacma/csf.htm.

[105] Treatment of hydrocephalus. 2010:http://www.hydroassoc.org/hydrocephalus-education-and-support/learning-about-hydrcephalus/treatment-of-hydrocephalus/.

[106] Go K, Ebels E, van Woerden H. Experiences with recurring ventricular catheter obstructions. Clin Neurol Neurosurg. 1981;83:47-56.

[107] Gower D, Lewis J, Kelly DJ. Sterile shunt malfunction. A scanning electron microscopic perspective. J Neurosurg. 1984;61:1079-84.

[108] Del Bigio M, Bruni J. Reaction of rabbit lateral periventricular tissue to shunt tubing implants. J Neurosurg. 1986;64:932-40.

[109] Kossovsky N, Snow R. Clinical-pathological analysis of failed central nervous system fluid shunts. J Biomed Mater Res. 1989;23:73-86.

[110] Koga H, Mukawa J, Nakata M, Sakuta O, Higa Y. Analysis of retained ventricular shunt catheters. Neurol Med Chir (Tokyo). 1992;32:824-8.

[111] Cinalli G, Maixner W, Sainte-Rose C. Abdominal complications of peritoneal shunts. Pediatric hydrocephalus. Milan: Springer. p. 326.

[112] Clyde B, Albright A. Evidence for a patent firbrous tract in fractured, outgrown, or disconnected ventriculoperitoneal shunts. Pediatr Neurosurgery. 1995;23:20-5.

[113] VandeVord P, Gupta N, Wilson R, Vinuya R, Schaefer C, Canady A, et al. Immune reactions associated with silicone-based ventriculo-peritoneal shunt malfunctions in children. Biomaterials. 2004;25:3853-60.

[114] Ellis M, Kazina C, Del Bigio MR, McDonald P. Treatment of recurrent ventriculoperitoneal shunt failure associated with persistent cerebrospinal fluid eosinophilia and latex allergy by use of an "extracted" shunt. J Neurosurg Pediatrics. 2008;1:237-9.

[115] Czernicki Z, Strzalkowski R, Walasek N, Gajkowska B. What can be found inside shunt catheters. Brain Edema XIV. Acta Neurochir Suppl. 2009;106 (Part 3):81-5.

[116] Thomale. Performation holes in ventricular catheters -- is less more? Childs Nervous System. 2010;26:781-9.

[117] Ono H, Moriyama T, Uneoka K, Matsumura H, Fujita Y. Percutaneous revision of shunt with obstructed ventricular catheter (author's transl). No Shinkei Geka. 1976;4:365-70.

[118] Ventureyra E, Higgins M. A new ventricular catheter for the prevention and treatment of proximal obstruction in cerebrospinal fluid shunts. Neurosurgery. 1994;34:924-6.

[119] Pattisapu J, Trumble E, Taylor K, Howard P, Kovach T. Percutaneous endoscopic recanalization of the catheter: a new technique of proximal shunt revision. Neurosurgery. 1999;45:1361-6; discussion 6-7.

[120] Ginsberg H, Drake J, Peterson T, Cobbold R. Recanalization of obstructed cerebrospinal fluid ventricular catheters using ultrasonic cavitation. Neurosurgery. 2006;59 ONS403-12.

[121] Camlar M, Ersahin Y, Ozer F, Sen F, Orman M. Can using a peel-away sheath in shunt implantation prevent ventricular catheter obstruction? Childs Nerv Syst. 2010;Epub ahead of print.

[122] Ames R. Ventriculo-peritoneal shunts in the management of hydrocephalus. J Neurosurg. 1967;27:525-9.

[123] Zumstein B, Landolt A. Untersuchung des an Ventrikelkathetern hydrozephaler Patienten haftenden Gewebes im Lichtund Electronenmikroskop. Acta Neurochir. 1974;30:287-98.

[124] Haase J, Weeth R. Multiflanged ventricular Portnoy catheter for hydrocephalus shunts. Acta Neurochir (Wien). 1976;33:231-8.

[125] Nakamura S, Moriyasu N. Floating ventricular catheter: A new shunting device. Monogr Neural Sci. 1982;8:191-4.

[126] Watson D. Process for creating an ingrowth preventing indwelling catheter assembly. United States. 2004;United States Patent # 7763142.

[127] Cagavi F, Akalan N, Celik H, Gur D, Guciz B. Effect of hydrophilic coating on microorganism colonization in silicone tubing. Acta Neurochir (Wien). 2004;146:603-10; discussion 9-10.

[128] Boelens J, Zaat S, Meeldijk J, Dankert J. Subcutaneous abscess formation around catheters induced by viable and nonviable Staphylococcus epidermidis as well as by small amounts of bacterial cell wall components. J Biomed Mater Res. 2000;50:546-56.

[129] Bayston R, Grove N, Siegel J, Lawellin D, Barsham S. Prevention of hydrocephalus shunt catheter colonisation in vitro by impregnatino with antimicrobials. J Neurol Neurosurg Psychiatry. 1989;52:605-9.

[130] Medtronic I. 2006;United States Patent Serial # 78887628.

[131] Lin J, Morris M, Olivero W, Boop F, Sanford R. Computational and experimental study of proximal flow in ventricular catheters. Technical note. J Neurosurg. 2003;99:426-31.

[132] Medow J. The permeable proximal catheter project: a novel approach to preventing shunt obstruction. American Association of Neurological Surgeons Annual Meeting, Pediatric Section. 2005.

[133] Patel K, Tang H, Grever W, Simon NK, Xiang J, Keep R, et al. Evaluation of polymer and self-assembled monolayer-coated silicone surfaces to reduce neural cell growth. Biomaterials. 2006;27.

[134] Liang X, Wang A, Cao T, Tang H, McAllister Jn, Salley S, et al. Effect of cast molded rifampicin/silicone on Staphylococcus epidermidis biofilm formation. J Biomed Mater Res A. 2006;76:580-8.

[135] Lee S, Pinney J, Khialeeva E, Bergsneider M, Judy J. Functional evaluation of magnetic microactuators for removing biological accumulation: an in vitro study. Conf Proc IEEE Eng Med Biol Soc. 2008;2008:947-50.

[136] Lee S, Vasquez D, Bergsneider M, Judy J. Magnetic microactuators for MEMS-enabled ventricular catheters for hydrocephalus. Conf Proc IEEE Eng Med Biol Soc. 2006;1:2494-7.

[137] Izci Y, Secer H, Akay C, Gonul E. Initial experience with silver-impregnated polyurethan ventricular catheter for shunting of cerebrospinal fluid in patients with infected hydrocephalus. Neurol Res. 2009;31:234-7.

[138] Blount J, Campbell J, Haines S. Complications in ventricular cerebrospinal fluid shunting. Neurosurg Clin N Am. 1993;4:633-56.

[139] Pujari S, Kharkar S, Metellus P, Shuck J, Williams M, Rigamonti D. Normal pressure hydrocephalus: long term outcome after shunt surgery. J Neurol Neurosurg Psychiatry. 2008;79:1282-6.

[140] Harris C, Resau J, Hudson E, West R, Moon C, McAllister J. Mechanical contributions to astrocyte adhesion using a novel in vitro model of catheter obstruction. Exp Neurol. 2010;222:204-10.

[141] Design control guidance for medical device manufacturers. In: Administration FaD, editor.1997.

[142] Chamberlain L, Godek M, Gonzalez-Juarrero M, Grainger D. Phenotypic non-equivalence of murine (monocyte-) macrophage cells in biomaterial and inflammatory models. J Biomed Mater Res A. 2009;88:858-71.

[143] Bleier R, Albrecht R. Supraependymal macrophages of third ventricle of hamster: morphological, functional and histochemical characterization in situ and in culture. J Comp Neurol. 1980;192:489-504.

[144] Winslow B, Tresco P. Quantitative analysis of the tissue response to chronically implanted microwire electrodes in rat cortex. Biomaterials. 2010;31:1558-67.

[145] Turner J, Shain W, Szarowski D, Andersen M, Martins S, Isaacson M, et al. Cerebral astrocyte response to micromachined silicon implants. Experimental Neurology. 1999;156:33-49.

[146] Stensaas S, Stensaas L. The reaction of the cerebral cortex to chronically implanted plastic needles. Acta Neuropathol. 1976;35:187-203.

[147] Polikov V, Tresco P, Reichert W. Response of brain tissue to chronically implanted neural electrodes. Journal of Neuroscience Methods. 2005;148:1-18.

[148] Menei P, Croue A, Daniel V, Pouplard-Barthelaix A, Benoit J. Fate and biocompatibility of three types of microspheres implanted into the brain. Journal of Biomedical Materials Research. 1994;28:1079-85.

[149] Giulian D, Baker T, Shih L, Lachman L. Interleukin 1 of the central nervous system is produced by ameboid microglia. J Exp Med. 1986;164:594-604.

[150] Brahmachari S, Fung Y, Pahan K. Induction of glial fibrillary acidic protein expression in astrocytes by nitric oxide. The Journal of Neuroscience. 2006;26:4930-9.

[151] Watson-Marlow. Marprene. 2006:http://www.watson-marlow.com/pdfs-global/wd-marprene-us-01.pdf.

[152] Anderson J. Mechanisms of inflammation and infection with implanted devices. Cardiovascular Pathology. 1993;2:33-41.

[153] Shen M, Horbett T. The effects of surface chemistry and adsorbed proteins on monocyte/macrophage adhesion to chemically modified polystyrene surfaces. Journal of Biomedical Materials Research Part A. 2001;57:336-45.

[154] Ertel S, Ratner B, Kaul A, Schway M, Horbett T. In vitro study of the intrinsic toxicity of synthetic surfaces to cells. J Biomed Mater Res. 1994;28:667-75.

[155] Taraska J, Zagotta W. Fluorescence application in molecular neurobiology. Neuron. 2010;66:170-89.

[156] Schwartz A, Wang L, Early E, Gaigalas A, Zhang Y, Marti G, et al. Quantitating fluorescence intensity from fluorophore: the definition of MESF assignment. Journal of Research of the National Institute of Standards and Technology. 2002;107:83-91.

[157] Harris C, McAllister JP. Systems and methods for simulating flow of cerebrospinal fluid. 2010;Attorney Docket # 21101.022UI.

[158] Detwiler P, Porter R, Rekate H. Hydrocephalus - clinical features and management. In: Choux M, Di Rocco C, Hockley A, Walker M, editors. Pediatric neurosurgery. New York: Churchill Livingstone; 1999. p. 253-71.

[159] Goldblum R, Pelley R, O'Donell A, Pyron D, Heggers J. Antibodies to silicone elastomers and reactions to ventriculoperitoneal shunts. Lancet. 1992;340:510-3.

[160] Cullen D, Simon C, LaPlaca M. Strain rate-dependent induction of reactive astrogliosis and cell death in three-dimensional neuronal-astrocytic co-cultures. Brain Research. 2007;1158:103-15.

[161] Basson M, Yu C, Herden-Kirchoff O, Ellermeier M, Sanders M, Merrell R, et al. Effects of increased ambient pressure on colon cancer cell adhesion. Journal of Cellular Biochemistry. 2000;78:47-81.

[162] Davies P, Robotewskyj A, Griem M. Quantitative studies of endothelial cell adhesion. Directional remodeling of focal adhesion sites in response to flow forces. J Clin Invest. 1994;93:2031-8.

[163] Wang N, Miao H, Li Y, Zhang P, Haga J, Hu Y, et al. Shear stress regulation of Kruppel-like factor 2 expression is flow pattern-specific. Biochemical and Biophysical Research Communications. 2006;341:1244-51.

[164] Tsuchiya T. Studies on the standardization of cytotoxicity tests and new standard reference materials useful for evaluating the safety of biomaterials. J Biomater Appl. 1994;9:138-57.

[165] Ostrow L, Sachs F. Mechanosensation and endothelin in astrocytes--hypothetical roles in CNS pathophysiology. Brain Res Brain Res Rev. 2005;48:488-508.

[166] Roca-Cusachs P, Gauthier N, Del Rio A, Sheetz M. Clustering of alpha(5)beta(1) integrins determines adhesion strength whereas alpha(v)beta(3) and talin enable mechanotransduction. Proc Natl Acad Sci U S A. 2009;106:16245-50.

[167] Razumovsky A, Hanley D. Intracranial pressure measurement/cranial vault mechanics: clinical and experimental observations. Curr Opin Neurol Neurosurg. 1992;5:818-25.

[168] Johanson C, Duncan Jr, Klinge P, Brinker T, Stopa E, Silverberg G. Multiplicity of cerebrospinal fluid functions: new challenges in health and disease. Cerebrospinal Fluid Res. 2008;5.

[169] Ross R. The pathogenesis of atherosclerosis: a perspective for the 1990s. Nature. 1993;362:801-9.

[170] Johanson C, Stopa E, McMillan P. The blood-cerebrospinal fluid barrier: structural and functional significance. In: Nag S, editor. The blood-brain and other neural barriers- biology and research protocols. New York: Humana Press; 2010.

[171] Sigal G, Mrksich M, Whitesides G. Effect of surface wettability on the adsorption of proteins and detergents. J Am Chem Soc. 1998;120:3464-73.

[172] Yung L, Colman R, Cooper S. Neutrophil adhesion on polyurethanes preadsorbed with high molecular weight kininogen. Blood. 1999;94:2716-24.

[173] Polikov V, Hong J, Riechert W. Soluble factor effects on glial cell reactivity at the surface of gel-coated microwires. J Neurosci Methods. 2010;190:180-7.

[174] Brydon H, Keir G, Thompson E, Bayston R, Hayward R, Harkness W. Protein adsorption to hydrocephalus shunt catheters: CSF protein adsorption. J Neurol Neurosurg Psychiatry. 1998;64:643-7.

[175] Brydon H, Hayward R, Harkness W, Bayston R. Physical properties of cerebrospinal fluid of relevance to shunt function. 2: The effect of protein upon CSF surface tension and contact angle. British Journal of Neurosurgery. 1995;9:645-51.

[176] Kim B, Peterson T, Papautsky I. Long-term stability of plasma oxidized PDMS surfaces. Conf Proc IEEE Eng Med Biol Soc. 2004;7:5013-6.

[177] Ratner B. Biomaterials science: overview and opportunities with special reference to organic and polymeric glow discharge plasma treatments. In: D'Agostino R,

Favia P, Fracassi F, editors. Plasma processing of polymers. Boston: Kluwer Academic Publishers; 1996. p. 453-64.

[178] Lampin M, Warocquier-Clerout, Legris C, Degrange M, Sigot-Luizard M. Correlation between substratum roughness and wettability, cell adhesion, and cell migration. J Biomed Mater Res. 1997;36:99-108.

[179] Fan Y, Cui F, Hou S, Xu Q, Chen L, Lee I-S. Culture of neural cells on silicon wafers with nano-scale surface topograph. J Neurosci Methods. 2002;120:17-23.

[180] Hillborg H, Ankner F, Gedde U, Smith G, Yasuda H, Wikstrom K. Crosslinked polydimethylsiloxane exposed to oxygen plasma studied by neutron reflectometry and other surface specific techniques. Polymer. 2000;41:6851.

[181] Keselowsky B, Collard D, Garcia A. Surface chemistry modulates focal adhesion composition and signaling through changes in integrin binding. Biomaterials. 2004;25:5947-54.

[182] Menei P, Croue A, Daniel V, Pouplard-Barthelaix A, Benoit J. Fate and biocompatibility of three types of microspheres implanted into the brain. J Biomed Mater Res. 1994;28:1079-85.

[183] Godek M, Malkov G, Fisher E, Grainger D. Macrophage serum-based adhesion to plasma-processed surface chemistry is distinct from that exhibited by fibroblasts. Plasma Process Polym. 2006;3:485-97.

[184] Xia Z, Triffitt J. A review on macrophage responses to biomaterials. Biomedical Materials. 2006;1:R1-R9.

[185] Winslow B, Christensen M, Yang W, Solzbacher F, Tresco P. A comparison of the tissue response to chronically implanted Parylene-C coated and uncoated planar silicon microelectrode arrays in rat cortex. Biomaterials. 2010;Epub ahead of print.

[186] Silverberg G. Normal pressure hydrocephalus (NPH): ischaemia, CSF stagnation or both. Brain. 2004;127:947-8.

[187] Deren K, Forsyth J, Abdullah O, Hsu E, Klinge P, Silverberg G, et al. Low levels of amyloid-beta and its transporters in neonatal rats with and without hydrocephalus. Cerebrospinal Fluid Research. 2009;6:4.

[188] Del Bigio MR. Neuropathology and structural changes in hydrocephalus. Dev Disabil Res Rev. 2010;16:16-22.

[189] Del Bigio MR, Enno T. Effect of hydrocephalus on rat brain extracellular compartment. Cerebrospinal Fluid Research. 2008;5:12.

[190] Del Bigio MR. Cellular damage and prevention in childhood hydrocephalus. Brain Pathology. 2004;14:317-24.

[191] Foltz E, Shurtleff D. Five-year comparative study of hydrocephalus in children with and without operation (113 cases). J Neurosurg. 1963;20:1064-79.

[192] Thi M, Tarbell J, Weinbaum S, Spray D. The role of the glycocalyx in reorganization of the actin cytoskeleton under fluid shear stress: a "bumper-car" model. Proc Natl Acad Sci USA. 2004;101:16483-8.

[193] Morais J, Papadimitrakopoulos F, Burgess D. Biomaterials/tissue interactions: possible solutions to overcome foreign body response. AAPS J. 2010;12:188-96.

[194] Ikada Y. Surface modification of polymers for medical applications. Biomaterials. 1994;15:725-36.

[195] Gombotz W, Guanghui W, Horbett T, Hoffman A. Protein adsorption to poly(ethylene oxide) surfaces. J Biomed Mater Res A. 1991;25:1547-62.

[196] Amiji M, Park K. Surface modification of polymeric biomaterials with poly(ethylene oxide), albumin, and heparin for reduced thrombogenicity. J Biomater Sci Polymer Ed. 1993;4:217-34.

[197] Merrill E, Salzman E. Polyethylene oxide as a biomaterial. ASAIO J. 1983;6:60-4.

[198] Lee J, Kopecekova P, Kopecek K, Andrade J. Surface properties of copolymers of alkyl methacrylates with methoxy (polyethylene oxide) methacrylates and their applications as protein-resistant coatings. Biomaterials. 1990;11:455-64.

[199] Green R, Frzier R, Shakesheff K, Davies M, Roberts J, Tendler S. Surface plasmon resonance analysis of dynamic biological interactions with biomaterials. Biomaterials. 2000;21:1823-35.

[200] Drury J, Mooney D. Hydrogels for tissue engineering: scaffold design variables and applications. Biomaterials. 2003;24:4337-51.

[201] Forster S, Platenberg T. From self-organizing polymers to nanohybrid and biomaterials. Angew Chem Int Ed. 2002;41:688-714.

[202] Du H, Chandaroy P, Hui S. Grafted poly-(ethylene glycol) on lipid surfaces inhibits protein adsorption and cell adhesion. Biochim Biophys Acta. 1997;1326:236-48.

[203] Sofia S, Premnath V, Merrill E. Poly(ethylene oxide) grafted to silicon surfaces: grafting density and protein adsorption. Macromolecules. 1998;31:5059-70.

[204] Bergstrom K, Osterberg E, Holmberg K, Hoffman A, Schuman T, Kozlowski A, et al. Effects of branching and molecular weight of surface-bound poly(ethylene oxide) on protein rejection. J Biomater Sci Polymer Ed. 1994;6:123-32.

[205] Olofsson A, Hermansson M, Elwing H. N-acetyl-L-cysteine affects growth, extracellular polysaccharide production, and bacterial biofilm formation on solid surfaces. Appl Environ Microbiol. 2003;69:4814-22.

[206] Dixon A, Israelsen R, Odell D, Heredia A, Britt D. PEG silane modification of PDMS for improved hydrophilicity. 4th Annual Mountain West Biomedical Engineering Conference. Park City, 2008.

[207] Chen H, Zhang Z, Chen Y, Brook M, Sheardown H. Protein repellant silicone surfaces by covalent immobilization of poly(ethylen oxide). Biomaterials. 2005;26:2391-9.

[208] Akiyama S. Integrins in cell adheison and signaling. Hum Cell. 1996;9:181-6.

[209] Wei J, Yoshinari M, Takemoto S, Hattori M, Kawada E. Adhesion of mouse fibroblasts on hexamethyldisiloxane surfaces with wide range of wettability. J Biomed Mater Res B Appl Biomater. 2006;81B:66-75.

[210] Harris C, Resau J, Hudson E, West R, Moon C, Black A, et al. Effects of surface wettability, flow and protein concentration on macrophage and astrocyte adhesion in an in vitro model of central nervous system catheter obstruction. J Biomed Mater Res A. 2011.

[211] Bjugstad K, Lampe K, Kern D, Mahoney M. Biocompatibility of poly(ethylene glycol)-based hydrogels in the brain: an analysis of the glial response across space and time. J Biomed Mater Res A. 2010;95:79-91.

[212] Chen G, Shi J, Hu Z, Hang C. Inhibitory effect on cerebral inflammatory response following traumatic brain injury in rats: a potential neuroprotective mechanism of N-acetylcysteine. Mediators Inflamm. 2008;2008:716458.

[213] Stanislaus R, Gilg A, Singh A. N-acetyl-L-cysteine ameliorates the inflammatory disease process in experimental autoimmune encephalomyelitis in Lewis rats. J Autoimmune Dis. 2005;2:4.

[214] Ginsberg H, Sum A, Drake J, Cobbold R. Ventriculoperitoneal shunt flow dependency on the number of patent holes in a ventricular catheter. Pediatr Neurosurgery. 2000;33:7-11.

[215] Lintula L. How shunts are made. It's about life: 10th National Conference on Hydrocephalus. Park City, 2008.

[216] Duffy D, McDonald A, Schueller O, Whitesides G. Rapid prototyping of microfluidic systems in poly(dimethylsiloxane). Analytical Chemistry. 1998;70:4974-84.

[217] Mata A, Fleischman A, Roy S. Characterization of polydimethylsiloxane (PDMS) properties for biomedical micro/nanosystems. Biomedical Microdevices. 2005;7:281-93.

[218] Giang U, Lee D, King M, DeLouise L. Microfabrication of cavities in polydimethylsiloxane using DRIE silicon molds. Lab on a Chip. 2007;7:1660-2.

[219] Abramoff M. Image processing with ImageJ. Biophotonics International. 2004;11:36-42.

[220] Jenney C, DeFife K, Colton E, Anderson J. Human monocyte/macrophage adhesion, macrophage motility, and IL-4-induced foreign body giant cell formation on silane-modified surface in vitro. J Biomed Mater Res. 1998;41:171-84.

[221] Eymann R, Meier U, Kiefer M. Animal experiments to evaluate complications of foreign materials on silicone with shunt catheters: preliminary results. Acta Neurochir Suppl. 2010;106:91-3.

[222] Vartanian K, Berny M, McCarty O, Hanson S, Hinds M. Cytoskeletal structure regulates endothelial cell immunogenicity independent of fluid shear stress. Am J Physiol Cell Physiol. 2010;298:C333-41.

[223] Falkenhagen D, Bosch T, Brown G, Schmidt B, Holtz M, Baurmeister U, et al. A clinical study on different cellulosic dialysis membranes. Nephrol Dial Transplant. 1987;2:537-45.

[224] Watkins L, Maier S, Goehler L. Immune activation: the role of pro-inflammatory cytokines in inflammation, illness responses and pathological pain states. Pain. 1995;63:289-302.

[225] Sahar A, Tsipstein E. Effects of mannitol and furosemide on the rate of formation of cerebrospinal fluid. Experimental Neurology. 1978;60:584-91.

[226] Tsze D, Steele D. Neurosurgical emergencies, nontraumatic. In: Fleisher G, Ludwig S, editors. Textbook of pediatric emergency medicine. 6 ed. Philadelphia: Lippincott Williams & Wilkins; 2010. p. 1588.